Tornado Damage Assessment in the aftermath of the May 20th 2013 Moore Oklahoma Tornado

Andrew J. Graettinger, Ph.D., The University of Alabama, Tuscaloosa, AL
Chris C. E. Ramseyer, Ph.D., University of Oklahoma, Norman, OK
Seamus Freyne, Ph.D., Mississippi State University, Starkville, MS
David O. Prevatt, Ph.D., University of Florida, Gainesville, FL
Laura Myers, Ph.D., The University of Alabama, Tuscaloosa, AL
Thang Dao, Ph.D., The University of Alabama, Tuscaloosa, AL
Royce W. Floyd, Ph.D., University of Oklahoma, Norman, OK
Lisa Holliday, Ph.D., University of Oklahoma, Norman, OK
Duzgun Agdas, Ph.D., University of Florida, Gainesville, FL
Fred L. Haan, Ph.D., Rose-Hulman Institute of Technology, Terre Haute, IN
Jim Richardson, Ph.D., The University of Alabama, Tuscaloosa, AL
Rakesh Gupta, Ph.D., Oregon State University, Corvallis, OR
Robert N. Emerson, Ph.D., Oklahoma State University, Stillwater, OK
Christine Alfano, Colorado State University, Fort Collins, CO

March 2014

Table of Contents

Disclaimer

The opinions and views expressed by the authors in this report are theirs alone and do not represent the view of any funding agencies. All information in this report is believed by the authors to be factually correct, but readers should use any information contained herein at their own risk

Executive Summary - Moore Tornado Report

This report presents observations, findings, and recommendations from an engineering reconnaissance trip following the May 20th, 2013 tornado that struck Moore, Oklahoma. A team of faculty, research scientists, professional engineers, and civil engineering students were tasked with investigating and documenting the performance of critical facility buildings and residences, (IBC Occupancy Category II, III, and IV), in Moore, OK. The Enhanced Fujita (EF) 5 tornado created a 17-mile long damage swath destroying over 12,000 buildings and killing 24 people. The total economic loss from this single event was estimated at $3 billion. The May 20th tornado was the third major tornado to hit Moore in the previous 15 years.

The primary objectives of this study included describing a methodology for an easily-reproducible rapid damage assessment, assessing performance of building components, assessing performance of above and below ground storm shelters, analyzing how social media can positively impact communities in the wake of extreme events, and conducting specialized depth studies. The data and recommendations are presented to support future development and/or modification of design guidelines, standards, and the use of social media to mitigate loss caused by extreme events.

Tornado damage is particularly extensive when medium- to large-sized cities with dense concentrations of buildings are hit by strong tornados. Damaging effects from moderate (EF0 to EF2) winds may be avoided by following hurricane coastal design guides. EF0 to EF2 winds cover approximately 85% of a damage area that is produced by strong EF4 and EF5 tornados. These robust designs are rarely employed for residential construction in tornado-prone areas. The mortality rates from tornado events have not decreased in years, while building damage and overall economic losses continue to grow. New methods are needed to improve engineering design and construction practices in tornado-prone areas. In addition, revision of structural retrofit practices should be considered for mitigating future losses from tornadoes. The findings from this field study are instrumental in validating recent results on tornado loads from laboratory experiments and numerical analyses.

On May 26th, 2013 the reconnaissance team arrived in Moore, OK. Along a series of transects perpendicular to the tornado's path, the team observed a dramatic change in the severity of damage from the center of the path towards the edges. These damage severity profiles were used to produce a damage severity contour map of the study area. In addition to mapping damage, in-depth studies were performed to leverage the technical data observed in the field. These studies include: the use and performance of storm shelters, performance of building materials and construction techniques, progressive failures of residential buildings, and how collected data can be used to improve laboratory simulations. In addition, a detailed aerial assessment of damage and debris was also conducted.

The findings of the assessment team are based on observations over three days spent surveying damaged homes and storm shelters in Moore, OK.

- A geolocation data methodology was developed and tested for use by extreme event damage assessment teams to collect, attribute, store, and distribute perishable damage data.
- An analysis of residential storm shelter performance was conducted including above and below ground shelters. The results show that no inspected below ground shelters failed from perforation or penetration although these shelters were sometimes found flooded by rain and severed water pipes, and in some cases the exits were blocked by debris. One perforation, through an area of poorly consolidated concrete, was observed on an above ground insulated concrete form waffle-grid residential shelter.
- Residential structures in lower wind speed areas were examined and found to fail at garage door openings and at connections.
- The comparison between the damage data from this assessment and total force predictions from a laboratory tornado simulator showed promise for lab simulations.
- Remotely sensed aerial imagery gave an understanding of flow and spreading of debris. Using aerial imagery from Moore, it was observed that debris flow is typically manifested in thin "streak lines" spreading out from the direction of travel of the storm.

All data was geolocated and is stored in electronic format. A website was created (http://esridev.caps.ua.edu/MooreTornado/MooreTornado.html) and is used to disseminate the team's data and findings as well as to aid future researchers interested in the tornado damage data collected. The team received funding for travel and lodging from the National Science Foundation.

Chapter 1 - May 20th 2013 Moore Oklahoma Tornado Overview

On May 20th, 2013, an Enhanced Fajita (EF) 5 tornado struck the city of Moore, Oklahoma. In addition to over $2 billion in economic loss (NBC News 2013), 24 people were killed and over 350 others were injured. The weather system that produced this tornado formed 95 tornadoes from May 18th to May 20th, 2013. In the afternoon hours of May 20th, a supercell formed that produced the tornado that struck Moore. The tornado traveled 17 miles across rural farmlands and dense urban areas and at its widest the tornado created a 1.3 mile wide swath of destruction. Wind speeds were estimated at a maximum of 210 miles per hour, the highest in that area since the 1999 Bridge Creek-Moore Tornado which registered winds of 317 miles per hour (Weather Underground, 2013).

The National Oceanic and Atmospheric Administration/National Weather Service (NOAA/NWS) Storm Prediction Center issued a weather warning for May 20th stating that the development of supercells was a large risk based on weather conditions (Storm Prediction Center, 2013). At 1:17 a.m. CDT, an update was issued that stated the risk of severe thunderstorm development and a risk of a strong isolated tornado in the region surrounding Interstate 44, which included the Oklahoma City Metropolitan area. Tornado watch 191 was issued at 1:10 p.m. CDT by the Storm Prediction Center for central and eastern areas of Oklahoma and described the threat of a few isolated strong tornadoes in that area. The National Weather Service in Norman, Oklahoma issued a tornado warning for the storm at 2:40 p.m. CDT. The tornado touched down at 2:56 p.m. CDT in Grady County, southwest of Moore and 4.4 miles west of Newcastle, Oklahoma. The tornado stayed on the ground for almost 40 minutes, lifting at 3:35 p.m. CDT 4.8 miles east of Moore. Figure 1.1 shows the radar imagery of the tornado and parent supercell. The National Weather Service and local news stations warned residents to find a safe place such as a basement or storm shelter after the warning was broadcast.

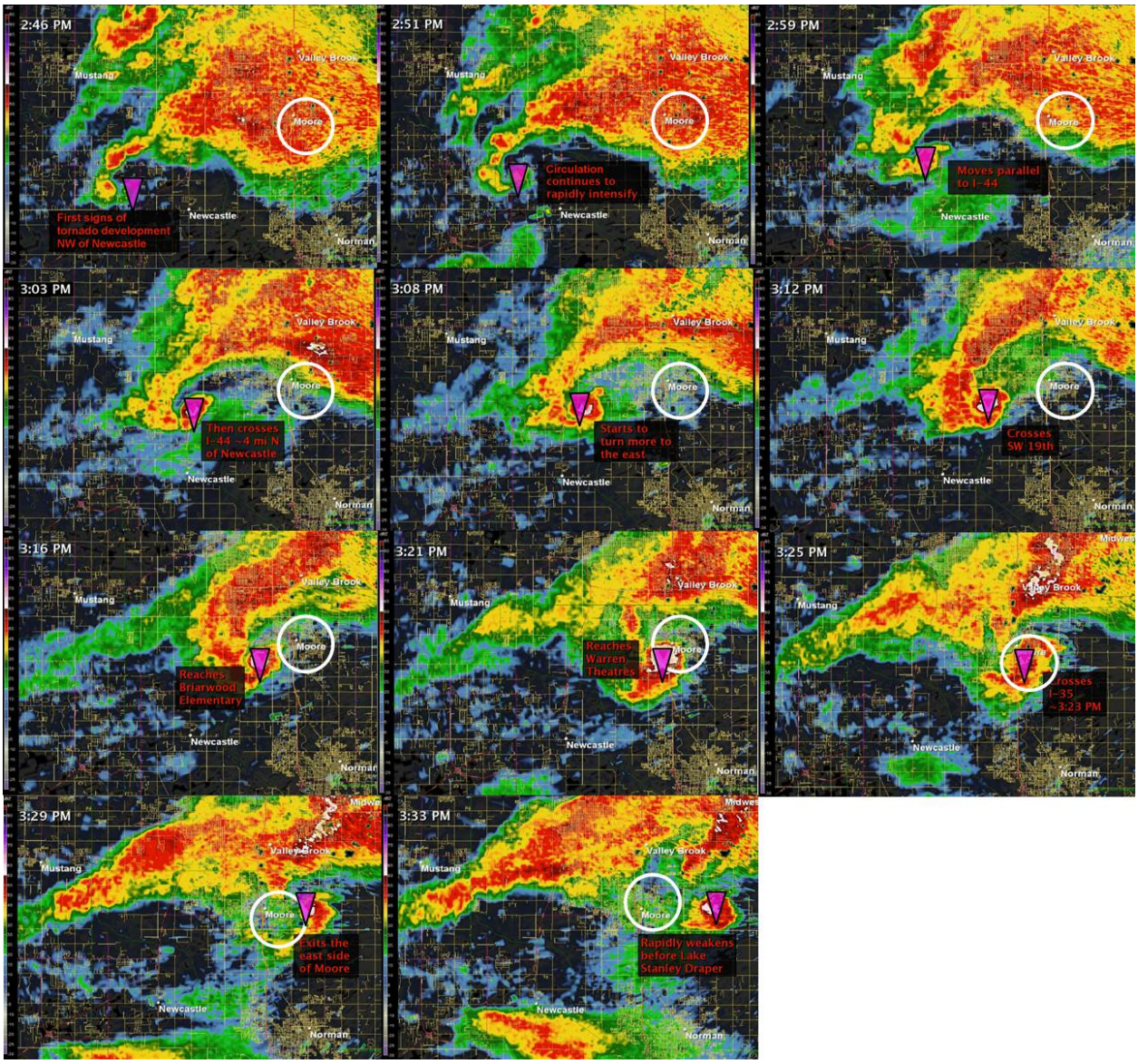

Figure 1.1, Radar imagery of the movement of the Moore, Oklahoma tornado. The pink triangle indicates the location of the tornado, while the white circle indicates Moore (modified from NWS 2013).

Moore has been hit by several large tornadoes in the past two decades, including an F5 tornado on May 3, 1999, an F4 tornado on May 8, 2003, and the EF5 tornado on May 20, 2013. Figure 1.2 shows the approximate paths of these three dangerous tornadoes. The 1999 tornado caused 36 deaths and 295 injuries, and its path was 38 miles long and up to 1 mile wide according to the National Weather Service (National Weather Service, 2013). This was one of the strongest tornadoes to hit a densely populated area and resulted in over $1 billion in property damage and received significant attention from engineers in America (Marshall, 2002; Gardner

et al, 2000; Pan et al, 2002). The May 2013 tornado crossed the path of the 1999 tornado near the intersection of S May Ave and SW 149th St., a rural intersection to the southwest of the residential areas in the city of Moore as shown in Figure 1.2.

Figure 1.2, Map of the paths of the three major tornadoes to hit Moore in the past 15 years with the May 20th, 2013 tornado shown in green (kfor, 2013).

The 2003 tornado caused no deaths, but 45 injuries were reported. The 2003 tornado took a northeast path through Moore. The 2013 tornado came close to the path of the 2003 tornado near the intersection of SW 4th St and N Santa Fe Ave.

The 2013 tornado affected mostly residential and light commercial areas, moving in an east-northeast direction through Moore as shown in Figure 1.2. An overview map of Oklahoma, Cleveland County, and the approximate 2013 tornado path is shown in Figure 1.3. A detailed map of Moore and the study area, along with the extents of the 2013 tornado damage path are shown in Figure 1.4. The major roads affected by the 2013 tornado included Santa Fe Avenue, Telephone Road, Interstate 35, and Eastern Avenue that run in a north-south direction, and 19th

Street and 4th Street running in an east-west direction. A freight line running parallel to Interstate 35 in Moore was also crossed by the tornado path.

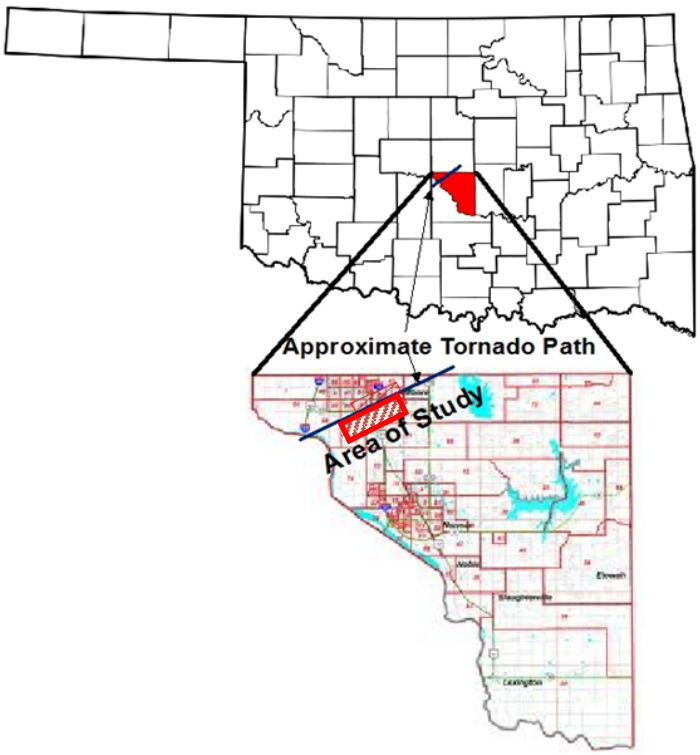

Figure 1.3, Map of Cleveland County, extracted from county map of Oklahoma along with the approximate path of the May 20th tornado shown by the line and the area studied by the research team in the hatched region.

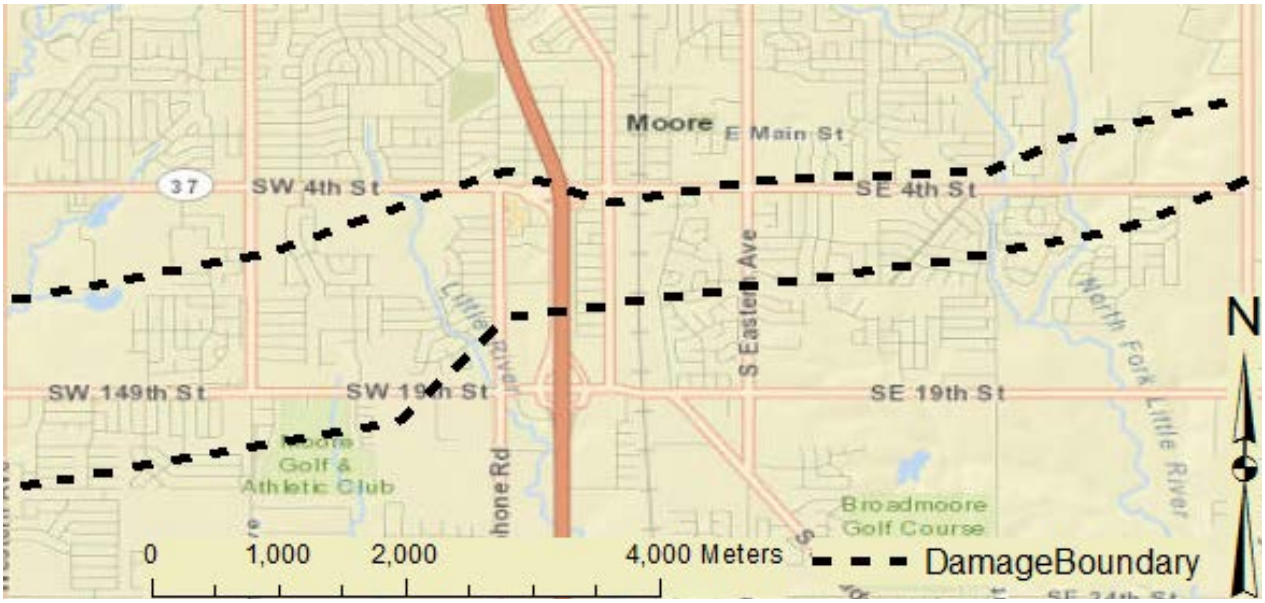

Figure 1.4, View of the Moore, Oklahoma inspection area street map with the damage boundary of the May 20th tornado.

The city of Moore is in Cleveland County. It is in the greater Oklahoma City metropolitan area and has a population of 57,810, making it the seventh largest city in the state of Oklahoma (U.S. Census Bureau, 2010). The May 20th 2013 tornado damaged or destroyed a reported 12,000 homes and 33,000 people were displaced or affected (Tulsa World, 2013). The study area is mostly comprised of single-family neighborhoods of single- and multi-story homes and light commercial structures such as restaurants and strip malls. The local hospital, Moore Medical Center, was in the path of the tornado and acted as a shelter for approximately 100 employees, 30 patients, and between 250 and 300 community members (Norman Transcript, 2013). Plaza Towers Elementary School and Briarwood Elementary School were heavily damaged by the tornado.

The city of Moore consists of around 21,000 housing units. According to the 2010 census, 73% of these units are single family homes. Fewer than one percent of these homes were built before World War II, 16% were built in the 60's, 53% of the homes in Moore were built between 1970 and 1989, and 36% were built since 1990 as shown in Figure 1.5. Most of the houses in Moore have between 4 to 7 rooms, with an average of 3 bedrooms as shown in Figure 1.6.

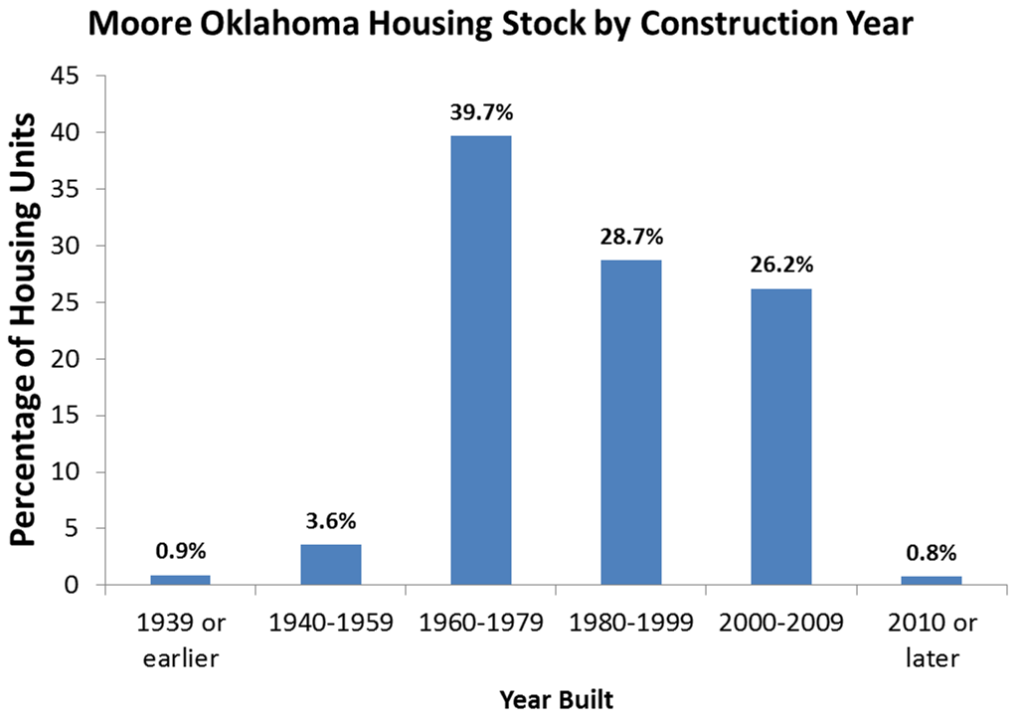

Figure 1.5, Housing unit construction in Moore, Oklahoma based on decade built (U.S. Census Bureau, 2012).

(a)

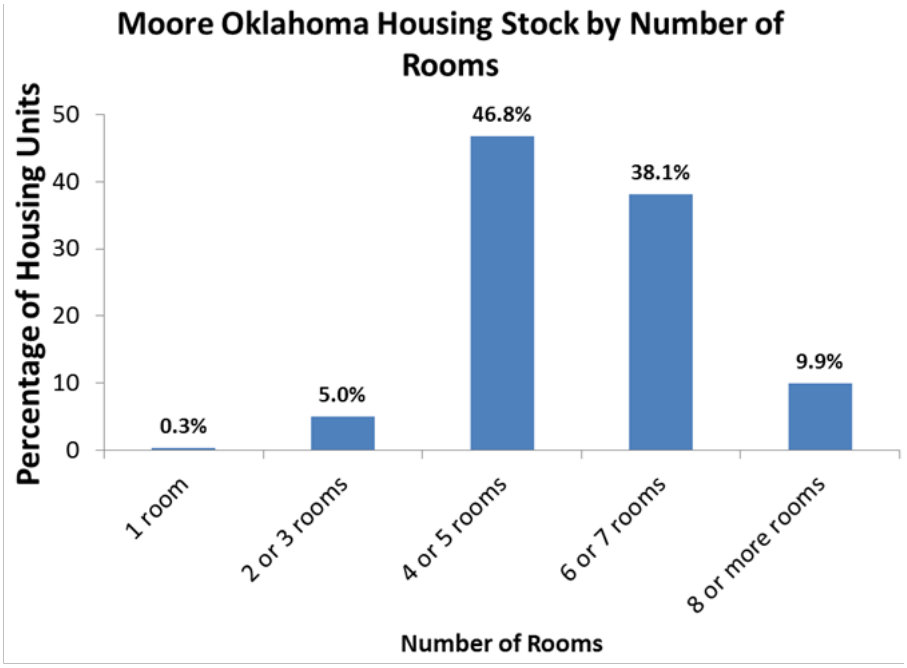

(b)

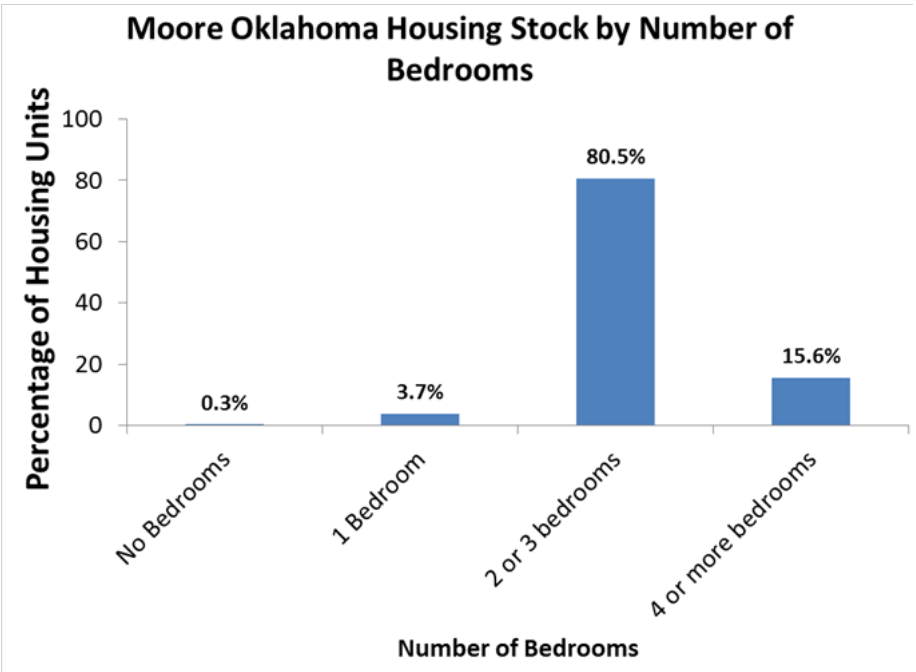

Figure 1.6, Housing stock percentages in Moore based on (a) number of rooms and (b) number of bedrooms (U.S. Census Bureau, 2012).

1.1 Report Organization

This report is divided into seven chapters. Chapter 1 presents an overview of the May 20th, 2013 tornado including the path across the city of Moore as well as a summary of the building stock. A description of the data collection methodology used by the reconnaissance team is presented in Chapter 2. Chapter 3 presents the social science findings from studying the effects of social media on early warning, response, and data collection methods. A study of above and below ground safe rooms inspected in Moore is presented in Chapter 4. Chapter 5 presents how tornado debris modeling was used in Moore. Chapter 6 contains in-depth studies conducted by the reconnaissance team. Chapter 7 provides summary conclusions about the research conducted by the reconnaissance team and how the research can be used to prepare and respond to these disasters going forward.

Chapter 2 - Inspection Methodology

This project investigated and documented damage and failure modes of wood-frame structures, inspected above- and below-ground storm shelters to evaluate performance, and studied the use of social media in the aftermath of the May 20th, 2013 tornado that struck Moore, OK. Data collected for this study included geolocated photographs, information for in-depth studies, aerial basemaps of the inspection area from before and after the tornado, and ground-based Light Detection and Ranging (LiDAR) scans. Typically, this data was collected along transects that crossed the tornado path perpendicularly. In addition to data that was actively collected by team members in the field, data was collected passively in the background throughout this investigation. Passively collected data consisted of vehicle-based photographs, Global Position System (GPS) tracks, and photographs that were mined from Twitter and geotagged within the study area.

The study employed a data fusion method based on time and space synchronization. The information gathered was temporal as well as spatial. Photographs were taken through instantaneous sensing, and GPS tracks were taken over time. A method to link these two types of data was employed. Using Geographic Information System (GIS) technology, the time and date of the collected photographs were correlated with the spatial location of the GPS unit at that same time, which allows for the data to be mapped to the location where the photograph was taken. This robust spatial-temporal dataset can be viewed, accessed, and downloaded from the internet.

2.1 Data Collection Methodology

Field data collection activities were conducted from May 27 through May 29, 2013, with extra data being collected in the following days and months by local members of the inspection team. The evening before field data collections activities began, the damage assessment team assembled and discussed the objectives of the study and planed the overall reconnaissance strategy. Key items of interest to be documented by all team members were described and discussed. These items included: building scale Enhanced Fujita (EF) damage rating, storm shelters, shear walls, hurricane clips and straps, identifiable debris displacement, and impacted

storm water infrastructure. Having all team members collect all items of interest produced a very robust dataset in the limited time spent in the field.

Daily data collection activities included synchronizing time kept on the GPS units and time kept on digital cameras, collecting photographs for EF scale damage ratings, visiting sites of above- and below-ground storm shelters, and collecting photos of other items of interest. Every night the team gathered to compile, geolocate, and rate photographs. GIS maps were created each night that showed areas that were inspected. These maps were used to plan the next day's inspection activities. In these planning meetings, the team also decided upon special-interest locations to perform detailed studies. Mined photos from Twitter were also located on GIS maps and used as points of interest to visit.

During field data collection each day, the damage assessment team would divide into groups of 4 or 5 members, and walk transects that ran roughly perpendicular to the path of the tornado, starting and ending in areas where no damage was visible. This yielded multiple paths across the tornado damage area and showed different damage widths and gradients. Team members who had an iPhone were able to track each other's location in the field by using the Find Your Friends application. A screen shot of the application being used in Moore is shown in Figure 2.1.

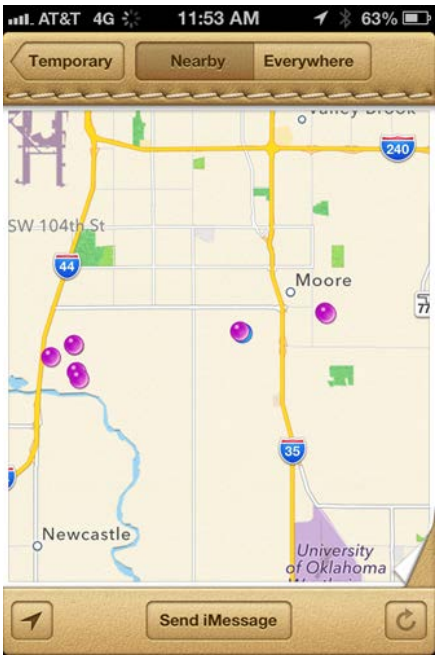

Figure 2.1 Screenshot of the Find Your Friends iPhone application used by the damage assessment team in Moore.

The main study area for the inspection team was a five-mile long section of the tornado path in Moore reaching from Western Avenue on the west to Sunnylane Road on the east. GPS units recorded the movements of team groups within the study area each day. Figure 2.2 shows the damage path created by the tornado as well as the tracks from the GPS units. Tracks from the first day (05-27-2013) are shown in blue, tracks from the second day are shown in red, and tracks from the third day are shown in green on Figure 2.2.

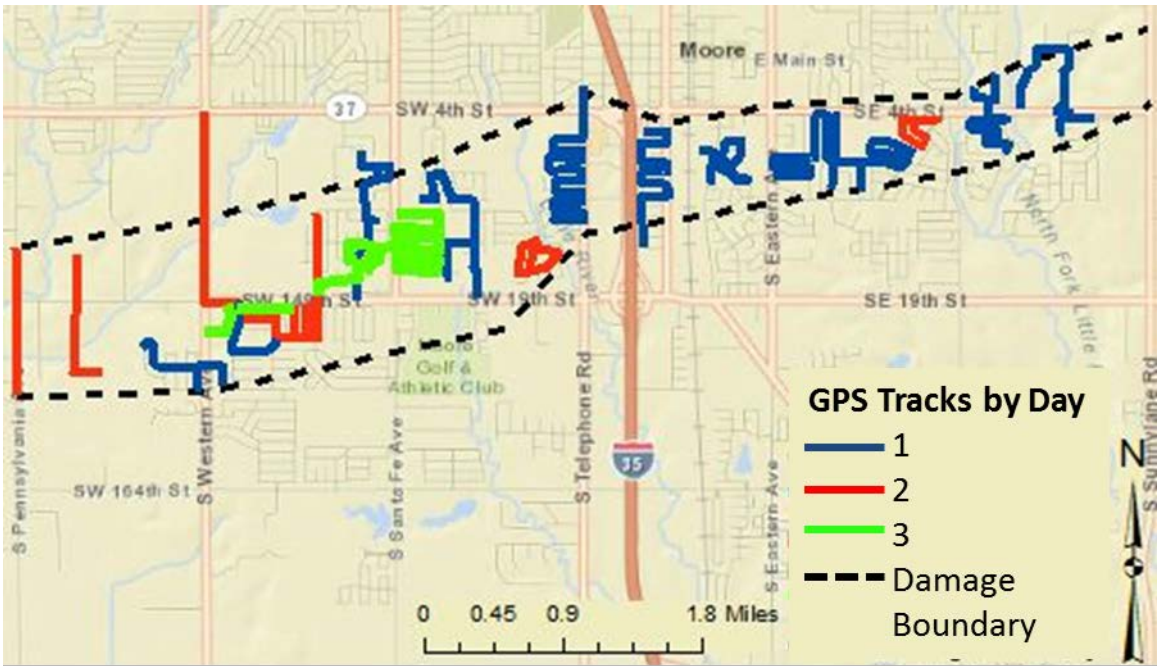

Figure 2.2, Map showing locations of all tracks where pictures were taken during the Moore Tornado study.

Cameras and GPS units were synchronized each morning by taking a picture of the GPS unit screen showing satellite time. This allowed for the time difference between each camera and GPS unit to be calculated. Using custom software developed at The University of Alabama called Time-Image Positioning Software (TIPS), a data file was created which correlated the location of every photo taken to a position in a GPS track. This data file was uploaded to a GIS software package, which showed the locations of each photo on a basemap of Moore. Pictures taken with smart phones or on GPS enabled cameras did not need to be correlated with a GPS track. These photos have the location automatically embedded in the metadata of the photo. These photos were also added to the GIS map. All pictures were hyperlinked to photo locations. Hyperlinking of photos allows for a photo to be viewed by selecting a location on the GIS map.

Photograph analysis took place each evening when the team returned from data collection activities. The reconnaissance team was divided into two member groups and given a copy of the Enhanced Fujita Scale document developed by Texas Tech University (Texas Tech, 2006) along with photographs taken by different team members. A spreadsheet was also provided with the name of each photograph, the latitude and longitude location of each photo, and columns to record damage ratings and items of interest in the photograph. Using the EF scale document as a guide, each group looked at photographs and rated the degree of damage of a building. Only one photo of each building was rated. This methodology was used by inspection teams following the Tuscaloosa and Joplin tornadoes in the summer of 2011.

As photographs were analyzed for building damage, items of interest were noted as an attribute to the photo. An "Item" column in the spreadsheet that would receive a number if the picture contained an item of interest: (1) storm shelter, (2) impacted stormwater infrastructure, (3) building connections, (4) shear wall, or (5) other interesting items. By coding the photographs with items of interest researcher can quickly query the database and locate information that pertains to specific research objectives.

After all photographs were analyzed, individual spreadsheets were combined and the end result was a single spreadsheet that contained columns for photograph name, latitude, longitude, degree of damage, item, photographer, date, and EF rating. The EF rating came from a correlation between the degree of damage expected wind speed and the EF wind speed. Each degree of damage is given an upper and lower boundary wind speed, as well as an expected wind speed. EF ratings are based on an upper and lower wind speed. The inspection team used a correlation between the expected wind speed of the degree of damage and the range of wind speeds given by the EF scale.

Additional ground level damage photos and low-oblique aerial photos of the damaged area were found on the FEMA website (FEMA, 2013). FEMA ground level damage photos were used in areas where the inspection team did not collect photographs. The photos were downloaded from the FEMA website and the same approach used to rate team member photos was used to rate FEMA photos. Although FEMA ground level photos were employed in the analysis and for contouring of wind speeds, a separate layer in the GIS map was created to display the FEMA ground level photos.

FEMA low aerial oblique photos were also downloaded, located on the GIS map, and used by the team. Arrows were added to the low-oblique photograph location to show the direction the camera was pointing when the picture was taken.

2.2 Field Equipment

Data collected in the field were captured using GPS units, digital cameras, smart phone cameras, and a ground-based Light Detecting And Ranging (LiDAR) laser scanner, as well as field measurements, sketches, and text descriptions of damage. GPS data was collected using Delorme GPS units including a PN-20, 2 PN-40s, and a PN-60. Smart phones and GPS digital cameras also captured GPS location as well as photos. The location accuracy of the units varied depending on unit, satellite orientation, and obstructions between satellites and units. The Delorme units were typically accurate within 10 m, as were the GPS cameras. The smart phones ranged in accuracy from 10 m to approximately 100 meters. Delorme GPS data was converted from the proprietary data storage method into a standard Geographic Exchange (GPX) format in order for the Time Image Positioning software to read the data. Photographs taken by the inspection team using digital cameras and smart phones were stored in a JPG format.

2.3 Field Data Collection Locations

Over 3000 photos were collected, cataloged, and geolocated as part of this data reconnaissance effort in the aftermath of the May 20th, 2013 tornado that struck Moore, OK. When the photograph rating process was complete, all photographs were mapped using the GPS tracks, the TIP program, or by using the embedded metadata from the smart phones and GPS cameras. Figure 2.3 shows the locations of all geo-tagged photographs.

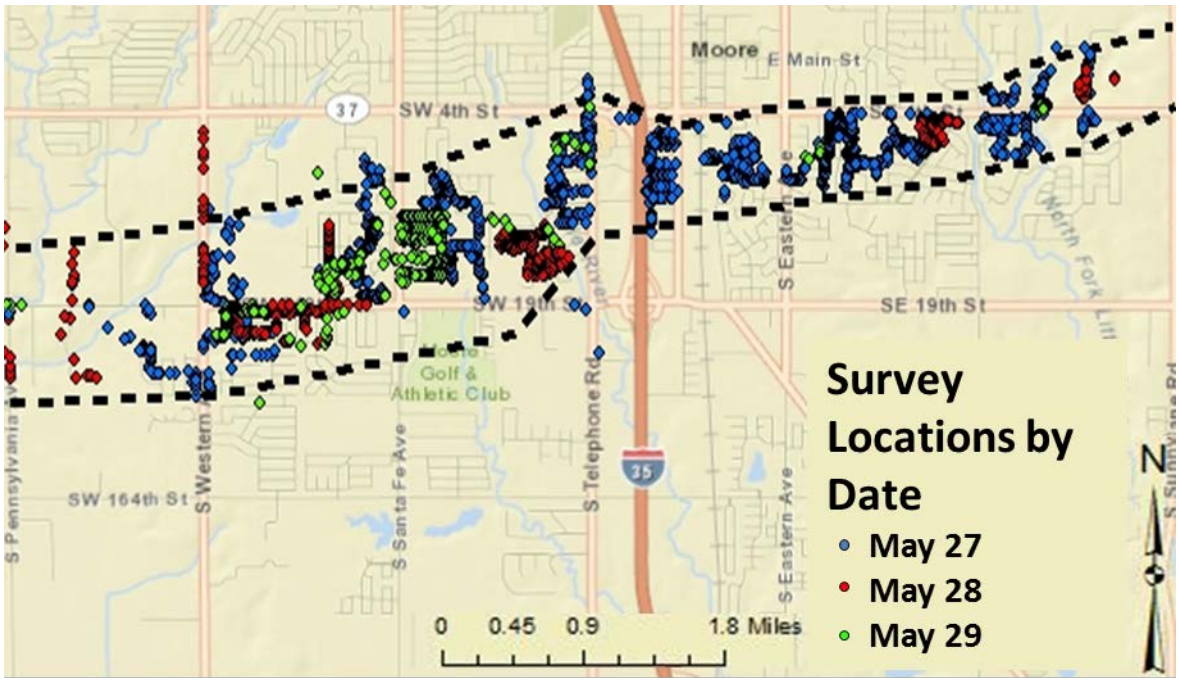

Figure 2.3, Map showing all geo-located photos colored by the day the pictures were taken.

Figure 2.4 shows a map with photos distinguished by EF rating. Degree of damage for the residential sectors of Moore ranged from no damage to EF4 level winds. As would be expected, the higher EF ratings are observed nearer to the center of the damage path and lower ratings are observed farther away from the center of the path. A damage contour map was created in GIS by interpolating between the EF-rated photos. The contour map of EF rating is shown in Figure 2.5. Table 2.1 provides the area of each EF rating as well as the percentage of damage that the EF rating represents.

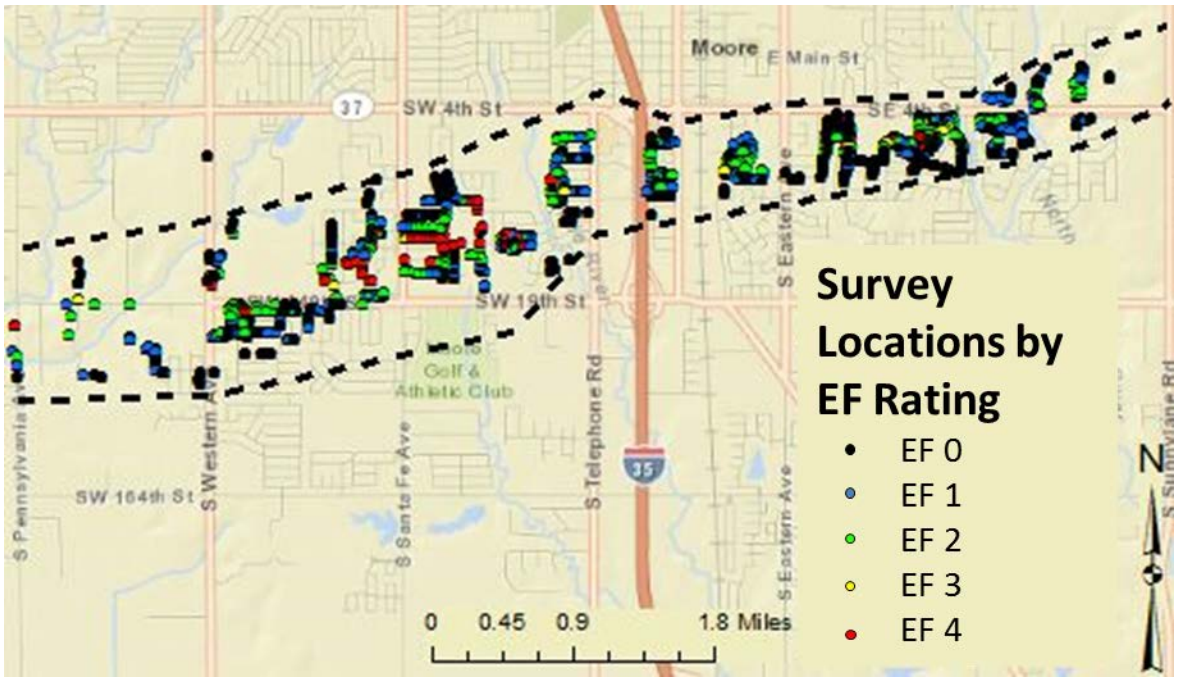

Figure 2.4, Map showing the EF rated photographs taken in Moore.

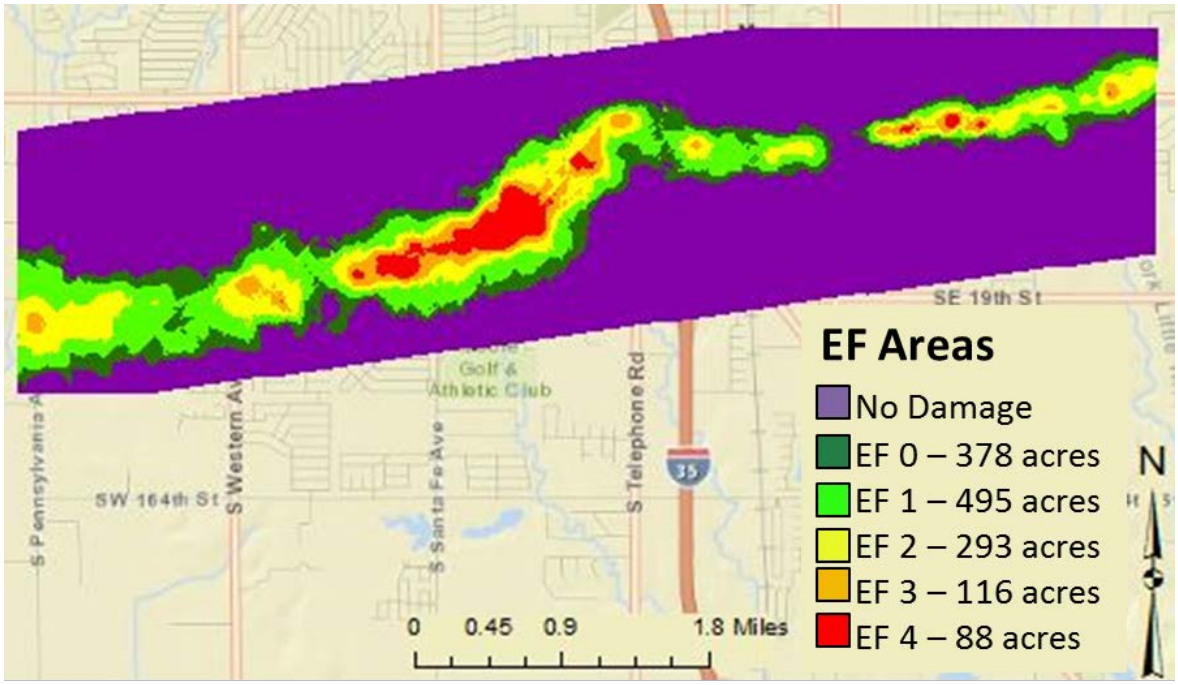

Figure 2.5, Contour map of EF wind speeds based on observed building damage.

It should be noted that the maximum expected wind speed for One- and Two- Family Residencies for a degree of damage rating of 10 "Destruction of engineered and/or well-constructed residence; slab swept clean" is 200 mph. An EF5 rating is over 200 mph; therefore,

by evaluating only wood framed constructed buildings in this study, an EF4 rating is the maximum rated photo and contour that can be achieved as shown on Figures 2.4 and 2.5.

Table 1.1, Areas and percentages of EF ratings in the inspection area.

EF Rating	Area (Acres)	Percentage
EF0	378	27.6%
EF1	495	36.1%
EF2	293	21.4%
EF3	116	8.5%
EF4	88	6.4%
Total	1370	

2.4 GIS-Based Interactive Web Map

The interactive web map containing the geo-located photographs taken while in Moore can be viewed at http://esridev.caps.ua.edu/MooreTornado/MooreTornado. In addition to the photographs, the web map also contains pre-and post-tornado aerial images, filters which allow the user to view photographs in categories such as storm shelter or crowd sourcing, the tornado contour map, and low aerial oblique photographs obtained from FEMA at the website http://fema.maps.arcgis.com/home/webmap/viewer.html.

2.5 3D Data Collection with Laser Scanning Technology

Terrestrial laser scanning technology was also employed for damage data collection. Terrestrial laser scanning is a robust technology used to collect 3D data with high precision and resolution. The position (x,y,z) of millions of points in a space are identified by a scanner through the reflection of a laser beam. The points are then reproduced to make a 3D virtual scene known as a point cloud. Some scanners include a built-in camera that allows the superposition of the true color to each point of the collected point cloud. Terrestrial scanners can produce dense point clouds in which the distances between measured points can be less than 5 centimeters. A 3D point cloud of damaged areas in the aftermath of a tornado enables remote engineers to virtually inspect damaged buildings. The rich and precise 3D information provided by scanners can potentially allow engineers to return to the virtual damage scene later for further investigations without missing perishable evidence.

Point cloud data was collected by a stationary scanner from two areas with two different scanning settings. Figure 2.6 shows the location of the scanned areas along the tornado path. The first dataset was collected from Eastmoore Ct area enclosed by a red rectangle, which includes several rows of buildings. In this area, the scanner was moved to several locations including both in the front yard and back yard of the buildings. Also, the built-in camera of the scanner was used to take panoramic images. The second dataset was collected from South Bouziden Dr, enclosed by a blue rectangle shown in Figure 2.6. In this area the scanner was used to scan the site from several locations but only on the street centerline. This scanning setting was selected to simulate scanning with mobile scanners that are mounted on vehicles. In addition, the built-in camera was not used in the second scenario. Therefore, data collection in this area was faster and easier, though the collected point cloud dataset includes neither the back side of buildings nor the true color.

Once captured in the field, the collected data was pre-processed using point cloud processing software and prepared for virtual damage analysis. Common points in separate scans such as roof or wall corners were identified and used to register individual scans together and

Figure 2.6, Location of the scanned areas along the tornado path

produce a complete 3D point cloud of the two sites. The panoramic images were employed to superimpose the true color to the first point cloud dataset. Animations that show the two 3D point cloud datasets are accessible at the project GIS website (http://esridev.caps.ua.edu/MooreTornado/MooreTornado.html). The point cloud datasets were also imported and geo-referenced into the GIS database as an additional layer of data.

2.6 Virtual Damage Investigation

Generated 3D point clouds of the damaged areas were employed to virtually investigate damage of buildings. The 3D nature of the scenes allows the investigator to navigate through the 3D scene, rotate or move the point of view, zoom in, or zoom out. This helps to properly understand the overall condition of the site and identify the location of the tornado path. Figure 2.7 illustrates a cross section of the second point cloud, which shows the damaged buildings on the west side of Bouziden Drive. The figure shows that damage gradually increases from the low damage at either end of the scan (south and north) to the total destruction at the center where the tornado has passed.

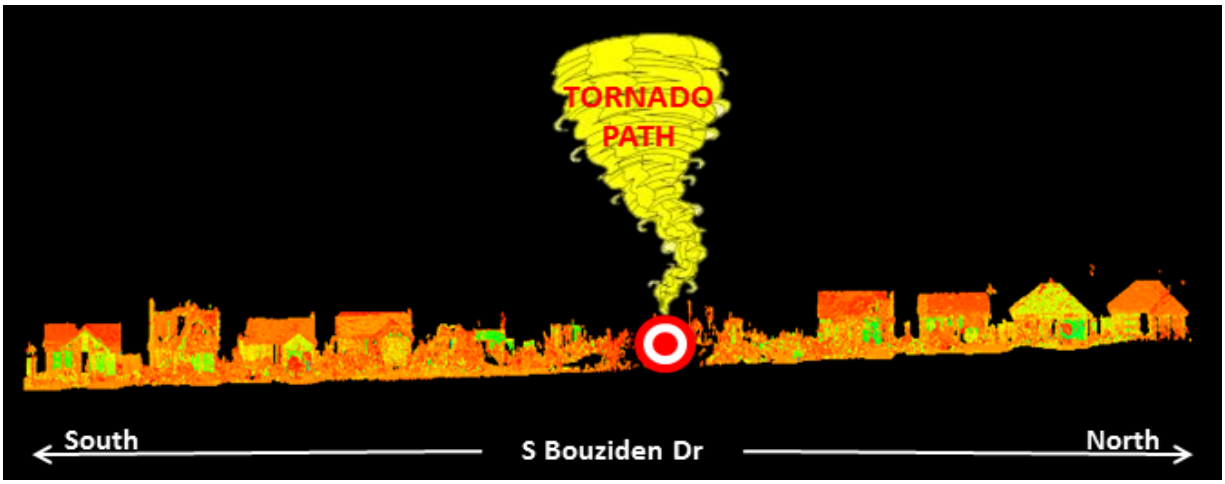

Figure 2.7, Point cloud of damaged buildings at west side of the Bouziden Drive and the tornado path.

Damage of individual buildings at the two sites was also virtually investigated and rated. To meet this goal a list of wind damage metrics was prepared based on wind damage descriptions of the Enhanced Fujita (EF) scale. Damage metrics included loss of roof or wall covering, broken glass of windows, failure of garage doors or walls, uplift of roof decks, failure of large section of roofs, failure of exterior or interior walls, and slab swept clean. The point

cloud of each building was investigated to detect those damage metrics. Figure 2.8 shows point clouds of three buildings and some detected wind damage metrics. Once the damage of each building was analyzed, an EF rate was assigned to the building based on the EF scale. Figure 2.9 and Figure 2.10 show the aerial view of damaged areas and results of the EF rating. Table A1 in the appendix presents the detailed results of the damage assessment and EF ratings for all individual buildings.

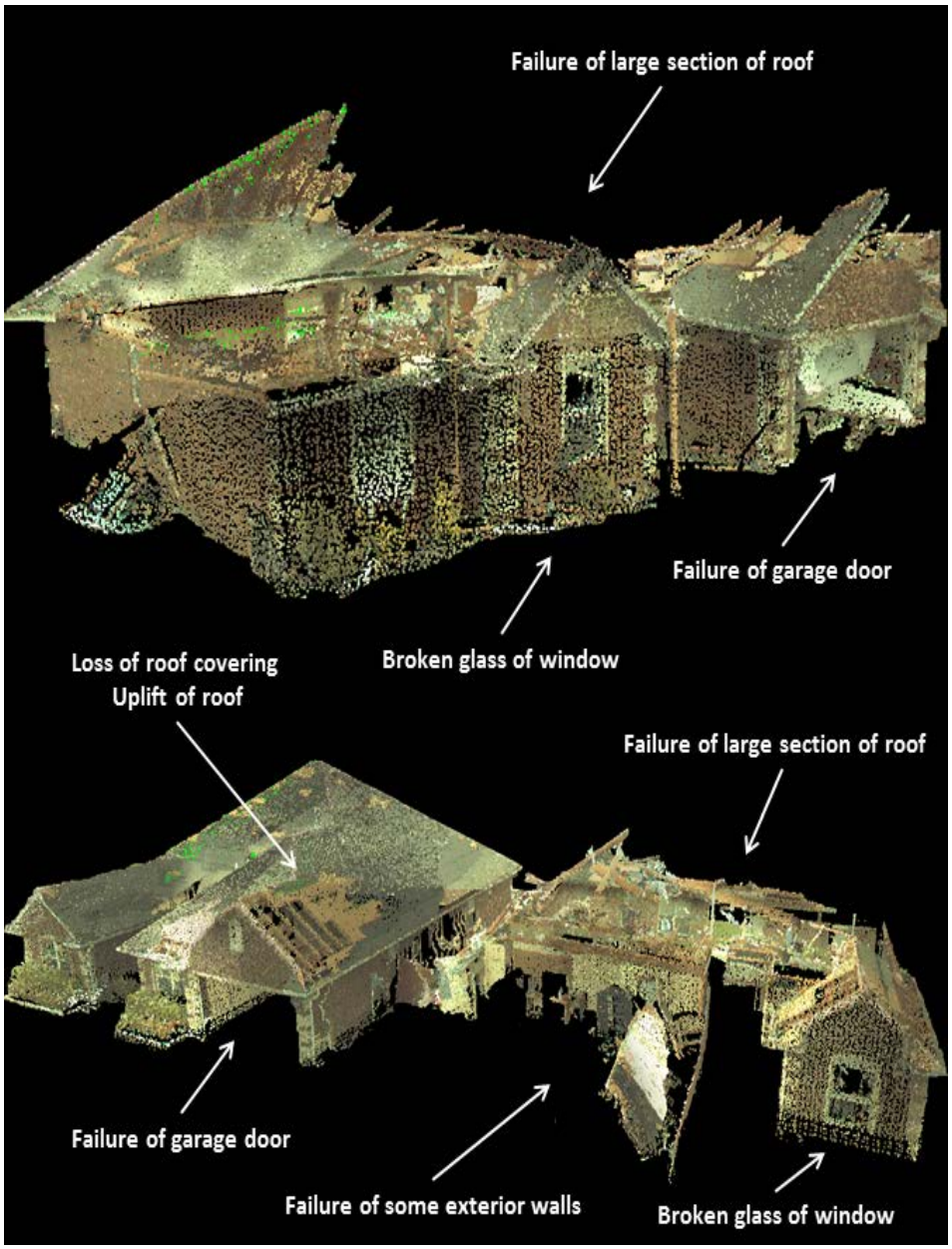

Figure 2.8, Point cloud of three damaged buildings and detected wind damage metrics.

Figure 2.9, Aerial images and EF rates of the area #1: (a) pre-tornado image and building IDs; (b) post-tornado image and EF rates.

Figure 2.10, Aerial images and EF rates of the area #2: (a) pre-tornado image and building IDs; (b) post-tornado image and EF rates.

2.7 Automated Damage assessment

Collected point clouds were used to test and validate the automated damage assessment tool developed by Kashani et al. (2013). This tool incorporates the 3D point cloud of damaged areas with pre-tornado aerial images and automatically identifies and compares pre- and post-tornado shapes of roofs and walls to quantify building damage. Figure 2.11 illustrates the roof and wall surfaces identified by the tool for the point cloud of buildings number 6 - 15 shown in Figure 2.9(a). Building number 11, shown with hatch area in Figure 2.9, had been cleaned up before the data collection. Therefore, the GIS tool did not identify any roof or wall surfaces associated with building 11.

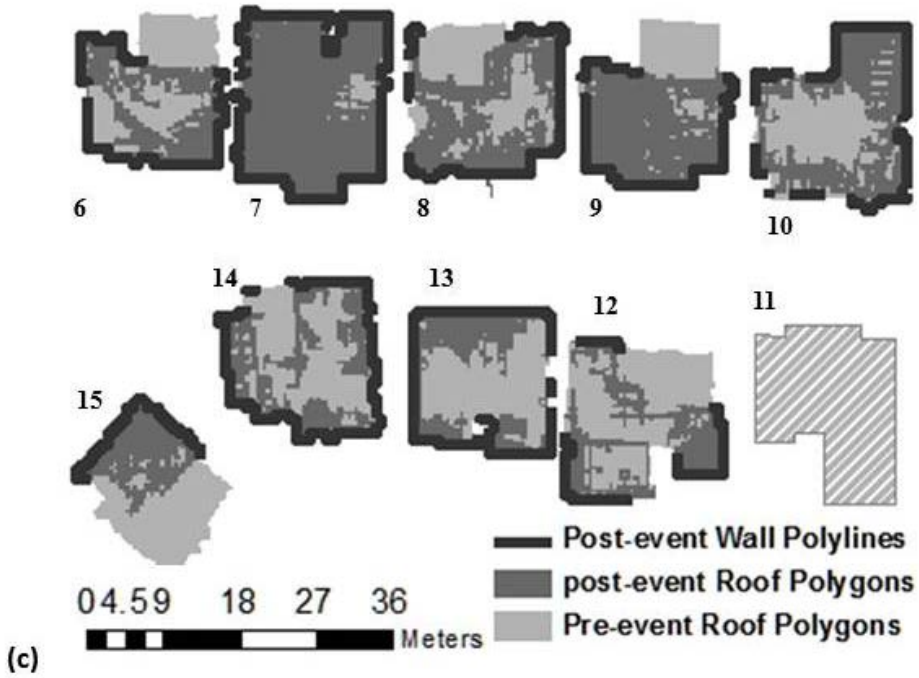

Figure 2.11, generated roof polygons and wall polylines with the GIS tool developed by Kashani et al. (2013).

2.8 Inspection Methodology Conclusions

The data collection methodology employed in this study successfully collected, geolocated, analyzed, and displayed information related to the May 20th 2013 Moore OK tornado. Techniques that were introduced and employed in past tornado events were again used to collect a robust data set that is available on the internet at http://esridev.caps.ua.edu/MooreTornado/MooreTornado. In addition, study specific attribute information such as storm shelters, shear walls, storm water infrastructure, etc. was collected and cataloged to enhance the

value of this data set. Mined social media data in the form of geolocated photos were also included in this study and used to locate features such as storm shelters within the damage extents.

This study also indicated that laser scanning technology can be used to preserve perishable damage data and perform virtual damage assessment and EF rating in the aftermath of tornadoes. In addition, the scanning of damaged buildings from the street without taking panoramic photos is an efficient way to collect 3D data for EF rating. Panoramic photos and back yard scans can improve the visual quality of the collected point cloud, however these datasets are not necessary for EF rating. Employing a mobile scanner mounted on a vehicle can speed up and facilitate the data collection procedure. This study also indicated the potential of laser scanning technology for automated damage assessment.

Chapter 3 - Social Media Data Mining

Engagement of society through social media is a key component of this research. Passively mining social media provided many spatially located photos that were used to direct the field data collection activities. Actively tweeting after the tornado and asking for engineering items of interest such as storm shelters, safe rooms, and homes built after 1999 allowed the research team to engage citizen sensors in the data collection process. These activities utilize citizens as sensors and promoted thought and discussion about infrastructure in relationship to tornado preparedness. Having social scientists on the team, allowed for new and creative ways to educate society. Utilizing social media to tweet information after this study will also educate society about improved building practice for tornado resiliency.

3.1 Mechanics of Mining Social Data

For this study, social science researchers were tasked with providing social media data to the on-site team to augment on-site visual documentation and to provide coordinates for specific types of visual data collection. Two types of data collections were undertaken, passive and active social media data collection.

3.2 Passive Social Media Data Collection

In passive social media data collection, messages from the Moore, Oklahoma area were collected via Twitter, a micro-blogging social media network. A software system developed by the Social Science Research Center at Mississippi State University, the Social Media Tracking and Analysis System (SMTAS) was used to collect the data. The social media team collected geo-located tweets from May 21 to May 29. Figure 3.1 shows the daily volume of tweets captured in Moore during this period.

Figure 3.1, The Daily Data Volume of Tweets, 5-21-13 to 5-19-13.

The data collection plan used an 11 miles x5 miles (55 square mile) sized bounding box along the tornado path to spatially filter tweets. The total number of geo-located tweets from the bounding box was 5022 tweets. Tweets were a primary form of communication in the early days of the event as cell communication was turned off and reserved for first responders. Texts and tweets were still working. These tweets were analyzed for relevant images and 157 tweets were sent to the engineering team. Figure 3.2 shows a map of tweets from the Moore area.

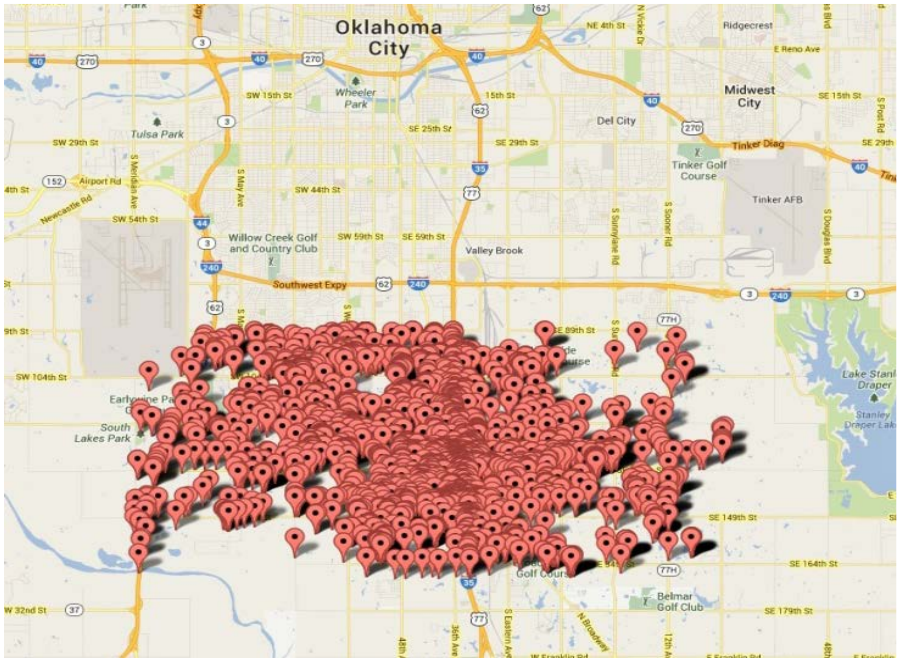

Figure 3.2, Map of Tweets from Moore, OK

The engineers used the images to find the exact coordinates of specific types of damage and the locations of storm shelters while on-site in Moore. With these images, the engineers taking pictures of locations were able to document the amount of clean up that had occurred between when the time the image appeared on Twitter and when the team reached the site. The Twitter images collected were also used in combination with the on-site images to develop the online interactive map of the damage locations.

Also, the social media team was able to match selected images of the structures with existing images of Google Street View prior to the tornado to observe different time points relevant to the damage. This provided structural images shortly after the tornado and from engineers doing their assessments. This level of documentation allowed the engineers to more accurately and comprehensively interpret the impacts of the event. This proved to be a successful and cost-efficient way to collect and expand visual documentation. Figure 3.3 shows comparison images.

Figure 3.3, Comparison of damaged home (a) pre- and (b) post-demolition

3.3 Active Social Media Data Collection

The social media team used the passive data collection phase to identify Twitter users frequently posting images from the Moore area. The team contacted these Twitter users to request specific types of visual documentation, such as the location of storm shelters and to also have them request their followers to send their tweet images. These images were sent with GPS coordinates to the on-site engineering team for investigation. This allowed for collection of data to document social barriers to home hardening, safe rooms, and storm shelters. By asking for images of particular types of damage, safe rooms, and storm shelters, the engineering team was able to collect enough field data to draw conclusions about how well homes were built, and how well safe rooms and different types of storm shelters withstood the storm.

During this process, the social media team was able to identify the types of individuals most likely to assist with data collection. News reporters documenting the event and storm chasers were the most willing to assist in providing information requested. See Figure 3.4 obtained through the active social media data collection.

Figure 3.4, Picture of local shelter obtained from active social media data collection.

3.4 Social Media Conclusions

The use of social media analysis in this study demonstrated the capacity to track social media at a potential storm site as soon as the National Weather Service releases warnings. This tracking can continue during and after the storm. Using geo-located tweets within the boundary areas of a storm will allow real-time data collection of damage locations. This permits actual damage assessment personnel, such as the National Weather Service, to locate damage locations immediately. Having the image immediately permits locating the damage more easily, and also helps determine if the location has been modified by the time research and damage assessment personnel reach the location.

Active social media data collection has much potential. This study indicates that volunteer groups are a likely group to help determine damage locations and send tweets. However, it was quickly learned that volunteer groups are there to volunteer and they do not have much interest in tweeting about damage. The social media team analyzed the senders of the passive tweets to determine other groups that might be more likely to assist. News reporters and storm chasers were obtaining and disseminating the most images. When they were approached for assistance, they were more than willing to share their tweets and images, as well as to disseminate the request to their followers, which grew the tweet count and images. This led to the conclusion that for future studies, citizen sensor requests should be directed to and disseminated through news reporters and storm chasers, as well as other "experts" on damage imaging. Such groups include structural engineers, professional photographers, amateur/ham radio operators, and storm spotters.

The use of social media in research of this nature will allow the public and particular expert groups within the public to serve as citizen sensors in the research process. In essence, the public can have a useful purpose in their social media activities relative to a severe weather disaster. This will allow researchers to begin collecting data immediately and to be able to geo-locate that data for field work. Social media will also reduce the time and resources needed by the field team to locate the work themselves when they arrive at the location. They can mobilize with a plan to reach particular locations quickly. Once on the scene, researchers can use active social media solicitations to obtain more images and information about items of interest. The

research team is essentially expanding the number of “boots on the ground” with the inclusion of the citizen sensors.

Another benefit of the citizen sensor data collection methodology is that researchers can also immediately share this data with other researchers and disaster response professionals who also need this time sensitive data. Response and recovery teams, weather service personnel, utility crews, and even volunteer groups can use this data to direct their efforts more efficiently.

Future studies will be able to explore the use of citizen sensors with the inclusion of more “expert” users to provide specific images and information. As this network grows, the intent is to also conduct studies where the “expert” citizen sensors have been pre-identified and already know their role in the research process. They can begin the data collection and dissemination process immediately. This will be relatively easy to do with storm chasers who are already in proximity to severe weather situations. Other “expert” citizens can be pre-identified in storm prone regions and they can also start their work immediately when an event occurs in their region. This will allow for more immediate data collection and also collection of data that these expert citizen sensors know is needed by the various end-users.

These citizen sensor social media networks that are grown with the continuation of citizen sensor inclusion will also permit the dissemination of knowledge back to the public about the outcomes of the research. Through social media, the public will become more aware of the types of research being done, what the issues are, what is being learned, and how this knowledge might serve them. In future studies, the dissemination of research outcomes through the citizen sensor networks will be tested and evaluated.

Chapter 4 - Residential Shelter Performance

One goal of the research team was to study the effects of any building practice changes in the city of Moore, especially because of the recent occurrence of violent tornadoes. One facet of this investigation focused solely on residential shelter availability and performance. In the 2011 tornadoes that hit Tuscaloosa, Alabama and Joplin, Missouri, residential shelters were not commonly observed, so there was an opportunity to assess whether this trend held true in Moore, especially given the city's recent history of tornadoes.

It is promising to note that at the time of the tornado, the city of Moore had 3,236 registered residential shelters (City of Moore, 2013). The locations of the registered residential shelters were obtained by the team after the damage survey and are shown in Figure 4.1 along with the locations of shelters observed by the team in the field and the damage boundary. According to the 2010 U.S. Census, there are 20,446 housing units in Moore. Based on the number of registered shelters, this would imply that approximately 16% of residential housing units have a shelter. This is an increase in the number of residential shelters observed in the aftermath of the 1999 F5 tornado when teams documented approximately 5-10% individual residential shelters (Gardner, 2000; Marshall, 2002).

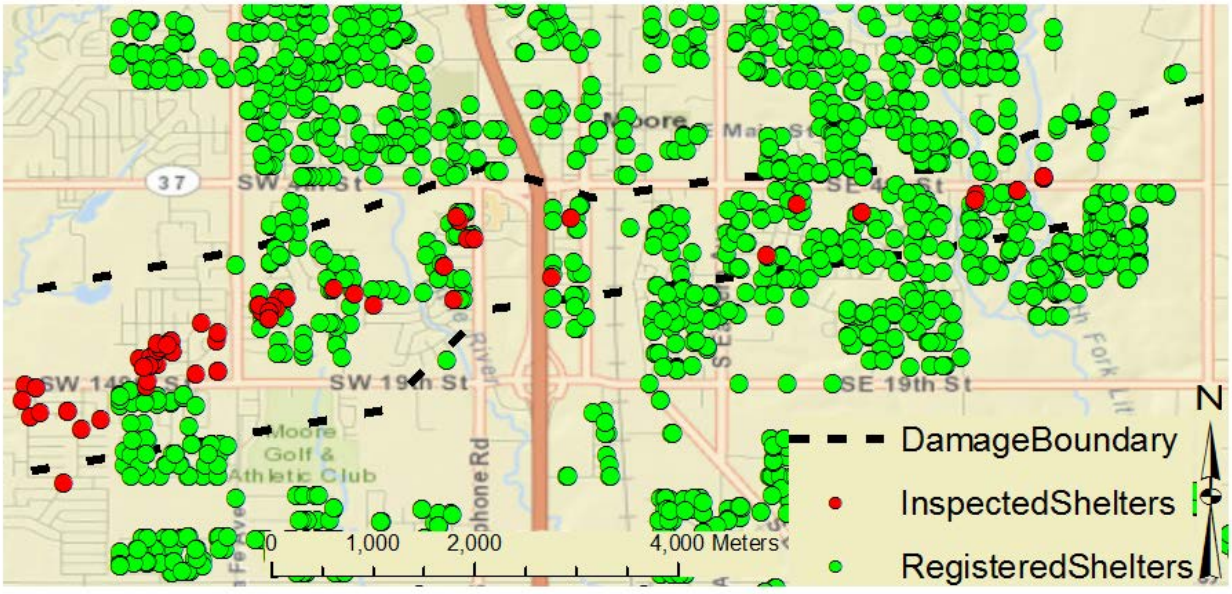

Figure 4.1, Locations of all registered and observed residential shelters in Moore city limits with the tornado path indicated by black dashes.

4.1 General Storm Shelter Observations

The term 'residential shelter' in this report has been used as a generic term to describe hardened locations where people took shelter from the storm. However, care is taken to differentiate between safe rooms, storm shelters, refuges, and safe spots. A safe room is classified as a hardened room built according to FEMA 320 design guidelines. The majority of the designs are above ground (FEMA, 2008). Secondly, a storm shelter is defined as a location either above or below ground which is approved and tested by the National Storm Shelter Association (NSSA), but not built to a FEMA recommended design. The majority of residential shelters observed are classified as storm shelters. In addition, a refuge describes a hardened room not built to FEMA guidelines, nor tested by the NSSA, and is often homemade. Finally, a safe spot is a non-hardened room in the interior of a home, typically a closet or bathroom. Table 4.1 provides a summary of these definitions. Furthermore, in this work, consistent with Federal Emergency Management Agency (FEMA) definitions, perforation occurs when projectiles breach exterior walls and are able to enter the residential shelter. Penetration is defined as damage to the exterior surface of the residential shelter walls without any perforation occurring (FEMA, 2008).

Table 4.1, Residential shelter classification.

Classification	Definition
Residential Shelter	Generic term to describe items below
Safe Room	Built according to FEMA 320 design guidelines
Storm Shelter	Approved and tested by NSSA, but does not fall under a FEMA recommended design
Refuge	Hardened room not built to FEMA design guidelines nor tested by NSSA
Safe Spot	Non-hardened interior room of a home

Of the 75 residential shelters observed by the assessment team in the damaged area, only 7 were above ground. The team relied on being able to observe the residential shelters from outside the home, thus, in some cases, shelters may have been present in a home, but were not immediately obvious from the outside and could not be documented. A total of 68 below ground

residential shelters were documented by the team with the majority referred to as prefabricated concrete or garage slab storm shelters.

There were 29 documented prefabricated concrete storm shelters within the damage path. These shelters were partially raised from the ground (~1/3 of the total height) and had the majority of the above ground portion covered with soil and vegetation. A steel door and ventilation spout were on the exposed concrete roof. A photo of a prefabricated concrete shelter is shown in Figure 4.2. Since these shelters were found outside homes, the assessment teams documented many instances where the owners would leave the shelter unlocked and open for neighbors to use in case of an emergency as described in more detail below. The second most common type of storm shelters observed were cut into the garage floor slab. There were over 25 garage floor shelters seen during the damage surveys with two door types: a sliding door and a hinged door. An example of a sliding door garage floor shelter is shown in Figure 4.3 which illustrates that this type of shelter was designed so a car could drive over them to preserve garage space. This type of storm shelter is a quick retrofit to an existing home, requiring approximately 12-15 hours to install, and allows occupants to enter the shelter without having to go outside into the elements. Although typically positioned behind a parking space, a car may have to be moved before occupants are able to enter.

Figure 4.2, Example of a prefabricated concrete storm shelter.

Figure 4.3, Example of a garage slab storm shelter.

While the majority of the garage slab shelters performed very well, there were some issues observed with these shelters. The first was that garage doors and attached garages often fail first during a tornado event (Marshall, 2002). In these instances, large objects and debris can block the doors of garage slab storm shelters. Figure 4.4 illustrates a garage slab storm shelter that was covered by debris after the garage and house collapsed. It should be noted that although debris can cover below ground shelter doors, and occupants may be trapped, first-responders are available very quickly after an event and occupants are typically assisted with in a half hour since the location of registered residential shelters is known. Another observation made was that in some cases the storm shelters were filled with water caused by heavy rains following storm passage or severed water lines in severely damaged homes. This was documented by the team several times with one shelter filling with 0.3 m (1 foot) of water before the occupants were able to safely exit the storm shelter. In the event of debris blocking the exit of the shelter, flooding could prove very dangerous to anyone remaining inside the storm shelter. An example of a flooded storm shelter is shown in Figure 4.5. Floating bottles and bench seats indicate that water had reached the top of the safe room. Another observation, while not directly related to the performance of garage slab storm shelters in the tornado, was that many of these shelters were left open after the occupants exited and were not closed. This is a hazard to first responders and

clean-up crews in the aftermath of a tornado, especially when the entry to the shelter is obscured by debris.

Figure 4.4, Debris blocked storm shelter after an attached garage failed.

Figure 4.5, Flooded storm shelter from severed water lines and rain. Floating debris indicates that water has reached the top of the storm shelter.

The majority of the above ground residential shelters observed were found in the moderate to severe damage range (EF3 - EF4), mainly because substantial home damage exposed the otherwise concealed shelters. The majority of above ground residential shelters performed very well and only had cosmetic damage on the exposed portions of the shelter due to debris strikes. When possible, specifications of the shelter were obtained from the home owner, or measurements were taken by team members in the field and used in the evaluation.

There were two observed instances of concrete or concrete masonry unit (CMU) safe rooms that were used as bedroom closets. Both of these safe rooms were stand alone and had no part of the home attached to the walls or ceilings as prescribed by FEMA 320. The first safe room was in an area that experienced EF3 level damage on Riverside Drive in eastern Moore. The safe room was built on the southwest corner of the home and is pictured in Figure 4.6. Inspection of this safe room indicated that the exterior dimensions were 3 m by 3 m (9.5 feet by 9.5 feet) and 2.5 m (8 feet) tall. The door had the FEMA recommended three dead bolts and three hinges and ventilation was noted at two locations on the ceiling. The second concrete/CMU safe room, shown in Figure 4.7, was found near the intersection of SW 149th St and S. May Ave. The home experienced EF4 damage with complete removal of the roof, second floor, and external walls. This house was near the intersection of the 1999 and 2013 tornado paths. The property also included a pool cabana, tennis courts, stand-alone garage, and greenhouse. The cabana, garage, and greenhouse were all removed from their foundations and blown approximately 45-90 meters (50-100 yards) according to the home owner. Likewise, trees on the property were badly damaged and debarked. The owner informed the team that he built the safe room according to the FEMA 320 specifications current at the time of home construction in 2001. The safe room door did have three dead bolts and hinges and adequate ventilation. Even though the home had an above ground safe room, the owner described to the team that his family felt safer below ground, so they also had an additional below ground garage slab storm shelter installed and were in that shelter when the tornado struck. Both the above and below ground residential shelters at this location performed well.

Figure 4.6, FEMA designed CMU safe room found near Riverside Drive in eastern Moore.

Figure 4.7, FEMA designed CMU safe room found near SW 149th St and S. May Ave. The safe room is centrally located among the remaining rooms and is indicated with the black circle.

Several additional above ground residential shelters, shown in Figure 4.8, are briefly discussed below. There were two instances of steel above ground storm shelters bolted to the garage slab. The first storm shelter was found near the intersection of SW 147th St. and S. Hudson Ave in an area of EF3 damage. The shelter and remnants of the home are pictured in

Figure 4.8(a). The shelter exterior was scratched and buffed from debris impact, but no major dent or perforation occurred. In addition, portions of the home's roof system fell on top of the storm shelter but no major damage was observed. The second above ground steel storm shelter was found at the intersection of SW 13th St and Penn Ln. This shelter was in an area of EF4 damage and is shown in Figure 4.8(b). The exterior of the storm shelter showed signs of significant scratching and buffing impact from windborne debris, however, no major damage or perforation was observed. Both of the above ground steel storm shelters successfully met their intended purpose.

Figure 4.8, Residential shelter images; (a) and (b) steel storm shelters bolted to the garage slab; (c) cylindrical steel exterior storm shelter; and; (d) homemade concrete dome refuge.

Near SW 151st St and Todd Way in an area of EF0 damage zone, an above ground storm shelter was documented by the team. The shelter had a cylindrical body capped with a dome and is shown in Figure 4.8(c). This type of storm shelter has been tested and approved by National Storm Shelter Association (NewDay Tornado Shelters, 2013). This shelter was made of 8 mm (5/16 inch) steel and stood about 2 m (6.5 feet) tall with a diameter of 102 cm (40 inches). Due

to the small footprint, this shelter is not recommended for more than 3 adults (NewDay Tornado Shelters, 2013).

A concrete dome refuge, shown in Figure 4.8(d) that appeared homemade without design guidelines was documented by the team. The dome refuge was found in a neighborhood that experienced EF4 damage and was near the intersection of SW 145th St and Briarcliff Dr. The door of the refuge was made of 5 mm (3/16 inch) steel and was 0.9 m (3 feet) tall and 0.6 m (2 feet) wide. The concrete exterior was measured at the midsection of the door frame and found to be 18 cm (7 inches) thick. The steel door had three hinges and each hinge was welded to the door frame and then welded to a pair of structural steel square tubes that ran across the door width. In addition, three slide barrel bolt locking devices were found on the door. Although homemade, the dome refuge performed very well in the tornado.

4.2 ICF Safe Room Missile Perforation

The team documented an insulated concrete form (ICF) house with an ICF safe. The house is located on NW 36th St in Newcastle, Oklahoma, near the touch down location of the tornado. This safe room suffered two missile perforations on the western wall. The home was built in 2001 using ICF waffle grid walls, which are now considered obsolete since flat ICF walls are now industry standard (Reward Wall Systems, 2013). The roof of the house was made of metal studs and a 5 × 20 cm (2 × 8 inch) wooden top plate which was attached to the ICF walls with anchor J-bolts. Damage to the home included complete removal of the attached garage (built with metal studs) and the roof. The ICF walls of the house experienced damage from debris impact resulting in the removal of some of the foam exterior. Overall the home was estimated to be in a region of EF4 strength wind primarily based on damage to neighboring homes.

The exterior walls of the home were built using the ICF waffle grid design which consisted of 3.8 cm (1.5 inches) of foam on the exterior and interior which encapsulated a concrete center. The walls were a total of 23.5 cm (9.25 inches) thick including the exterior and interior foam, the concrete core, and the interior sheet rock (Reward Wall Systems, 2013). The concrete fill ranged from a maximum thickness of 15 cm (6 inches) within a cell to a minimum thickness of 6.4 cm (2.5 inches) in the thin area between cells. The centers of the cells were

spaced at 30.5 cm (12 inch) increments consistent with FEMA specifications. Vertical and horizontal reinforcing steel was placed in every other cell of the exterior walls (61 cm spacing) according to the home owner. The reinforcing bar was estimated to be approximately No. 4 rebar (1.3 cm diameter) by the home owner.

An above ground ICF waffle grid safe room was found at this home. Although waffle grid ICF is no longer an industry standard, ICF waffle grid safe room design is still included in the current FEMA 320 guidelines (FEMA, 2008). This ICF safe room doubled as a storage closet. The safe room measured 2.4 m by 2.6 m (8 feet by 8.67 feet) with walls that were 2.4 m (8 feet) tall. A FEMA recommended door with three dead bolts was used. An exterior schematic of the home showing the location of the safe room and an inset image of the safe room are shown in Figure 4.9. As seen in Figure 4.9, one of the walls of the safe room is also an exterior wall.

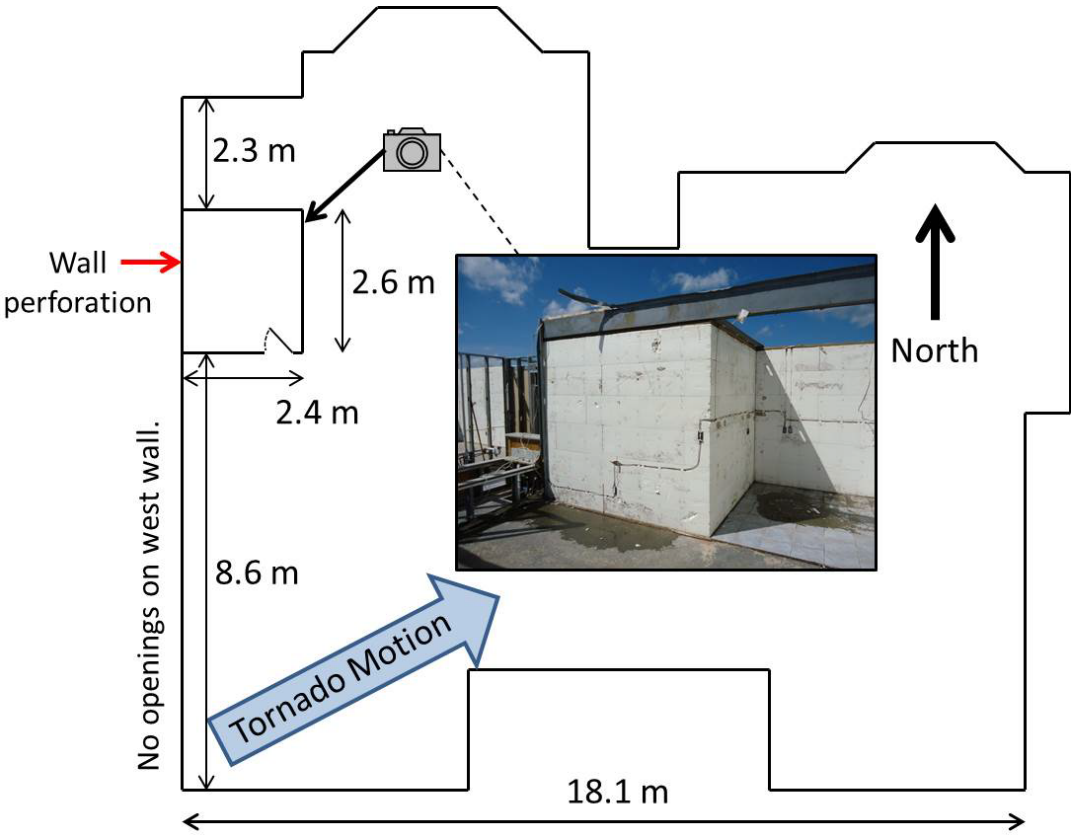

Figure 4.9, Floor plan of ICF home where failure of an above ground safe room occurred. An exterior image of the safe room is shown as well as the tornado motion. The red arrow indicates the location of perforation by two metal poles.

The west exterior wall of the safe room was perforated by two square metal poles shown in Figure 4.10(a). It should be noted that in Figure 4.10(a), only one projectile is shown. The second projectile was removed but evidence of the perforation is indicated by a hole on the right side of the image. The homeowner was seeking shelter in the safe room during the tornado and was nearly injured when the poles came through the wall inches from his head. The poles entered the safe room and extended approximately 0.6 m (2 feet) into the room. Based on inspection of the exterior wall of the safe room, it is likely that the poles struck some part of the thick cell center and, due to the rounded shape, deflected to the thinner portion of concrete where the metal was able to penetrate into the interior of the safe room. A pole taken from the site measured to be approximately 2.5 cm (1 inch) square with a thickness of 0.23 cm (0.09 inches). The pole was bent and had a tip to tip length of 99 cm (39 inches) and an arc length of 104 cm (41 inches) along the curve. Detailed images of one of the projectiles are shown in Figure 4.10(b-d).

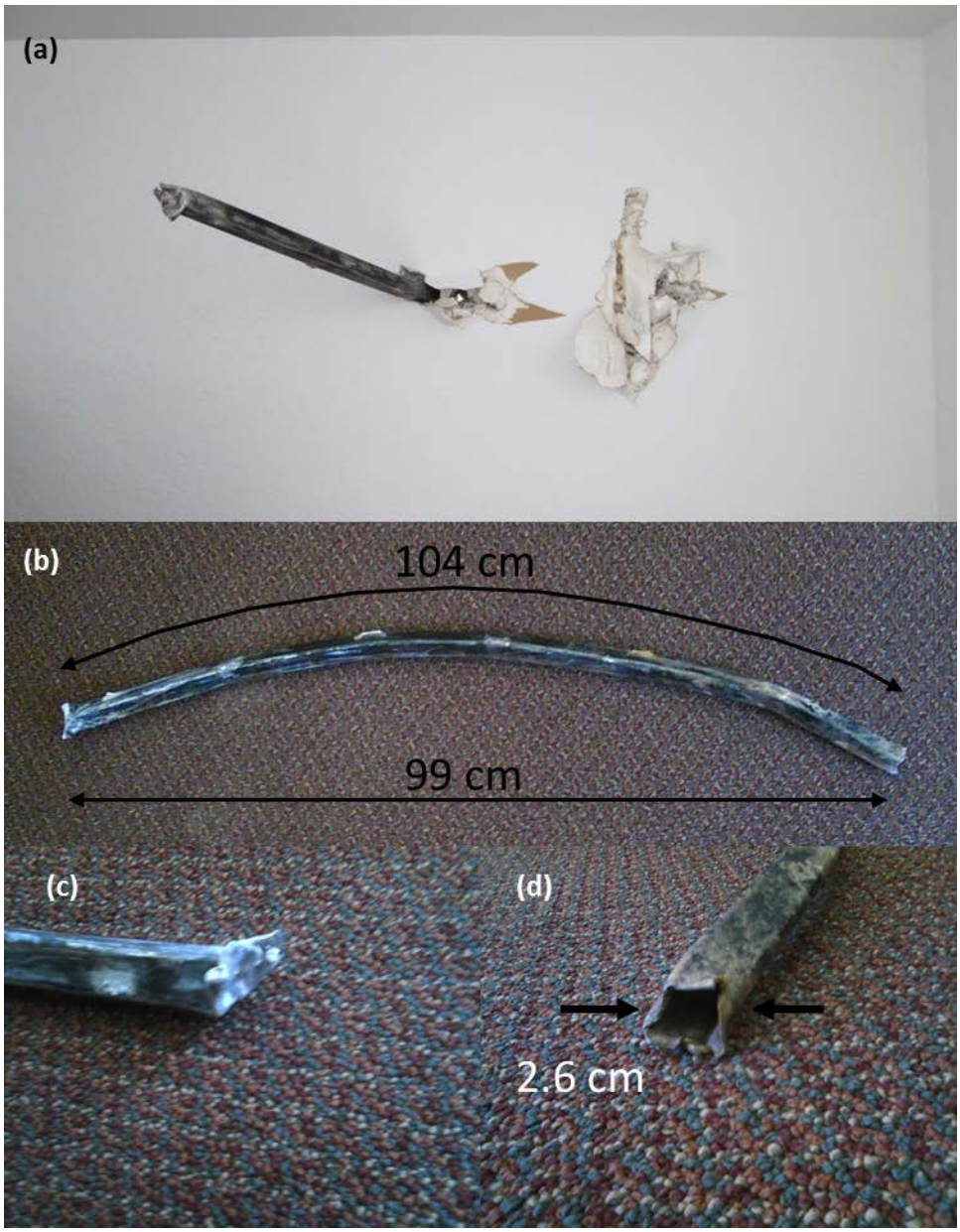

Figure 4.10, Illustrated is (a) the wind borne projectiles which punctured the ICF safe room wall nearly striking the home owner (one projectile has been removed); (b) detailed dimensions of one projectile; (c) the end which punctured the wall; and (d) the other end used for thickness measurements.

This particular safe room was built to the FEMA 320 (2008) ICF safe room recommended design, although FEMA ICF drawings were not available at the time of home construction. FEMA prescribes the use of #4 horizontal steel reinforcing bar every 40.6 cm (16 inches) and #5 vertical reinforcing steel every 30.5 cm (12 inches) for the waffle grid safe room design. The exact size of the steel reinforcement is not known; however, since the steel

reinforcement was not impacted by the missile, this detail is not considered critical for explaining the missile perforation.

FEMA recommends, but does not require, that safe rooms be built as an interior room of the home. Similar to the idea of an interior closet or bathroom safe spot, it is best to have as many walls as possible between a safe room and the exterior of the home. This typically helps to reduce the likelihood of missile impact, penetration, or perforation. However, since this is not a design requirement, safe rooms can have up to three walls exposed to the outside (FEMA, 2008). This particular safe room had a single wall coincident with the exterior of the home and this wall was on the western portion of the home as shown in Figure 4.9. Estimates from tornado climatology indicate that average tornado motion is from the southwest to the northeast (Gonzalez, 2013) causing the southern and western faces of homes to receive the worst brunt of tornado impacts. The safe room location on the west side of the home and having a wall on exterior portion of the building were two design components that may have contributed to the observed failure.

Another likely explanation for the failure was issues with workmanship and construction quality. Several large holes and voids were observed in the concrete at the location of the perforations as shown in Figure 4.11. FEMA 320 states that the compressive strength of concrete used in safe rooms must be at least 20.7 MPa (3000 psi), however, there is no requirement for testing of concrete used in safe room construction. Concrete compressive strength for the safe room that was perforated was estimated using ASTM method C805 (2013) and a Soiltest CT-320 concrete test hammer. The average curves provided with the instrument were used to convert the rebound results to compressive strength. Two locations were examined on both the roof and the west wall of the safe room. Those on the west wall were located directly between the missile impact points and at a location with no damage. For each location, the surface of the concrete was smoothed with a carborundum stone and ten readings were taken spaced at a minimum of 2.5 cm (1 inch). The average of the ten readings was then input into the curves provided with the instrument in order to determine an estimate of compressive strength. Results from the rebound hammer tests indicate a concrete compressive strength of approximately 23.4 MPa (3400 psi) for the walls of the safe room and 15.2 MPa (2200 psi) for the safe room roof. The curves used to convert the rebound values to compressive strength were

based on average concrete mixtures and curing conditions and have a margin of error of ±20%. Considering the margin of error, the measured values indicate that the wall concrete had a compressive strength most likely in excess of the 20.7 MPa (3000 psi) specified by FEMA (2008). However, the compressive strength of the safe room roof concrete may have had a compressive strength less than the specified minimum.

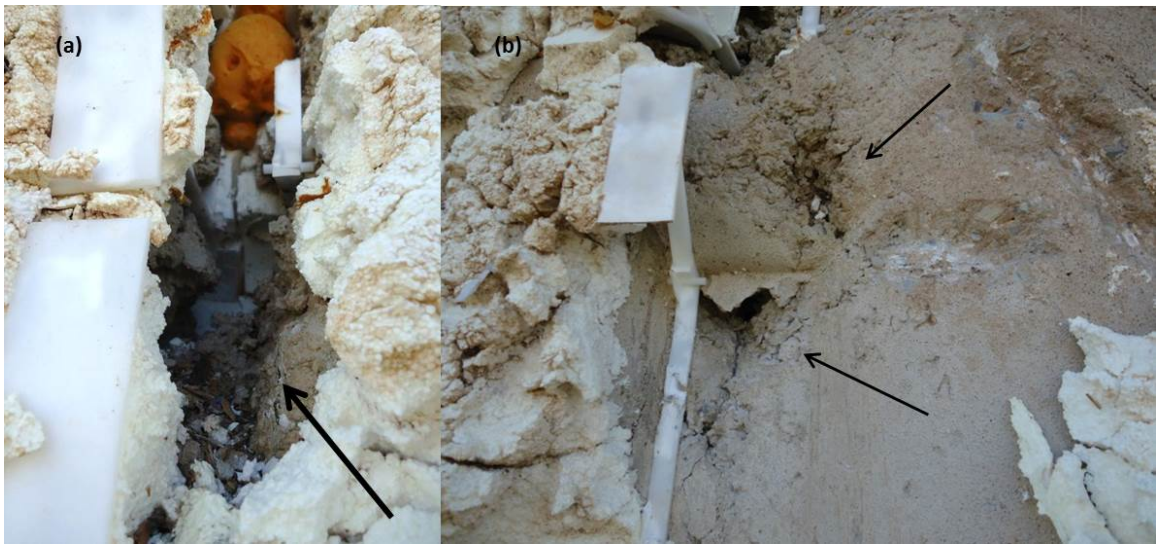

Figure 4.11, Inadequate concrete pour indicated by; (a) a large area of poorly consolidated concrete below missile perforation and (b) a large void in the concrete in the thinned area of the waffle grid and in the vicinity of a plastic clip.

In addition, the location and configuration of the plastic cross ties caused concrete flow issues and the actual concrete thickness at the location of missile impact was measured to be approximately 2.5 cm (1 inch). This measurement is less than the FEMA required minimum thickness of 5.1 cm (2 inches). This highlights the point that care must be taken to assure that all areas of safe room walls are properly filled with adequate strength concrete and to avoid plastic cross ties along the thinned portion of ICF waffle grid safe rooms when possible.

4.3 Shared Shelter Use

The social media analysis study of shelters and safe rooms in Moore, OK provided insight on how well these structures held up against the strength of tornadic winds and debris impact, and also how these structures were used to protect people. The choices that people made to use these structures had a great deal to do with how they survived.

The social media data that accompanied the pictures of these shelters and safe rooms indicated how shelters had saved lives. Observations of the shelters revealed that the shelters had withstood the tornadic winds and debris impact, and it also appeared that these shelters were well used and shared among large numbers of people. Regardless of the type or age of the shelter, families and neighbors shared these small protective fixtures in significant numbers. Using an informal neighborhood network of knowledge about the locations of these shelters and the open door use of these shelters, people went to the closest shelter and took protection with their neighbors. An example of this type of behavior is shown and described in Figure 4.12. Many of the shelters in the Moore tornado event housed multiple neighbors and their pets, in several cases, over ten people and their pets took refuge in shared shelters. This same story was told about many shelters observed in Moore.

Figure 4.12, This woman's family and neighbors sought protection in her shelter. The woman was not home at the time, but called her friends and family and told them to get into the shelter. This location is about 100 feet west of the Moore Medical Center and the Warren Theatre, where the tornado was at one of its strongest points.

Through the use of social media data and discussion with people at the site of the shelters, researchers were told how people knew which neighbors had shelters and that they were welcome to go to those shelters when it became necessary. In many of the locations in the path

of the tornado, there was at least one shelter on a street and in many cases multiple shelters on a street. The age of these shelters also varied. Some were very old as shown in Figure 4.13 or had been constructed by homeowners. Others were more modern and some were new, many having been installed within the last 6 months. The locations of the shelters also varied with many described as below ground and others installed above ground in garages or built into the homes as safe rooms.

Figure 4.13, This shelter was one of the older observed shelters in the area.

Neighbors talked about either going to the closest shelter or at least sending their families to those shelters when they could not go. These shelters filled to a capacity that belied what they should be able to hold. Structures that looked like they could hold maybe five or six people held many more people, including pets, in one case a German Shepherd dog.

Storm shelters are only successful if people use them. Properly designed shelters can stand up to the winds of an EF4 or EF5 tornado or withstand debris impact is irrelevant if few people are in those shelters when the time comes. These shelters were well used and there were a large number of them to be shared by neighbors. The informal neighborhood networks that were in place allowed neighbors to know the locations of these shelters with the awareness of

open invitations to use them. This provided many people with a safe place during the tornado and allowed these shelters to do their jobs well. In one case, the homeowners were out of town and they called their neighbors to tell them that the gates were unlocked and they could get into the shelter. This shelter ended up protecting over ten people, including multiple children, plus a dog from the surrounding homes. Figures 4.14 and 4.15 illustrate the interior walls of this particular shelter. Over the years, the homeowner has allowed the neighborhood children to decorate the interior walls of the shelter with their handprints and drawings with the hope that they won't fear the shelter when they need it. In the Moore tornado, the sharing of this shelter kept many people safe, including many of those children.

Figure 4.14, Storm shelter with walls decorated by children taking refuge.

Figure 4.15, Message on interior of storm shelter indicating the informal network of storm shelter shared use.

4.4 Storm Shelter Analysis Conclusions

Over 3000 registered residential shelters exist in the city of Moore. These shelters kept many people safe on May 20th, 2013. The large number of residential shelters can likely be attributed to the recent history of violent tornadoes in Moore. There were few instances of above ground safe rooms or storm shelters, with the majority of storm shelters classified as below ground. Below ground shelters performed well, although issues with access, debris blocking exits, and water intrusion from rain and severed water lines should be considered. The majority of above ground safe rooms and storm shelters performed well and had no cases of perforation by windborne debris except for one ICF safe room. Overall, this type of perforation is not acceptable for safe room and can likely be attributed to poor construction quality associated with improper concrete consolidation, especially in the thinned areas where plastic cross ties were located. This was evident by the large voids on the exposed portions of the ICF walls. In addition, the location of the safe room was less than ideal within the building envelope. Having a wall of a safe room coincident with an exterior wall of the home increases the risk of missile

impact and possible penetration and/or perforation. This exterior wall was also on the western face of the house which is a vulnerable region for tornadic winds.

Another facet of the residential shelter investigation was the concept of shared shelters. In many cases, people knew the location of residential shelters in their neighborhood and would take refuge at these locations in the event they did not have a safe place to go. Often, residential shelters were left unlocked so that neighbors could use the shelter in the event the home owner was not home. There were several instances where these shelters were filled in excess of their capacity holding up to 10 adults and pets.

Chapter 5 - In-depth Studies and Observations

5.1 Roof Failures Leading to Wall Collapse

Surviving an EF2 or greater tornado from within a wood-frame house requires protection from the debris-filled winds that can exceed 100 mph. While the level of protection is not up to the standards of a properly designed and constructed tornado shelter, survivability inside a wood-frame house is certainly enhanced by the presence of standing walls. Inspection of wood-frame houses damaged during the Moore tornado led to the conclusion that once a house's roof is removed, wall collapse is imminent.

Wind speeds at the center of a tornado path are greater than along the fringes. Observing the progression of damage from the edge of the tornado path inward can provide clues regarding likely collapse mechanisms. For example, damage to roofs of houses along the fringe of the tornado path consisted mainly of missing sheathing; roof framing (trusses or rafters) was still intact. Houses adjacent but closer to the center of the tornado path were missing roofs and had collapsed walls. One obvious conclusion is that the roof framing provided lateral support to the tops of the walls. Once the roof was removed, the walls collapsed soon after.

This in-depth study describes four likely roof failure mechanisms and their effect on lateral support to walls. The failure mechanisms are proposed based on observed damage to wood-frame houses from the Moore tornado.

1. Failure of light-gage metal garage doors, particularly on garages that extend out from the house, led to pressurization of the garage, subsequent loss of roof over the garage, and collapse of the garage walls.
2. Prefabricated wooden roof trusses resisted uplift better than rafter/ridge-beam roofs.
3. Removal of roofs supported by prefabricated roof trusses left the tops of walls with little lateral support. On the other hand, removal of rafter/ridge-beam roofs typically left the separate ceiling joists in place; and thus the tops of the walls were still laterally supported.
4. "High profile" roofs had relatively long unsupported spans (compared to other roof types) leaving them more vulnerable to uplift. Fewer intermediate supports led to larger

bending moments and shear forces in the rafters; and longer distances between lateral support to the rafter bottom edge (compression edge for uplift) decreased resistance to lateral-torsional buckling of the rafters.

The following sections describe in words and photos the observed damage supporting each of the four postulated failure mechanisms described above.

1. Loss of light-gage garage doors.

Some houses on the fringe of the 2013 Moore OK tornado path had partially collapsed garage doors as shown in Figure 5.1 below. Though slight in terms of property damage, the consequences of losing the garage door were frequently severe.

Figure 5.1, Partially collapsed light-gage metal garage door of house on tornado damage fringe.

Loss of the garage door ruptures the building envelope and allows the inside of the garage to be pressurized by tornado winds. Garages that protruded from the main footprint of the house seemed to be especially vulnerable. The combination of positive pressure inside the garage and negative pressure outside the garage roof likely caused the garage roof to be pulled

up and off. This resulted in essentially complete loss of lateral support to the tops of the garage walls on either side of the large garage door as shown in Figure 5.2 and Figure 5.3. The short walls adjacent to the garage door opening were typically not sheathed (e.g. with plywood) and therefore had minimal shear stiffness.

Figure 5.2, Garage removed from house on left with protruding garage.

Figure 5.3, Missing garage on house with "protruding" garage.

The garage walls in the houses shown in Figures 5.2 and 5.3 had properly anchored sill plates (see Figure 5.4 for example). The anchored sills are effective in resisting uplift, but not torsion (caused by collapsing wall) and uplift.

Figure 5.4, Failed sill plate with anchor bolt still attached.

2. Prefabricated wooden trusses.

Prefabricated roof trusses resisted uplift better than rafter/ridge beam construction. See Figure 5.5 for a house with rafter/ridge beam roof framing flanking a house with prefabricated wood roof trusses. The prefabricated roof trusses are still intact, but the entire roofs of the rafter/ridge beam roofs have been removed. The better performance of the prefabricated roof trusses is likely due to the better connections (metal truss-plates loaded in shear), and the more web members connecting the top chord to the bottom chord.

3. Removal of rafter/ridge-beam roofs frequently left ceiling joists in place.

Note in Figures 5.5 and 5.6 that although the roofs, ridge beams and rafters are missing, the ceiling joists are still intact. These ceiling joists provide lateral support to the walls. Houses missing prefabricated truss roofs (not shown here) did not have ceiling joists, since the bottom chords of the roof trusses serve as the ceiling joists. This implies that although the prefabricated roof trusses performed better than ridge beam/rafter roofs at one wind speed, at higher wind speeds the situation may be reversed.

Figure 5.5, Missing rafter/ridge beam roof on house to left of house with largely intact prefab truss roof.

Figure 5.6, Missing roof but intact ceiling joists.

4. High-profile roofs had rafters with long unsupported spans for uplift

High-profile roofs have a distinctive architectural look but may lack utility. Another weakness of rafter/ridge beam roofs observed and shown in Figures 5.7 and 5.8 is the relatively long unsupported spans of the rafters (see Figure 5.7). The rafter has minimal vertical support to resist gravity loads and also the support to resist uplift loads depends on a weak connection between the rafter and the vertical support. In addition, while ample lateral support is provided to the compression side (top) of the rafter for gravity loads from the sheathing, only one point of lateral support is provided to the compression side (bottom) of the rafter for uplift loads from the purlin. Figure 5.8 shows a house with intact garage doors but completely missing its high-profile roof.

Figure 5.7, Long unsupported spans of rafters on typical "high profile" roof. Lateral support to bottom of rafters indicated by red arrow.

Figure 5.8, Progression of roof damage to "high profile" ridge beam/rafter roofs.

5.2 Truss Connections in Single Family Dwellings (EF2 wind speed 110 - 137 mph)

Two homes located diagonally across the street from one another on one of the narrowest sections of the tornado path (i.e. visible damage width was ~200 yd) were compared for performance of the roof trusses. The home at 808 S. Silver Leaf Drive was located approximately 180 ft south of the center of the damage path on the east side of the north-south street and the home at 805 S. Silver Leaf Drive was located approximately 150 ft south of the center of the damage path on the west side of the street. The homes directly to the south of both 808 and 805 S. Silver Leaf sustained substantially less damage, while the homes directly to the north of both were nearly completely destroyed. Locations of the homes in both before and after aerial views are shown in Figure 5.9.

Both homes were single story, wood frame structures with brick veneer, an attached garage, and a fireplace. Both homes had gable roofs consisting of 2 × 4 trusses spaced at 24 in. connected with press plates and attached to the 2 × 4 wall plates with two 16d toe-nails at each truss, 1x6 roof sheathing, and asphalt shingle roofing. The roof of 808 S. Silver Leaf had a pitch of 5.5:12 and the truss height was 74 in. The roof of 805 S. Silver leaf had a pitch of 5:12 and the truss height was 97 in. The 2 × 4 stud walls were connected to the foundation slab using ½ in. anchor bolts for both homes. Walls were sheathed with insulating fiberboard sheathing at all locations except for the corners of the homes, which each had one sheet of plywood sheathing in each direction.

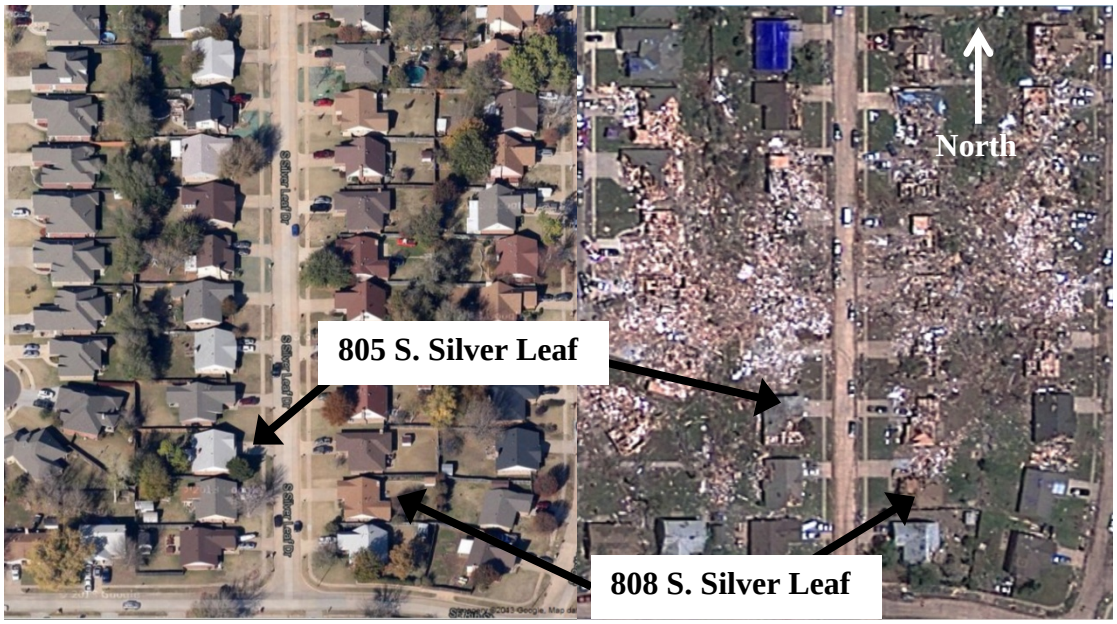

Figure 5.9, Before (left) (Google Maps 2013) and after (right) (Google Crisis Response, 2013) photos showing home locations.

808 S. Silver Leaf Drive

This single family home was built in 1978 and was a 1306 ft^2, 3 bedroom, 2 bath home according to zillow.com (Zillow, 2013). Before and after views of the home are shown in Figure 5.10. Damage to the home consisted of:

- The northern, approximately 50% of roof structure missing
- Approximately 30% of the roofing material was missing from the remaining structure
- Garage and living room exterior walls on north and west sides destroyed
- Remaining back wall (east) slanted outward and front wall (west) slanted inward
- Chimney toppled
- Remaining westward windows broken, likely by flying debris

Figure 5.10, 808 S. Silver Leaf Drive (a) before (Google Maps, 2013) and (b) after the tornado. The Degree of Damage (DOD) on the EF scale was 6 based on the removed roof structure and most walls remaining intact, which suggests wind speeds between 104 and 142 mph with an expected speed of 122 mph. The collapsed walls indicated a DOD nearer to 7 and wind speeds toward the high end of this range.

All walls that were completely destroyed were connected to the garage or garage walls. Anchor bolts provided for the wall bottom plate to slab foundation connection had no evidence of nuts or washers in most of the exposed locations. Brick ties were provided on all walls, but structural sheathing was only provided at the corners of the home, probably as intermittent bracing as allowed by the building code. The roof truss geometry is shown in Figures 5.11 and 5.12. The truss connector plates used for the roof trusses were approximately 1/16 in. thick, made of steel with unknown properties, and were provided on both sides of the truss at each connection. The pressed in connector plates were very small or poorly aligned at many connections and many of the smallest connection plates (1 in. by 4 in. connecting intermediate bracing) failed as shown in Figures 5.11 through 5.14. These smallest plates were oriented in the direction of the intermediate braces and were theoretically in pure tension or compression. Each

had approximately 32, 3/16 in. points pressed into the wood, distributed across the two members being connected. The failures of these smallest plates in the trusses that remained intact were on the east side, as shown in Figure 5.13, whereas those on the west side did not fail. The connection to the wall top plate was intact on the east side, but not on the west side due to the severe lean of the wall shown in Figure 5.12. Only connectors on two of the intact trusses were broken, but other failures of the 1 in. by 4 in. connector plates were observed in the portions of the roof structure piled in the yard on the east side of the home.

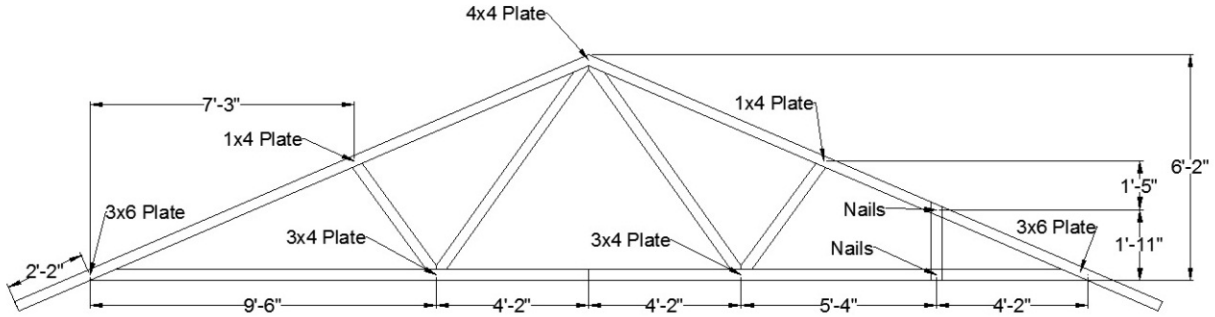

Figure 5.11, Geometry of roof trusses at 808 S. Silver Leaf.

Figure 5.12, Intact roof truss with plate failure location indicated.

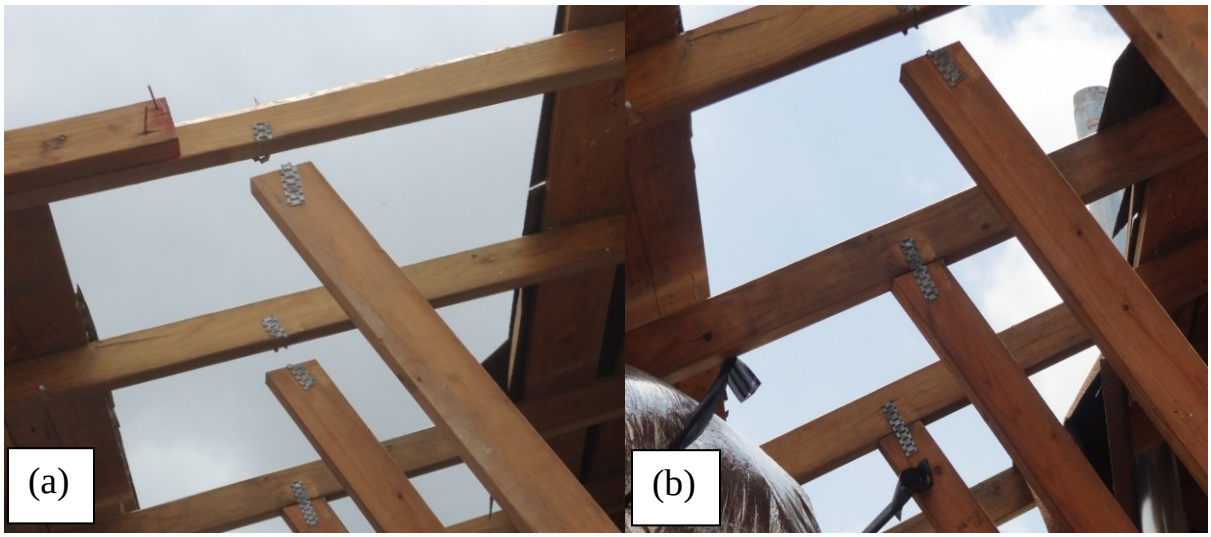

Figure 5.13, Examples of (a) small truss connector plate failures at location indicated and (b) small connector plates that remained intact.

Figure 5.14, Example of connector with unequal overlap of the connector similarly observed in several locations. The gap between the wood members was within the range allowed at the time.

805 S. Silver Leaf Drive.

This single family home was built in 1975 and was a 1366 ft^2, 3 bedroom 2 bath home according to zillow.com (Zillow, 2013). Before and after views of the home are shown in Figure 5.15. Damage to the home consisted of:

- Approximately 40% of roof structure destroyed on south end
- Approximately 20% of roofing material missing from remaining structure
- Roof was shifted east off of the walls in the areas where it remained intact
- Gable end siding removed from remaining structure (north end)
- Garage walls leaning outward (east and north)
- Chimney broken at roof level
- Most windows broken on south and east sides, likely from flying debris

All walls remained intact as seen in Figure 5.16, but the building only had plywood structural sheathing at each corner, probably for intermittent bracing as allowed by the building code. The roof truss pattern and field measured dimensions are shown in Figure 5.17. The truss connector plates had the same thickness, but were more robust in their dimensions and of a different type than those in 808 S. Silver Leaf, as shown in Figure 5.18. The properties of the steel were also not known. The truss members were the same size (2×4) as those in the roof structure of 808 S. Silver Leaf.

The smallest truss plate connectors were 2 in. by 4 in. instead of the 1 in. by 4 in. connectors observed in 808 S. Silver Leaf and the largest connectors were 5 in. by 8 in. instead of the 3 in. by 6 in. plates observed in 808 S. Silver Leaf. No evidence of connection plate failures was observed in 808 S. Silver Leaf, with all failures located within the truss members similarly to the piece shown in Figure 5.18(b).

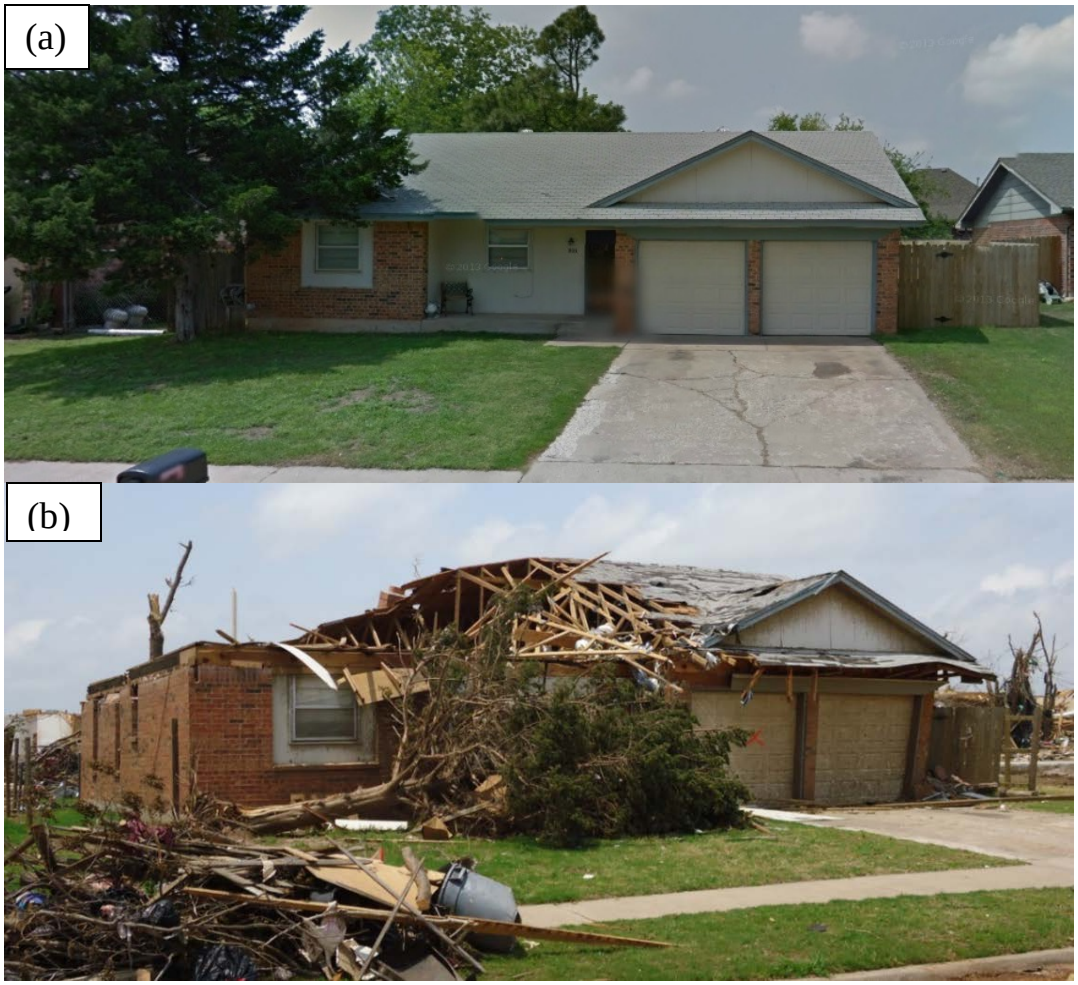

Figure 5.15, 805 S. Silver Leaf Drive (a) before (Google Maps, 2013) and (b) after the tornado. The Degree of Damage (DOD) on the EF scale was 6 based on the removed roof structure and most walls remaining intact, which suggests wind speeds between 104 and 142 mph with an expected speed of 122 mph.

Figure 5.16, 808 S. Silver Leaf Drive after the tornado.

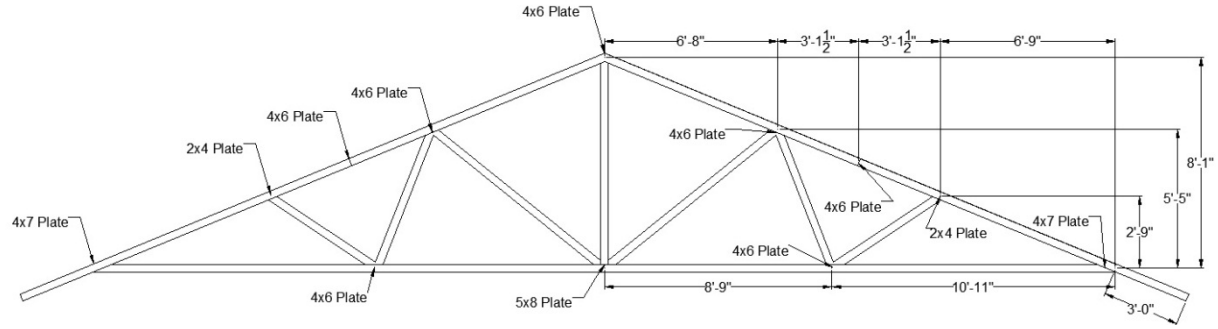

Figure 5.17, North end and truss arrangement for 805 S. Silver Leaf Drive.

Figure 5.18, (a) Larger truss connector plates than for 808 S. Silver Leaf and (b) example of failure within the truss members.

The directional location of the major damage and portion of the home affected was different for these two homes. The loss of structure for 808 S. Silver Leaf began with the westward facing garage whereas the damage to 805 S. Silver Leaf began with the southern gable end. In both cases, evidence was observed of the lost trusses being pulled from the toe-nail connections on the remaining walls. Uplift of the 1 × 6 roof sheathing and flying debris may have contributed to the failure of members within trusses that remained connected to the walls for 805 S. Silver Leaf, by producing loadings other than tension and compression and exceeding the capacity of the 2 × 4 sections. The connector plate failures in 808 S. Silver Leaf were likely caused by tension in the bracing members resulting from outward pressure on the east side roof not considered in design. The 24 in. truss spacing produced a substantial tributary area for each of the previously mentioned loadings and subsequent failures. Both the truss to wall connection and connections within the trusses were important factors in the behavior of these homes.

5.3 House Shifting from Foundation

The objective of this in-depth study is to report on the absence of homes that had shifted from their foundation in the 2013 Moore tornado compared to those found on similar assessment trips prior to this tornado in Joplin and Tuscaloosa in 2011 and Moore in 1999.

Damage assessment surveys conducted after previous tornadoes in Tuscaloosa, Joplin, and Moore showed a few cases where houses had shifted from their foundations, but remained intact as seen in 5.19 and Figure 5.20. This particular failure mode was not observed in Moore on this damage assessment survey. This is unusual because Marshall (2002) observed houses surveyed after the 1999 Moore tornado that failed in a similar manner as seen in Figure 5.21.

Figure 5.19, House shifted off of foundation in Joplin, MO after 2011 Tornado.

Figure 5.20, House shifted off of crawlspace foundation in Tuscaloosa, AL after 2011 Tornado.

Figure 5.21, House shifted off foundation 90 m in Moore, OK after 1999 tornado (Marshall, 2002).

FEMA (1999) stated that residential structures built in Moore were required to meet design requirements listed in the one and two-family dwelling building code published by the Council of American Building Officials (CABO). However, houses built prior to 1995 were governed by a less restrictive building code.

The CABO (1995) building code requires that walls be anchored to concrete foundations by 1.3 cm (0.5 in) diameter steel anchor bolts spaced a maximum of 1.8 m (6 ft) apart. According to this code, anchor bolts also should extend a minimum of 18 cm (7 in.) into the concrete.

Most houses observed by Marshall (2002) were fastened to foundations by 5 cm (2 in) long, tapered cut nails driven through the top sides of the sill plates at intervals of 30 to 130 cm (12–51 in). The sill plates at 3.8 cm x 8.9 cm (1.5 in × 3.5 in) allowed the tapered cut nails to extend a maximum of 1.3 cm (0.5 in) into the concrete foundation. As seen in Figure 5.22 scrape marks found on concrete slabs that extended from the points where tapered cut nails had been installed indicated that the walls moved laterally in the tornado. These connections, although

able to keep the walls in place under normal gravity loads, are not adequate when wind forces are applied.

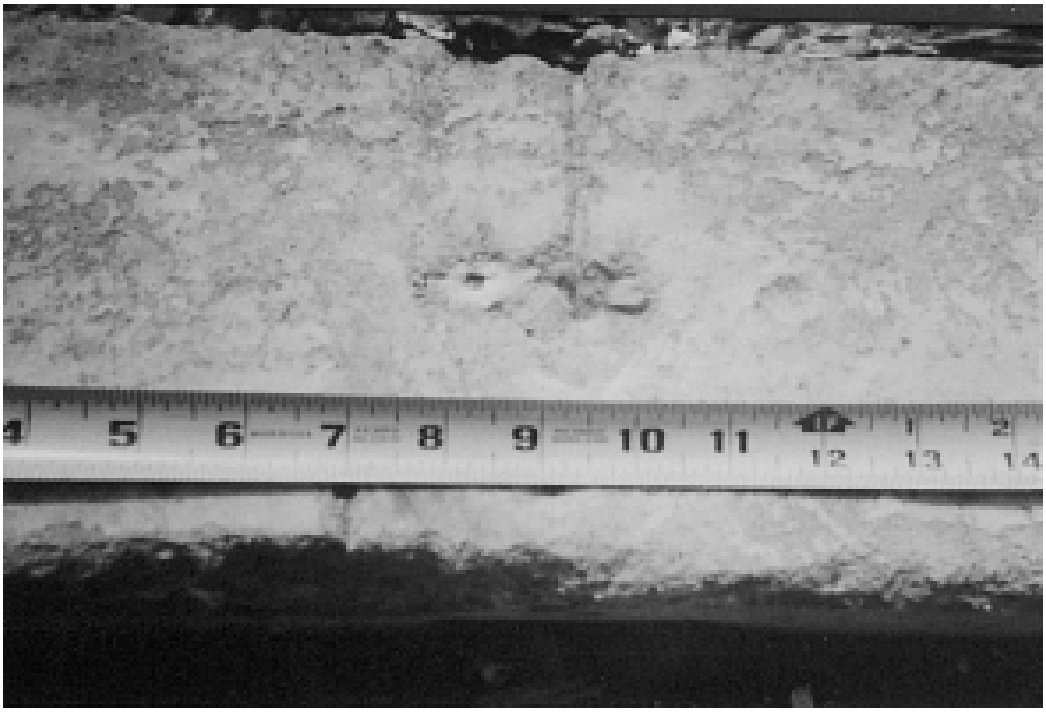

Figure 5.22, Scrape mark in the surface of concrete slab foundation indicating where the wall bottom plate along with the tapered cut nail connection were moved laterally (Marshall, 2002).

The uplift pressure of wind can exceed the weight of an average residential structure at around 125 – 135 mph in straight-line winds (Prevatt, 2012). Once the uplift pressure reaches the weight of the building, the lateral wind pressure is able to push the house off of the foundation. Sufficiently embedded anchor bolts provide resistance to this uplift pressure and sliding failure.

The absence of observed houses sliding off of foundations in Moore can most likely be attributed to the requirement of anchor bolts securing the foundation in recent construction. Many anchor bolts were found without nuts and washers, which would keep them from resisting uplift force, but the bolts themselves were able to resist lateral loads trying to push a house off the foundation.

5.4 Progressive Failure of Residential Garages

Within the context of this report, a superstructure failure is any failure of the framing system in a residential building. This includes failure of the roof, rafters, joists, load bearing

walls and non-load bearing walls. According to the majority of data gathered in this investigation, framing failure in a wood-frame residential structure appears to follow an ordered and predictable mechanism in the presence of tornado forces. This sequence is illustrated in five basic stages in Figure 5.23 through Figure 5.27. In this study, observations made immediately after the storm clearly demonstrate that failure of single-family homes begins in the garage. The most likely explanation for this observation is that the metal paneling construction of the overhead door represents the weak link in the building shell. In order to resist severe wind pressure effects, it is critical that the building shell not be punctured. However, the lightweight garage door typically has significantly lower lateral strength than the surrounding walls. In addition, garage doors in Oklahoma are not typically wind rated. For instance, while the design wind speed is 115 mph according to ASCE 7-10, most doors are not designed to meet this minimum. As a result, the door is the first element to give way under abnormally high wind loading, as shown in Figure 5.23 and Figure 5.24.

Figure 5.23, Stage 1 -- Wind Pressure Initiates Failure of the Garage Door

Figure 5.24, Stage 2 -- Garage Door Completely Destroyed

As soon as the garage door has been breached, the shell of the building is no longer intact and immediately begins to function as a “partially enclosed” structure, rather than an “enclosed” one. When the home begins to behave as a partially enclosed structure, ASCE 7-10 dictates that the internal pressure coefficient is boosted from GCpi = + 0.18 to GCpi = + 0.55. The typical result of this transition to a partially enclosed structure is that the internal wall pressure and uplift within the garage moves to a range far beyond what the wood-frame walls and roof trusses can resist and literally attempts to blow the structure up like a balloon. This also serves to explain why garages that have failed in this manner (such as shown in Figure 5.25 and 5.26) often give the appearance of having “blown up”, rather than simply collapsing. Once the garage has been completely destroyed, the front of the home is left exposed (see Figure 5.27), and the damage progresses into the structure in a similar manner.

Figure 5.25, Stage 3 -- Home Becomes Partially Enclosed Structure; Roof Begins Peeling Off

Figure 5.26, Stage 4 -- Garage Wall Framing Starts to Fail

Figure 5.27, Stage 5 -- Garage Completely Destroyed; Main Roof Begins Peeling Off; Attic is now partially Enclosed

At this point, with the garage completely destroyed, the main portion of the house becomes vulnerable due to increased exposure. This exposure leads to wind loading in two different manners: wind pressure on the windward side of the roof slope and wind suction on the leeward side of the roof slope. This combination of pressure and suction has the potential to rapidly deteriorate the roof truss structure via connection failure. In a typical wood-frame residential structure, the roof framing have connections as shown in Figure 5.28, with kickers directly bracing the roof rafter. Or they have connections as shown in Figure 5.29, with the kickers supporting a roof purlin that then acts as a brace point for the roof rafter.

Figure 5.28, Typical Roof Truss Connections

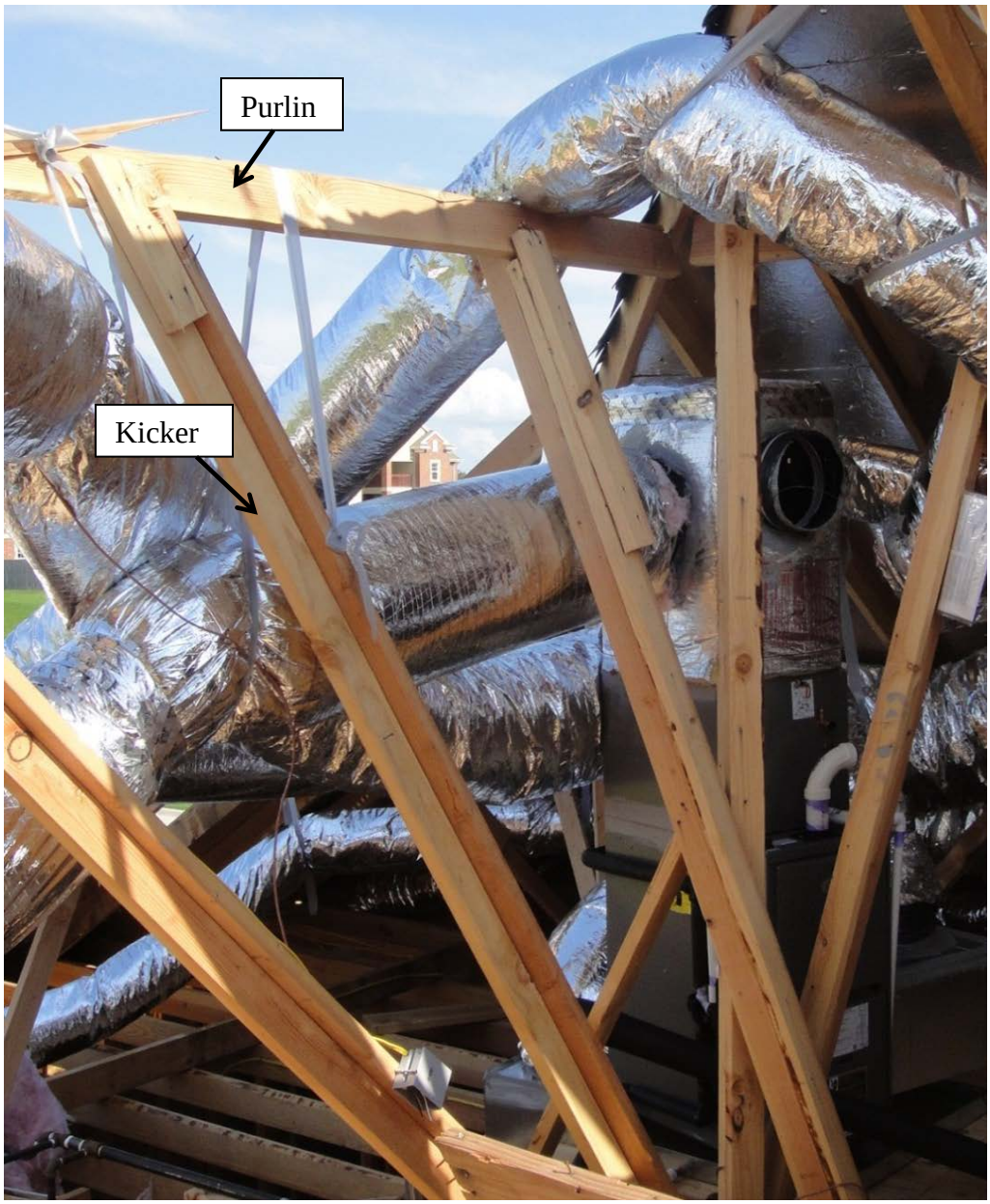

Figure 5.29, Typical Roof Truss Connections

In general, these nailed connections are intended to perform well in compression, but tend to be highly vulnerable to tension forces. Tension is induced when the leeward slope of the roof is subjected to uplift. The resulting failure mechanism is illustrated in Figure 5.30.

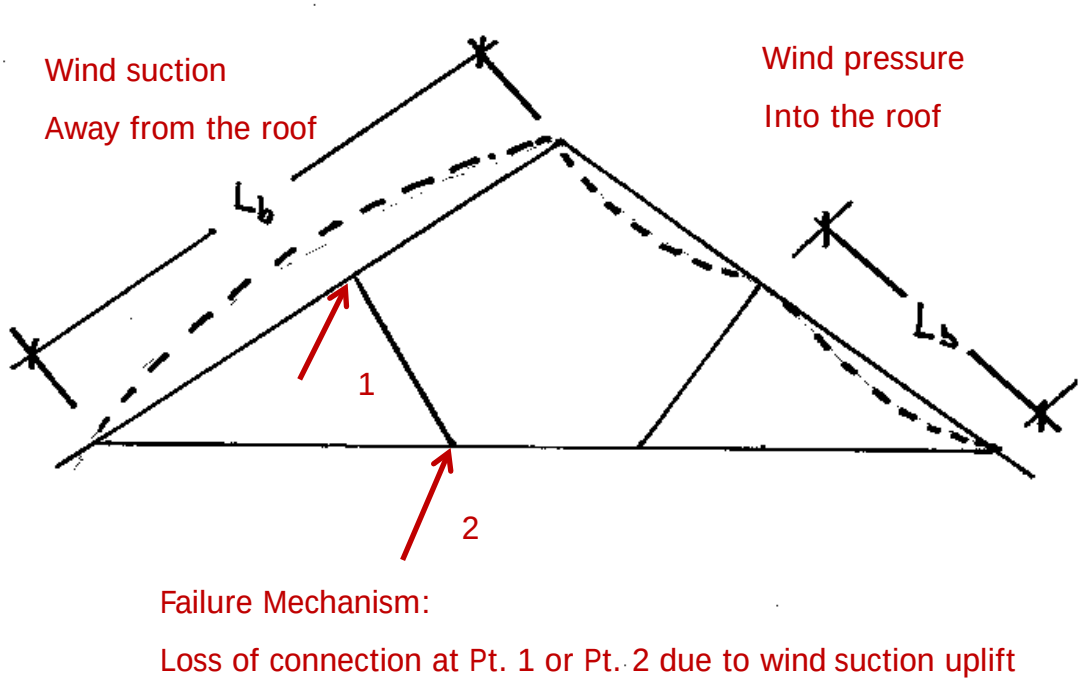

Figure 5.30, Roof Truss Failure Mechanism

In the event of a failure as illustrated in Figure 5.30, the following sequence occurs:

1. Due to connection failure, the rafter loses a brace point, effectively becoming twice as long.
2. Doubling the rafter length stresses the rafter beyond design capacity.
3. The rafter fails in flexure, causing a general failure in the roof system on the leeward slope.

5.5 In-depth Studies Conclusions

The in-depth studies performed in the aftermath of the Moore tornado lead to the following conclusions.

- Failure of garage doors causes the shell of a building to function as a “partially enclosed” structure, rather than an “enclosed” structure. The typical result of this transition is that the internal pressure and uplift within the garage moves to a range far beyond what the wood-frame walls and roof trusses can resist. This leads to pressurization of the garage, subsequent loss of roof over the garage, and collapse of the garage walls.

- Prefabricated wooden roof trusses were observed to resist uplift better than rafter/ridge-beam roofs. But removal of roofs supported by prefabricated roof trusses left the tops of walls with little lateral support. Removal of rafter/ridge-beam roofs typically left the separate ceiling joists in place; and thus the tops of the walls were still laterally supported. Truss to wall connection and connections within the trusses were important factors in the behavior of these homes.
- "High profile" roofs had relatively long unsupported spans (compared to other roof types) leaving them more vulnerable to uplift.
- The absence of observed houses sliding off of foundations in Moore can most likely be attributed to the requirement of anchor bolts securing the structure to the foundation.

Chapter 6 - Aerial Assessment of Damage

The methodology for this investigation consisted of assessing the May 20th, 2013 tornado damage using aerial images available through Google Earth. This software is equipped with a time history tool that allows the user to view a specific area at an arbitrary point in time (if images were captured at or close to that date). Using this time history tool, a user may view pictures of Moore that were captured on May 21, 2013, one day after the devastating tornado struck. This provides a complete aerial view of the tornado path from start to finish. Having access to the aerial image of the tornado path affords a unique opportunity to study the results of the storm, since it makes it possible to analyze patterns and behaviors that are not visible from ground level.

These tools may be utilized in many different ways in order to analyze the behavior of the May 20th tornado. In this section, aerial images will be used to evaluate the tornado on the basis of residential damage intensity. This assessment will span the entire length of the tornado path, from Newcastle to eastern Moore, and will include not only identifying buildings that suffered top-of-the-scale damage (EF4 – EF5), but also identifying buildings very nearby that were significantly less damaged. In order to carry out this evaluation, the path of the tornado was broken down a total of 5 distinct residential areas that were impacted. The path of the tornado and various residential areas influenced by the storm are indicated by labels in Figure 6.1. Note that these residential areas are arbitrary and approximate, but serve to give a general sense of the areas impacted by the storm.

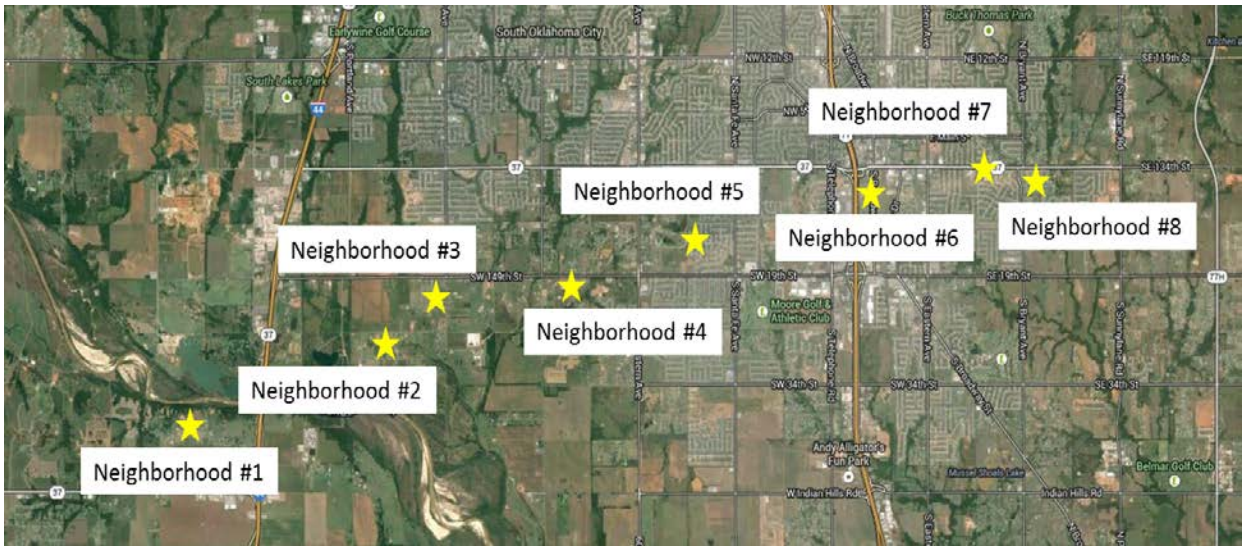

Figure 6.1, Neighborhoods and Labels.

6.1 Damage Intensity along Tornado Path

The purpose of this section is to examine the path of the May 20th tornado in order to identify areas where heavy damage occurred. The first inspected area of damage to residential structures caused by this tornado was observed in a small subdivision on NW 36th St. labeled Neighborhood #1 in Figure 6.1. Figure 6.2 shows a pre-event aerial view of this subdivision.

Figure 6.2, Location of first inspected neighborhood (Newcastle, OK).

The damage sustained by this neighborhood is shown in Figure 6.3. Although extreme, the tornado did not completely destroy the homes and left many walls still standing. It is interesting to note that the most severely damaged home in the neighborhood (completely leveled) is located very close to a home that was almost undamaged. This observation is illustrated in greater detail in Figure 6.4.

Figure 6.3, Damage in Newcastle neighborhood (NW 36th).

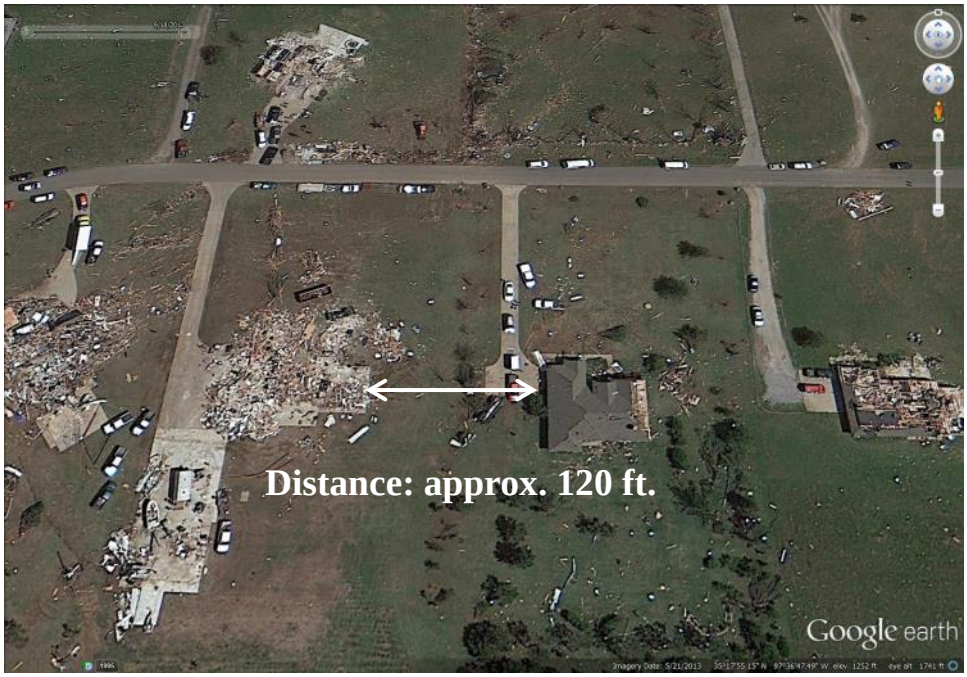

Figure 6.4, Damage Separation in Newcastle neighborhood (NW 36th).

The next residential area impacted by the tornado was located further to the northeast after the storm crossed the H.E. Bailey Turnpike (I-44). This neighborhood, labeled Neighborhood #2 in Figure 6.1, is located approximately 2.5 miles to the west of Moore. The pre-event view of this neighborhood is shown in Figure 6.5.

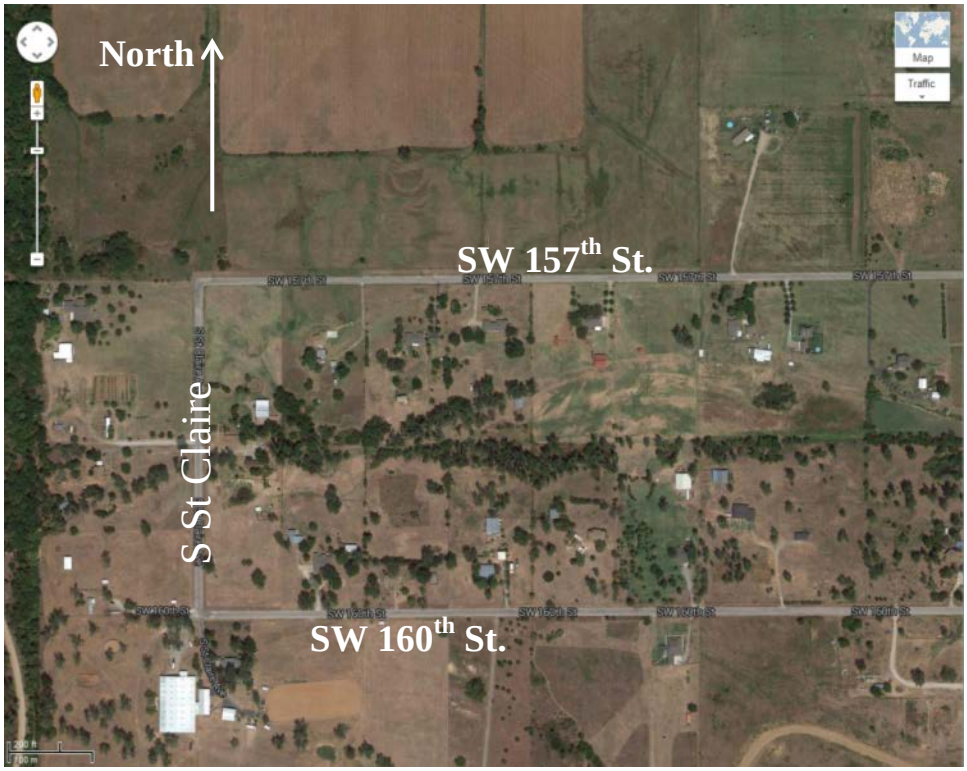

Figure 6.5, Neighborhood #2 Undamaged Condition (Sparse Residential Area Near Moore, Oklahoma).

An aerial assessment of Neighborhood #2 indicates that the damage intensity was low compared to areas to the west. A visual inspection of the post-event aerial image indicates that no homes in this neighborhood were completely leveled. The damage was not extreme, as seen in Figure 6.6 and Figure 6.7, in this neighborhood. The only home completely destroyed in this neighborhood was a single-wide mobile home, seen in the upper right-hand corner of Figure 6.6.

Figure 6.6, Neighborhood #2 – Damage 1

Figure 6.7, Neighborhood #2 – Damage 2

Up to this point, the tornado path can only be tracked by the presence of damage and debris spreading. Shortly after crossing the neighborhood at SW 157th and S St Claire, however, the tornado reached a level of strength high enough to leave a trail of bare soil. This transition is illustrated in Figure 6.8.

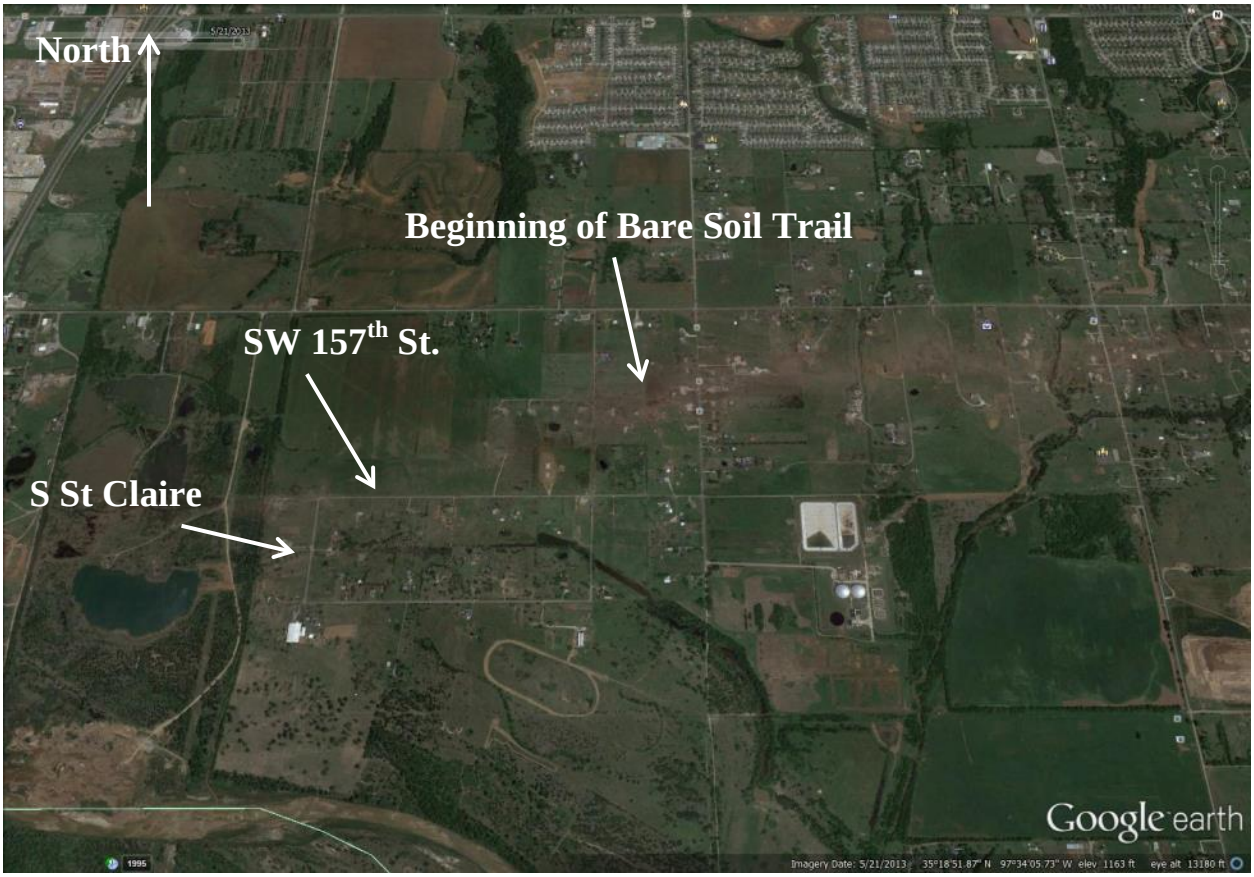

Figure 6.8, Beginning of Soil Trail

This simple observation also appears to mark a turning point in the severity of damage inflicted by the tornado. From the point that visual inspection from an aerial perspective indicates a bare soil trail, residential structures directly in the tornado's path appear to sustain more extreme levels of damage. This is readily illustrated by the damage to the residential area seen in Figure 6.9.

Figure 6.9, Neighborhood #3 Location and Undamaged Condition

The damage across the width of this neighborhood, which is labeled Neighborhood #3 in Figure 6.1, is shown in Figure 6.10 and Figure 6.11. Notice that at this point in the tornado path, the damage is very severe for most homes. Figures 6.12 and 6.13, 6.14 and 6.15, 6.16 and 6.17, 6.18 and 6.19, and 6.20 and 6.21 show the images before and after the tornado for Neighborhood #4, #5, #6, #7, and #8 shown in Figure 6.1, respectively.

Figure 6.10, Neighborhood #3 – Damage 1

Figure 6.11, Neighborhood #3 – Damage 2

Figure 6.12, Neighborhood #4 Location and Undamaged Condition.

Figure 6.13, Neighborhood #4 Damage

Figure 6.14, Neighborhood #5 Location and Undamaged Condition

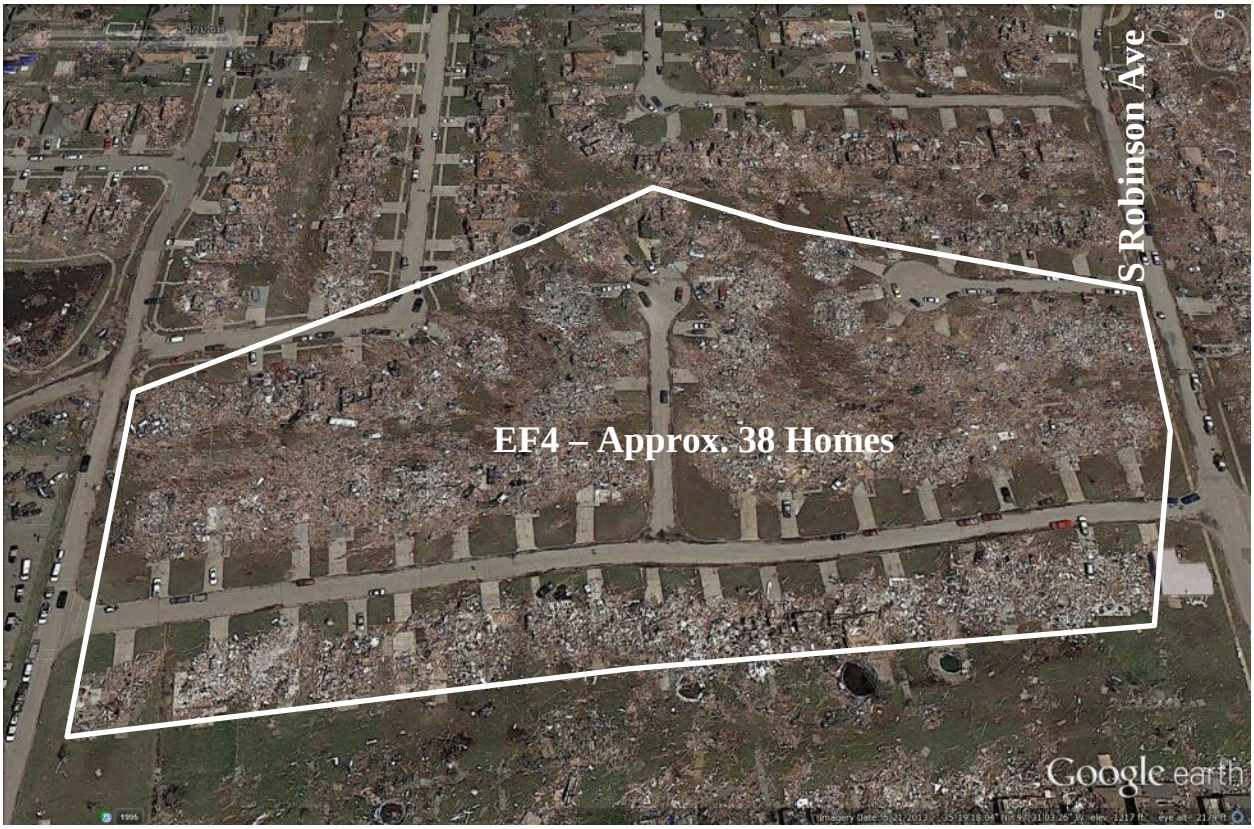

Figure 6.15, Neighborhood #5 – Damage overview

Figure 6.16, Neighborhood #6 Location and Undamaged Condition

Figure 6.17, Neighborhood #6 Damage

Figure 6.18, Neighborhood #7 Location and Undamaged Condition

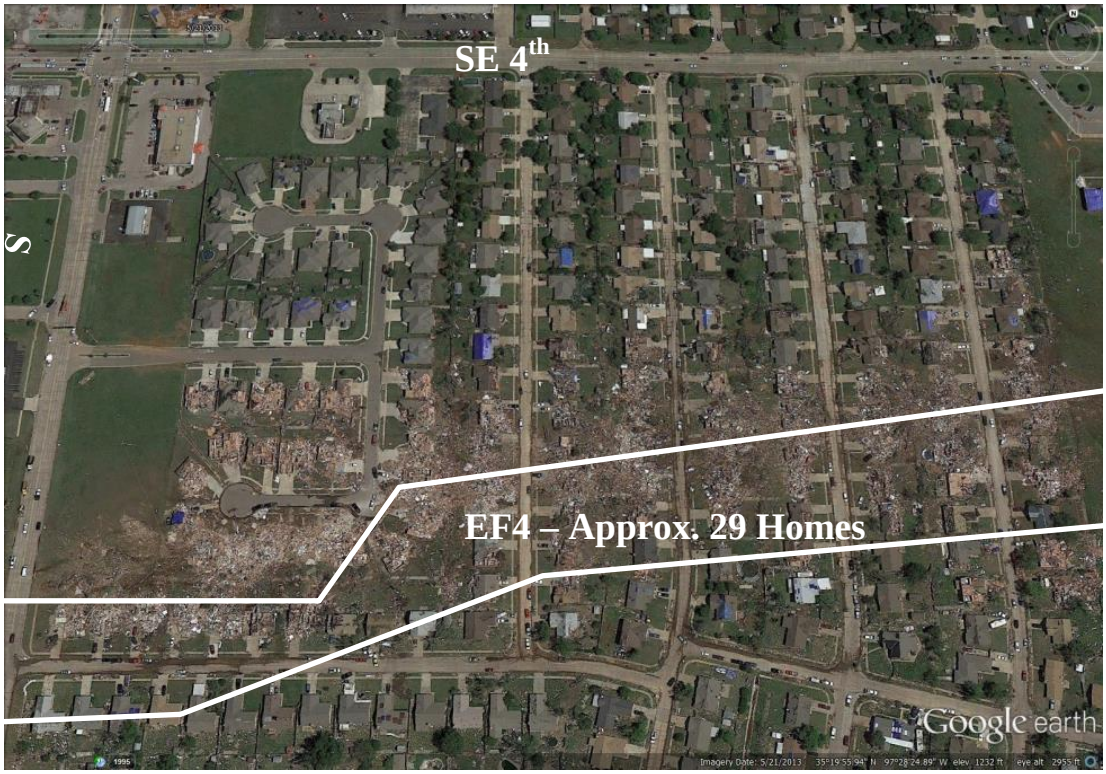

Figure 6.19, Neighborhood #7 Damage

Figure 6.20, Neighborhood #8 Location and Undamaged Condition

Figure 6.21, Neighborhood #8 Damage

6.2 Debris Flow Patterns Assessment Methodology

The same assessment methodology used in the aerial assessment of damage was employed to find the debris flow patterns. This methodology consisted of studying aerial imagery taken from Google Earth on May 21, 2013. This aerial assessment uses physical evidence left by the storm to investigate two specific topics related to debris patterns. First, the debris flow (the patterns and scattering of debris left by the tornado) and second is debris transport (the ability of a tornado to carry both light and heavy debris tremendous distances).

6.3 Observed Debris Flow Patterns

Debris flow refers to the pattern and final resting positions of debris after the event. The objective of this investigation was to study debris flow patterns in order to better understand wind behavior associated with a tornado and the relationship between wind direction and the direction of the tornado path. As Figures 6.22 through 6.25 indicate, the most common mode of debris flow in the May 20th tornado was very straightforward and highly consistent. In almost all cases where discernible debris flow was observed, the flow took the form of a "streaking" effect in the direction of the tornado path. In other words, trails of debris were laid out in thin lines from the debris source, pointing in the direction of the tornado travel. This pattern is seen consistently throughout this section. The only case where such behavior is not observed is in densely populated neighborhoods where there are too many debris piles to distinguish any streak lines. Each case of debris flow in this section is documented with two images. The upper image in each figure shows the pre-event undamaged condition, while the lower image of each figure shows the pattern of debris spreading (with arrows to indicate direction of flow). Debris trails, or streaking, are more evident in locations were the topography of the ground slopes downhill in the same direction as the tornado path (i.e. the elevation drops in the direction of the tornado path).

Figure 6.22, Debris Flow 1 -- Approximately Parallel to Tornado Path

Figure 6.23, Debris Flow 2 -- Spreading in direction of tornado travel

Figure 6.24, Debris Flow 3 -- "Streak Lines"

Figure 6.25, Debris Flow 4 – Debris Lines from Highland East

6.4 Old US 62 Steel Truss Bridge Debris Transport

When the tornado passed through this location, it generated sufficient force to destroy two spans of the bridge, knocking them off their piers and shredding the truss structure, as seen by comparing the pre-event photo, Figure 6.26(a), with the post-event photo, Figure 6.26(b).

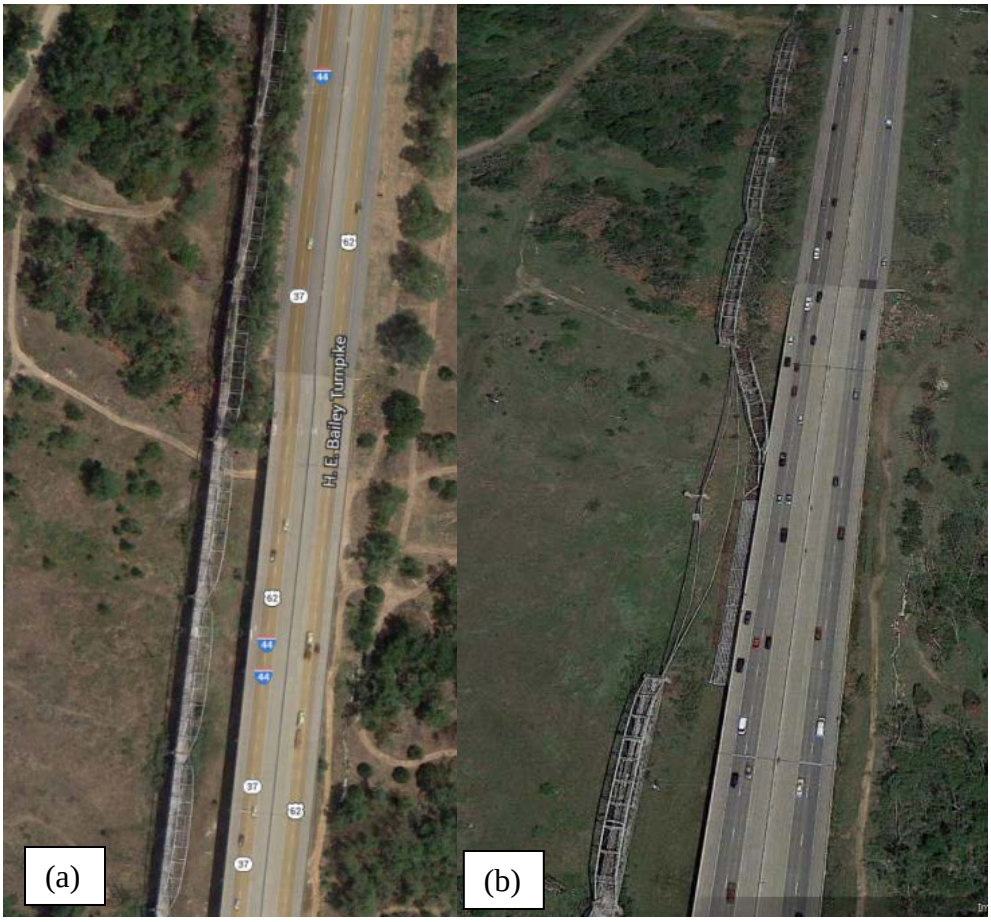

Figure 6.26, Old US 62 Steel Truss Bridge near I-44, (a) pre-event photo, (b) post-event photo.

The damage shown in Figure 6.26(b) indicates the strength of the tornado in terms of its ability to transport heavy debris. In this case, the power of the tornado is demonstrated by its ability to lift a bridge off of its piers and turn it upside down.

6.5 Oilfield Tank Farm Debris Transport

Among the many components of infrastructure destroyed by the May 20th tornado, several oilfield pumping and/or storage sites equipped with multiple storage tanks were hit. This generated identifiable debris that was scattered across the city of Moore. The largest tank farm (believed to be the source of this debris) is shown before and after the storm in Figure 6.27 and 6.28 respectively. This facility is located a few miles west of Moore on SW 149th.

After the tornado event, the facility was left in the condition shown in Figure 6.28. Six of the ten original tanks at the facility were carried away by the storm, and the tanks still on site were displaced and severely damaged. After the tornado struck this site, several of the tanks were torn loose and transported to various locations to the northeast along the path of the storm. The post-storm investigation identified several of these tanks in the city of Moore: one had been dropped on the roof of Briarwood elementary school and another landed in the yard north of Briarwood elementary school as shown in Figure 6.29. These resting places indicate a carried distance of roughly 4,400 feet. Resting places of this debris is shown in Figures 6.30 and 6.31.

Figure 6.27, Tank Farm Undamaged Condition.

Figure 6.28, Damaged Tank Farm

Figure 6.29, Tank Debris Transport

Figure 6.30, Oilfield Tank on Briarwood Elementary School Roof

Figure 6.31, Oilfield Tank on Briarwood Lawn

6.5 Aerial Damage Assessment Conclusions

This study generated several important conclusions based on an aerial investigation. First and foremost, the study demonstrated the tremendous benefit of having access to a comprehensive aerial overview of a tornado-impacted area. In addition to being crucial for search and rescue efforts in the first 24 hours after a destructive storm, access to aerial imagery is also useful for a comprehensive damage assessment. While certain failure mechanisms and damage patterns are best determined from ground-level, there are many patterns and behaviors that may be detected far more easily and accurately from the air. These patterns include overall direction of the tornado path, width of the damage path, flow and spreading of debris, long-distance transport of debris, and general distribution of damage intensity.

Of the behaviors and patterns listed above, the two behaviors of interest in this study were flow/spreading of debris and long-distance transport of debris. The first (and most obvious) finding of this report is that debris flow patterns are far easier to distinguish in relatively open areas. When damage occurs in a densely populated neighborhood, any pattern in

spreading of debris is difficult (if not impossible) to discern. The second finding is that, in general, debris most commonly flows in the direction of the tornado path. This flow is typically manifested by a series of "streak lines" where debris from a demolished structure spreads out in thin lines that point away from the source and towards the tornado travel direction. In the case of a small group of homes being destroyed, these thin lines of debris may even converge with one another as the tornado moves onto open ground. In this study, no cases were identified in which any well-defined pattern of debris flow occurred opposite to the direction of tornado travel.

An evaluation of debris transport patterns indicated that most heavy structural debris tends to be carried in the forward direction (parallel to tornado travel). This was evidenced by both the Old US 62 Bridge deck components and by the scattering of oilfield tanks across the city.

Chapter 7- Failure Progression, Fragility, and Laboratory Correlations

7.1 Failure Progression and Building Fragility within a Tornado Wind Field

Data collected from recent tornadoes in Tuscaloosa, Joplin, and Moore show a consistent pattern of damage to residential structures. For an EF4 or EF5 tornado, damage levels increase from the outer edges towards the center line of a tornado track. From the damage data collected, this study tries to explain the residential structure failure progression within a tornado wind field to get a better understanding of the correlation between tornado wind speed and structural damage. In general, the progression of residential structure failure often depends on wind speed, wind direction, windborne debris impact, and the capacity of building components.

7.1.1 Damage Pattern in a Tornado Path

General observation:

Residential building damage in tornados is caused by high wind loading or debris impact or both. Failure of residential buildings in tornado winds is often due to:

- Lack of continuous sheathing, fiberboard sheathing, lack of gable end sheathing, garages without anchor bolts.
- Lack of garage wall sheathing, a limited use of plywood with most of the sheathing fiberglass or hardboard siding.
- Observation from recent tornadoes (Tuscaloosa, AL, April 27, 2011 (van de Lindt et al, 2013); Joplin, MO, May 22, 2011 (Prevatt et al, 2012); and Moore, OK, May 20, 2013 shows that structures often did not have continuous load path from the foundation to the roof.

When a house was hit by windborne debris, the internal pressure changed causing progressive damage of the structure. The failure progression depends on where the debris impacts occurred; the relative location of the house to the tornado track; and the orientation of the house with respect to the tornado path.

Damage pattern in tornado wind field:

In order to document the damage due to tornadic wind, the assessment team collected damage data in a neighborhood at the western edge of Moore as indicated by the circle on Figure 7.1. This fairly new neighborhood was located on Kyle Dr. and SW 151st Street and was built around 2006. The buildings in this neighborhood were believed to be less affected by windborne debris because the tornado traveled from west to east, and west of this neighborhood the area is flat open fields with only a few residential houses with minimal damage. Therefore, it was believed that the damage to the houses in this neighborhood primarily came from tornado wind loading rather than debris impact. The houses in this area had similar structural configuration, which made it easier to identify the wind field from the damage patterns as compared to other areas.

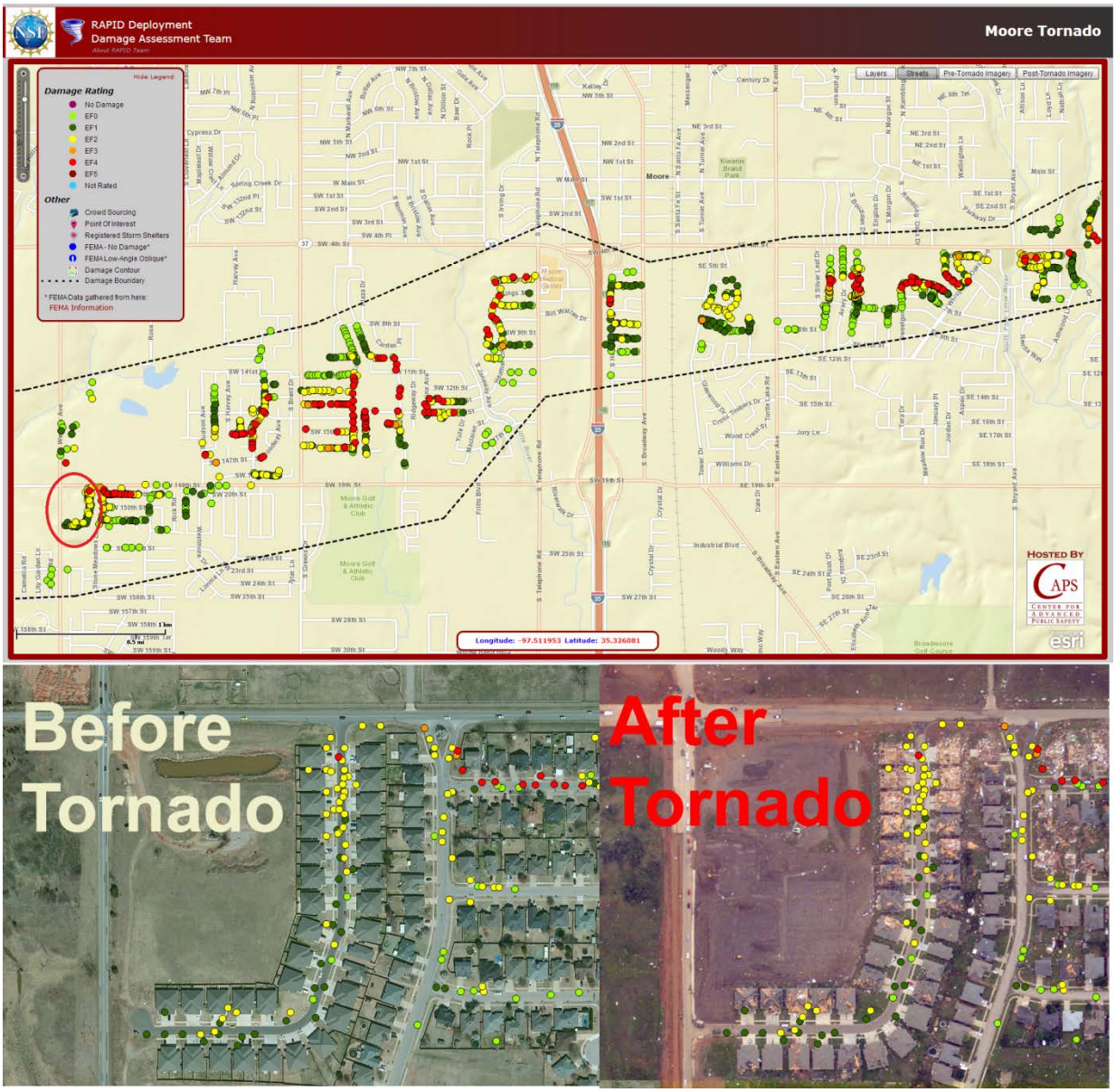

Figure 7.1, Neighborhood used in this discussion section.

Figure 7.2(a) shows the damage to residential structures on SW 151st Street looking west. This figure shows houses on both sides of the street, and one can see that all homes on the left side still have garage doors and sustained little or no damage, while homes on the right side of the street lost garage doors that blew inward. Since all the garage doors had similar design and were installed on rails inside of the door opening, the reinforcement bars are placed inside of the door, and these garage doors had higher capacity when experiencing negative pressure (outward load) as compared to lower capacity with positive pressure (inward load). This is because with the outward load case the load is transferred to the wall and rails through compression, while in

the inward load case, the rails failed by bending into the garage. With this reasoning, it can be seen from Figure 7.2(a) that the residential houses in this picture experienced mainly one wind direction as the tornado passed this street, and the garage doors on the left were on the leeward walls (negative wind pressure) while those on the right side of the street were on the windward walls (positive pressure). This behavior can also be seen on streets where the direction of the street changes, and the garage doors change from leeward to windward as shown in Figure 7.2(b). This means that when the tornado passed this area, these houses only experienced horizontal winds (the failure pattern was similar to straight line winds seen during hurricanes). For those houses having garage doors on the windward side in straight wind, the garage doors often fail before roof sheathing panels.

Figure 7.2, Different garage door damage levels (a) on both sides of SW 151st Street and (b) when house directions change.

Homes on Kyle Dr., a north-south street shown in the circled area on Figure 7.1, indicated an increase in damage to homes that are located closer to the center line of the tornado

track. This damage pattern is similar to what was observed in the aftermath of Tuscaloosa and Joplin tornadoes. Figure 7.3 shows the damage pattern of houses on the Kyle Dr. in which the camera was pointed to the south looking away from the centerline of the tornado. It should be noted that the tornado vortex was counter-clockwise and this neighborhood was on the south side of the tornado center line. Therefore, the houses on the south edge of the damage area experienced west-to-east winds, which is right-to-left in Figure 7.3. In Figure 7.3, the houses on the right side (west) near the middle of the street had the roof fail before the garage door failed. Failure of the roof happened on the leeward side of the roof and the roof was intact on the windward side. The garage doors, on the leeward side, were not damage on these homes. Similar damage was observed on the roof of the houses on the left side (east) of the street (failure happened on the leeward roof, intact on the windward roof), but the garage doors on the left side of the street all failed. This is because roof sheathing panels are weaker in uplift and stronger in compression due to nail withdrawal capacity. This failure pattern indicated that these houses experienced higher wind speed than at the edge of damage area and mainly in one direction of horizontal winds. It can also be seen in Figure 7.3 that garage doors and roofs failed on both sides of Kyle Dr. to the north where the photo was taken and several walls were collapsed in the house on the north-east end of Kyle Dr., far left in Figure 7.3.

Figure 7.3, Damage pattern on Kyle Dr., Moore, Oklahoma (Camera pointed to the south).

A closer inspection near the northern segment of Kyle Dr. indicated that the homes in this area experienced wind in one direction, as shown in Figure 7.4. Again, the house on the left had roof failure and the garage door survived, while the house on the right had the garage door blown in and only a minimal amount of sheathing panels failed.

Figure 7.4, Failure of roofs and garage doors on (a) west side and (b) east side of Kyle Dr.

7.1.2 Failure Progression in Residential Structures

To explain the different types of structural failure observed within a tornado wind field, a sketch of a tornado wind field is introduced in Figure 7.5. This sketch is based on the residential building damage that was observed in the aftermath of several tornadoes. In large tornados, the damage area along the tornado track can be divided into three bands. In Figure 7.5, Band 1 is the area right outside of the tornado core, in this area, buildings often experience straight winds in one direction, and the damage to residential structures is similar to what was observed in hurricane winds: garage doors fail on the windward side and some roof sheathing fails on the leeward side, as seen in Figure 7.2. In Band 1, the wind velocity has a much larger horizontal than vertical component. Band 2 is where the wind field in a tornado has significant vertical wind and the horizontal wind is also strong. A building in Band 2 experiences horizontal winds in two different directions as the tornado moves over the building. As can be seen in Figure 7.5, buildings in Band 2 also experience straight line wind before transitioning into a horizontal plus vertical wind filed. Therefore, buildings in Band 2 often have failure of garage doors on the windward side and the roof damage on both windward and leeward sides. This failure pattern is because uplift occurs on both sides of a roof as seen in Figure 7.4. Buildings in Band 3 often have higher damage levels not only due to higher wind speeds at the core, but also because the building experiences winds from all directions. As the tornado passes over a building, horizontal winds will go in two opposite directions. In addition, buildings in Band 3 also experience large uplift wind suction. Damage to buildings in Band 3 is extreme and often consists of roof loss, exterior wall loss, interior wall loss, and even total destruction of the structure.

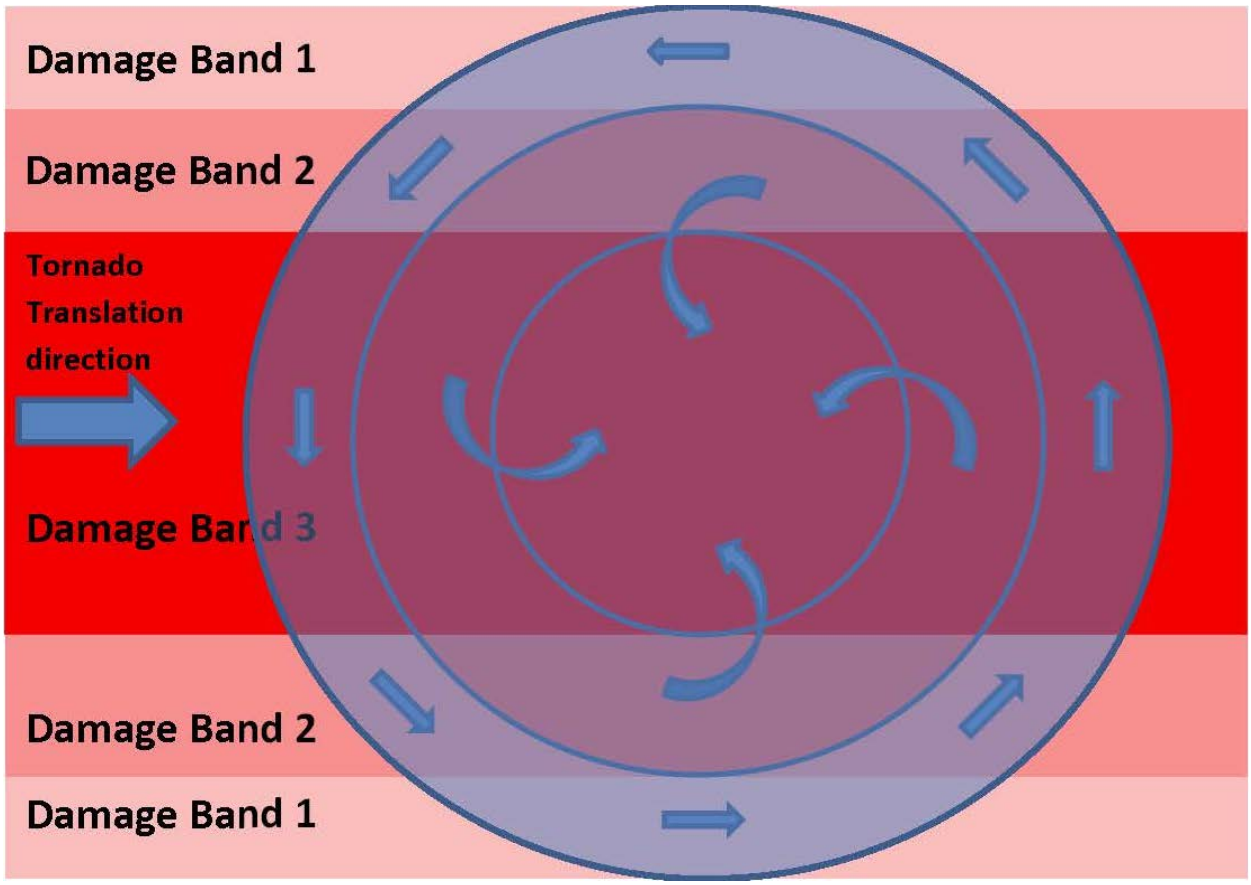

Figure 7.5, Damage zone on a large tornado track.

7.1.3 Building Component Fragility

In order to make a quantitative assessment based on the structural failure progression discussed above, this section introduces some conditional fragilities based on several previous studies. In general, the failure probability can be defined through the expression of the following limit state function:

$$P[G(X)<0]=\sum_{y}P[G(X)<0|D=y]P[D=y] \tag{7.1}$$

where D is the random variable representing the demand on the system (e.g., 3-sec gust wind speed) and $P[D=y]$ is the natural hazard probability, $P[G(X)<0|D=y]$ is the conditional limit state probability, and denotes the so-called fragility (Ellingwood et al, 2004). For roofing components, the limit state function $G(R, W, D) = R – (W – D)$, where R is component resistance, W is wind load and D is dead load. For lateral wind load bearing component such as shear walls or garage doors, there is no dead load component in lateral direction, therefore the

limit state function $G(R,W) = R - W$ was used to calculate the fragility. Component fragility functions were constructed for a typical house along Kyle Dr. in Moore, OK. The house has a plan area of 35ft × 35ft and the mean roof height of 16 ft and a roof slope of 35^o. The un-factored wind load applied on low-rise building components and cladding can be computed as:

$$W = q_h \left[GC_p - GC_{pi} \right] \tag{7.2}$$

where q_h is the velocity pressure evaluated at the mean roof height, G is gust factor, C_p is external pressure coefficient and C_{pi} is internal pressure coefficient. The velocity pressure is calculated following ASCE-7 (2010) as:

$$q_h = 0.00256 K_h K_{zt} K_d V^2 \tag{7.3}$$

where K_h is the exposure factor, K_{zt} is the topographic factor (taken equal to unity so as not to make the results dependent on local topography surrounding the building); and K_d is the directional factor (in this study, because the wind direction is determined from Figure 7.5 and was not considered as a random variable, K_d is set to unity); and V is wind velocity, i.e. basic wind speed. The statistics of the component resistance (or capacity) is listed in Table 7.1 for different building components and Table 7.2 lists the statistics of the dead load and the wind load parameters used in this study. For wind load in damage Band 2 and damage Band 3, the total pressure coefficient is scaled by a factor K_c to accounts for vertical wind velocity pressure increases (van de Lindt et al, 2013) based on the study by Haan et al. (2010).

Table 7.1, Resistance statistics of building component.

Building component	Capacity			Source
	Mean	COV	Distribution type	
Roof cover (asphalt shingle)	51 psf	0.4	Normal	Cope (2004)
Garage Door	52 psf	0.2	Normal	Cope (2004)
Roof Sheathing	69 psf	0.22	Normal	van de Lindt et al. (2013)

Table 7.2, Load Statistics.

Variables	Statistics parameters			Note
	Mean	COV	Distribution	
Dead Load D	3.5 psf (168 N/m^2)	0.10	Normal	Lee and Rosowsky, 2005
K_h	1	0.14	Normal	Lee and Rosowsky, 2005
GC_p (C&C)			Normal	
Roof Zone 1	0.855	0.12	Normal	Based on ASCE 7-10 and
Roof Zone 2	1.615	0.12	Normal	Ellingwood et al (2004).
Roof Zone 3	2.470	0.12	Normal	
Wall Zone 4	0.900	0.12	Normal	
GC_{pi}				
Enclosed	0.15	0.33	Normal	Lee and Rosowsky, 2005
Partially enclosed:	0.46	0.33	Normal	

Figure 7.6 presents fragility functions for different components of a building in damage Band 1, shown in Figure 7.5. The fragility functions of these building components were calculated with the condition that the building had no windward window broken or garage door failure (the internal pressure does not change and the building remains partially enclosed). It was also assume that in damage Band 1, the vertical component of wind velocity was small and the wind load applied on the building components is similar to straight wind. The wind load was calculated based on Equation (7.2). From the fragility functions shown in Figure 7.6, it can be seen that roof cover (asphalt shingles) often fail first. If one looks at the median value, 50% roof cover loss in roof zone 3 (corner, defined by ASCE7 for C&C) occurs around EF1 wind speed and 50% roof cover loss in roof zone 2 (roof edge, defined by ASCE7 for C&C) occurs around EF2 wind speed. In partially enclosed buildings, roof sheathing panels in roof zone 3 often starts to come off in EF1 to EF2 wind speeds.

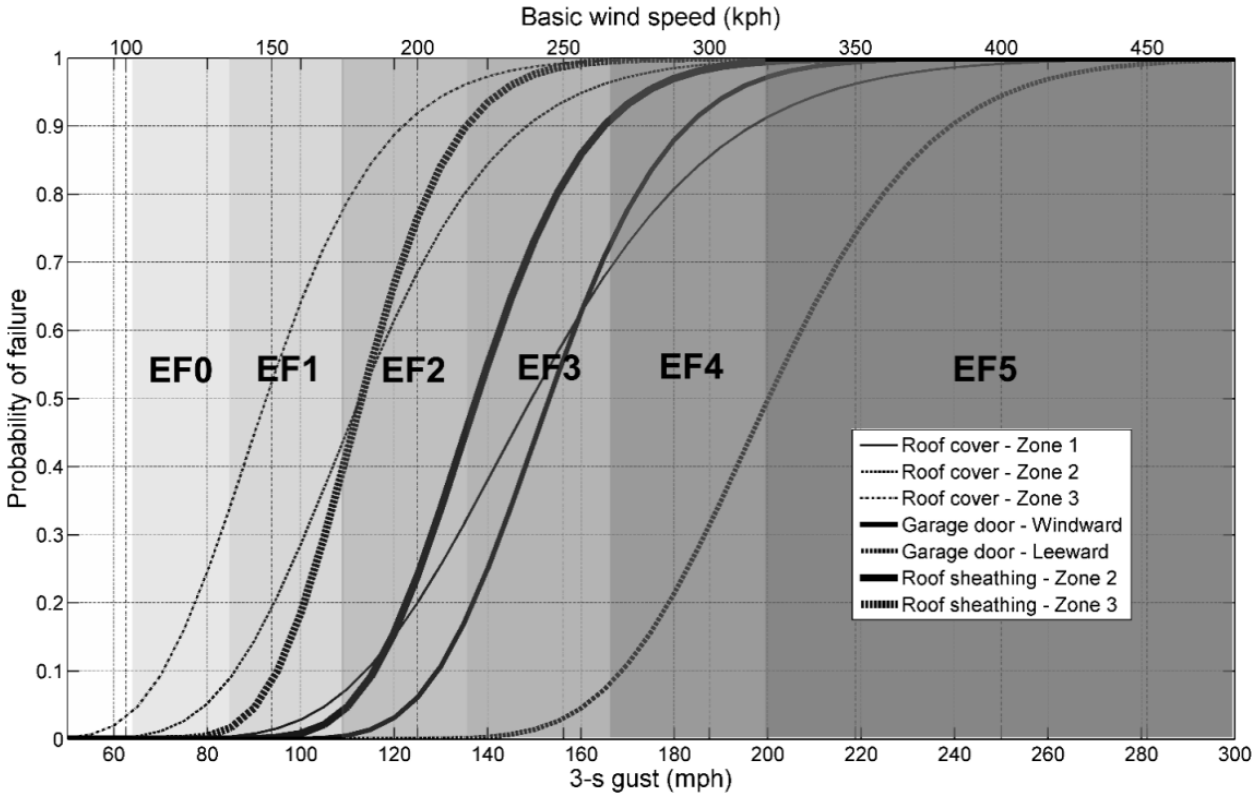

Figure 7.6, Component fragility in damage Band 1, partially close building.

Broken windows and garage door failures were observed in many buildings in damage Band 1, which has a major impact on the internal building pressure. Figure 7.7 shows the fragility of roof cover and roof sheathing panels in partially open buildings, in which the mean value of internal pressure coefficient changes from 0.15 to 0.46 (Table 7.2). In partially open buildings in damage Band 1, 50% of the roof cover in zone 3 and zone 2 often fails around EF1, and 50% of roof sheathing panels in zone 3 and zone 2 fails around EF2 wind speeds. Recall that in damage Band 1, the wind load does not include the effect of vertical wind velocity pressure increases.

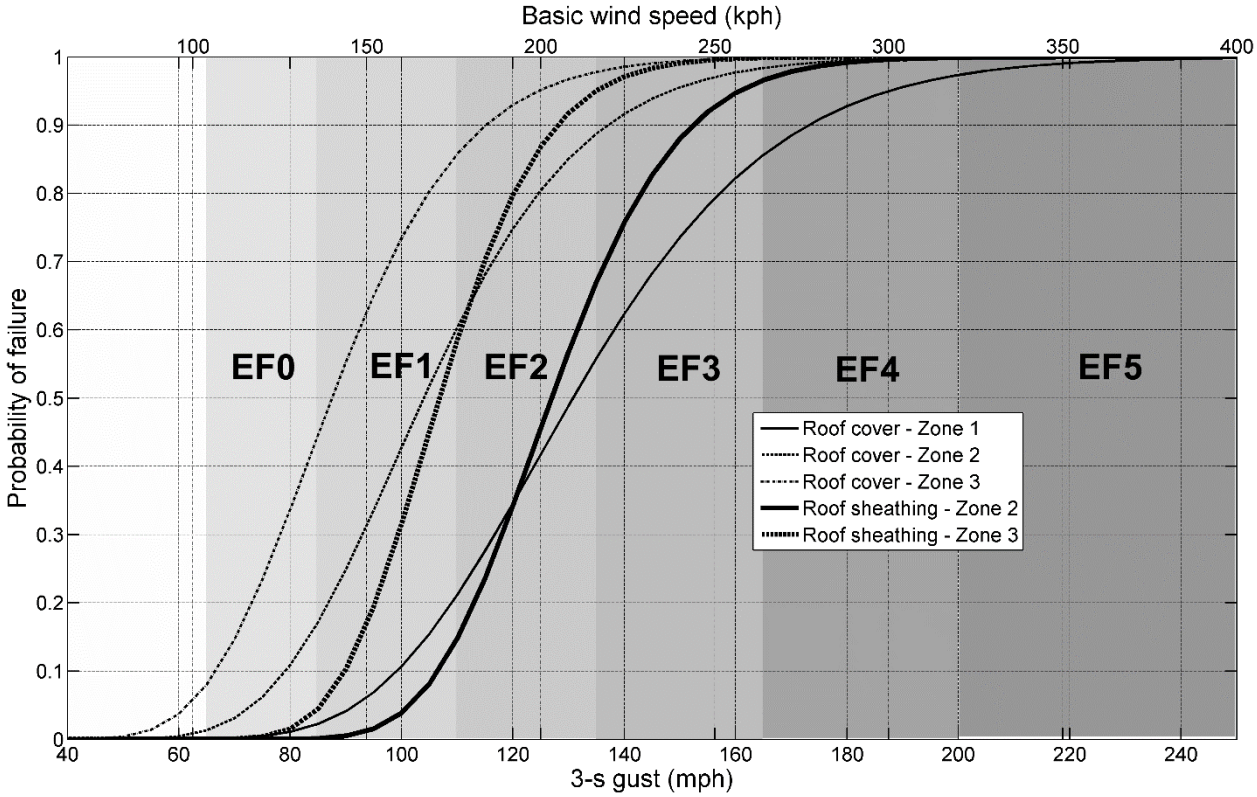

Figure 7.7, Component fragility in damage Band 1, partially open building.

In damage Band 2, broken windows and garage door failures were observed in most of the buildings. The fragility functions in Figure 7.8 are presented for roof cover and roof sheathing panels in roof zone 2 and 3, and garage door windward and leeward walls in partially open building in damage Band 2. Recall that in damage Band 2, calculated wind load includes the effect of vertical wind velocity pressure as a result of the high vertical component of wind speed in a tornado. It can be observed from this figure that up to 96% of roof sheathing panels in roof zone 3 and 72% of roof sheathing panels in roof zone 2 fail at wind speed EF1 range, much higher than 60% of roof sheathing panels in roof zone 3 and 15% roof sheathing panels in roof zone 3 in buildings in damage Band 1. For wind load in damage Band 2, the factor K_c was taken as a uniformly distributed random variable range from 1.4 to 1.8.

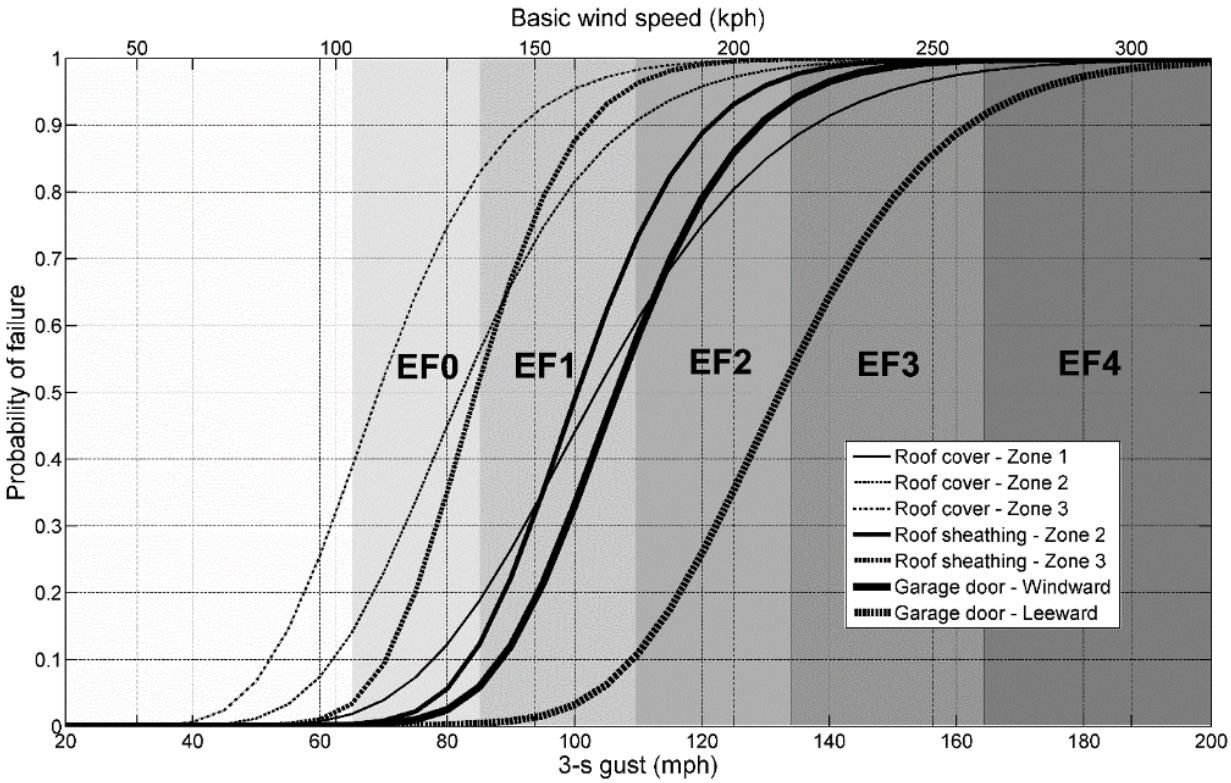

Figure 7.8, Component fragility in damage Band 2, partially open building.

Because of the higher vertical wind speed component in damage Band 3, in wind load calculations, the factor K_c was taken as a uniformly distributed random variable with a range from 1.8 to 2.4. Figure 7.9 shows the fragility function for components of partially open buildings in damage Band 3. It can be seen in Figure 7.9 that at EF1, almost 100% of roof sheathing panels in roof zone 3, and up to 93% of roof sheathing panels in roof zone 2 failed. These values were also higher than those of buildings in damage Band 2. It should be noted that garage doors designed for straight wind speed of 140 mph (Figure 7.6) would fail at tornado wind speed of EF1 to EF2.

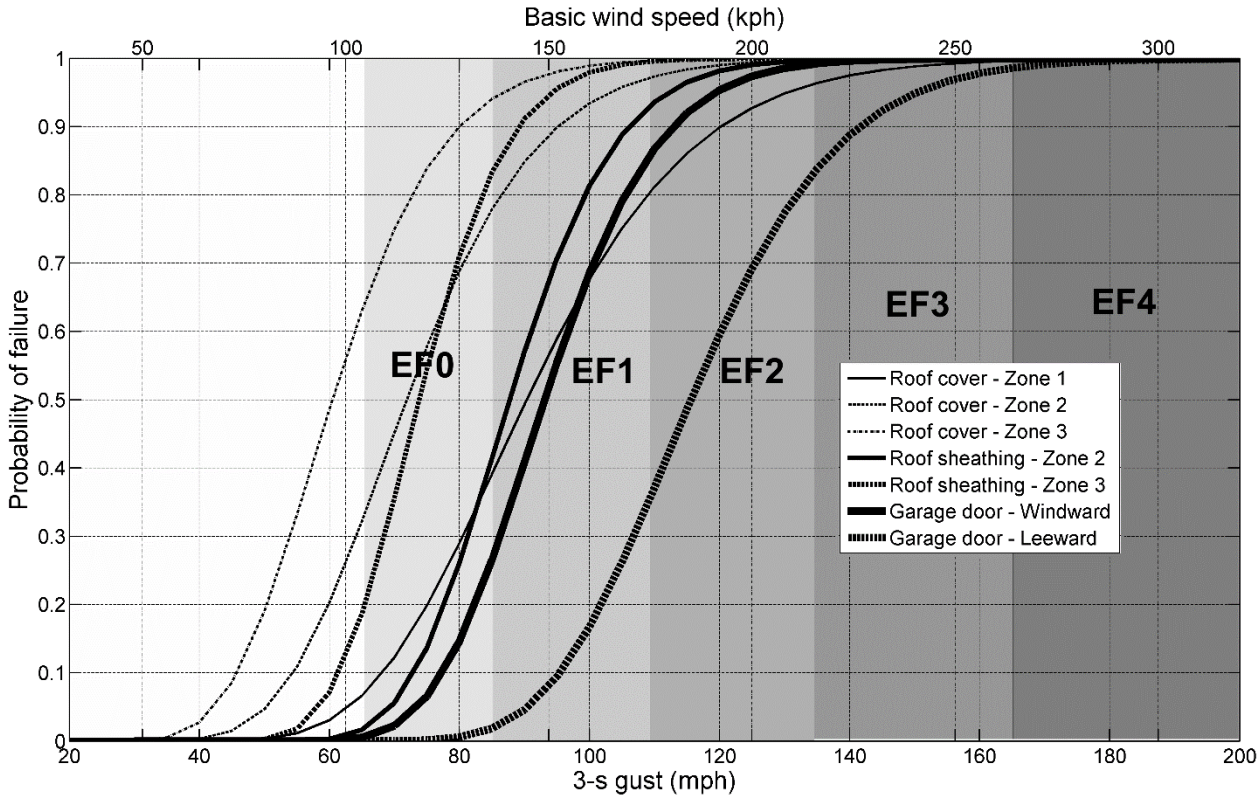

Figure 7.9, Component fragility in damage Band 3, partially open building.

It can be seen from the fragility functions presented in Figures 7.6 through 7.9 that with the same damage observed, the buildings may experience different lateral wind speeds in different damage bands. The observed damage depends not only on the relative location of the buildings to the tornado core, but also the building failure progression.

7.1.4 Fragility Analysis Conclusions

Analysis of building damage patterns after the May 20, 2013 Moore, Oklahoma tornado showed that the failure progression of residential structures within a tornado wind field depends on the relative location and orientation of the house to the tornado track. Specifically, if similar damage is observed, two different structures may have experience different wind speeds if located at different relative distances from the center-line of a tornado track. Also, different damage levels can be seen for structures at the same relative location to the center-line of a tornado. This can be caused by differences in house orientation (garage door/windows on the windward versus leeward side) and/or windborne debris impact, which leads to a change in internal wind pressure. The distance from the centerline of a tornado and the orientation of a

building should be considered when making predictions of tornado wind speed from observed residential structural damage.

7.2 Using Tornado Damage Surveys to Improve Laboratory Simulations

Laboratory tornado simulators were developed decades ago to study tornado vortices. In the past ten years, however, laboratory simulators have been employed for the new task of estimating tornado-induced wind loading on structures. If some structures are to be designed to withstand tornado wind loads, the mechanisms and magnitudes of these loads must be understood. To design a safer home, to design a tornado-resistant hospital or power plant, to design safe buildings, a laboratory simulator with model structures can be used to estimate wind loads. While several facilities for conducting such work are operational or in various stages of development around the world (at Texas Tech: Mishra et al. (2008), in Canada: Natarajan and Hangan (2012), and in Japan: Sabareesh et al. (2012)), this section summarizes a comparison of the tornado damage observed in Moore to the residential building loads measured at Iowa State University. More details of the work from Iowa State can be found in Haan et al. (2010).

Validating such a facility is a challenge due to the difficult and dangers of placing instrumentation in the path of a tornado vortex. Ideally validation would consist of an instrumented house or other structure being hit with a tornado. Since this is nearly impossible from a practical standpoint, other validation approaches must be employed. Past validation attempts have been made using radar data and ground pressure data (see Haan et al. 2008). Geo-located structural damage data from an event such as the Moore tornado presents another validation possibility. This section of the overall report compares laboratory estimates of tornado-induced loading with structural damage observed in Moore with the purpose of improving such simulations for the future.

This section is organized into three subsections. The first summarizes the experimental approach of the laboratory tornado simulator, the second summarizes the character of tornado-induced wind loading and the scaling required to relate the laboratory to the field, and the third subsection discusses the comparisons between the Moore damage and the laboratory estimates.

7.2.1 Details of the Experimental Approach

The experimental approach involved use of the tornado simulator at Iowa State University. This section will describe the simulator, the gable-roof model used in these tests, and the test conditions included in this analysis.

Tornado Simulator Facility

Iowa State University houses a tornado simulator that was conceived and built for testing model structures in tornado-like vortex flows. The facility consists of a 6 ft (1.83m) diameter fan surrounded by an 18 ft (5.49m) annular duct. The *fan* is fixed in the middle of the facility and draws air upward. This upward flow is redirected back downward through the annular duct. The downward flow is given rotation with adjustable guide vanes. The rotating inflow forms a vortex beneath the fan near the updraft. This vortex-generation mechanism is qualitatively similar to that of full-scale tornadoes. The fan and duct system is mounted on an overhead crane to allow the vortex to translate past models that are mounted on a ground plane beneath the system. Figure 7.10 shows the system in the laboratory. Further details of the facility development are described in Haan et al. (2008).

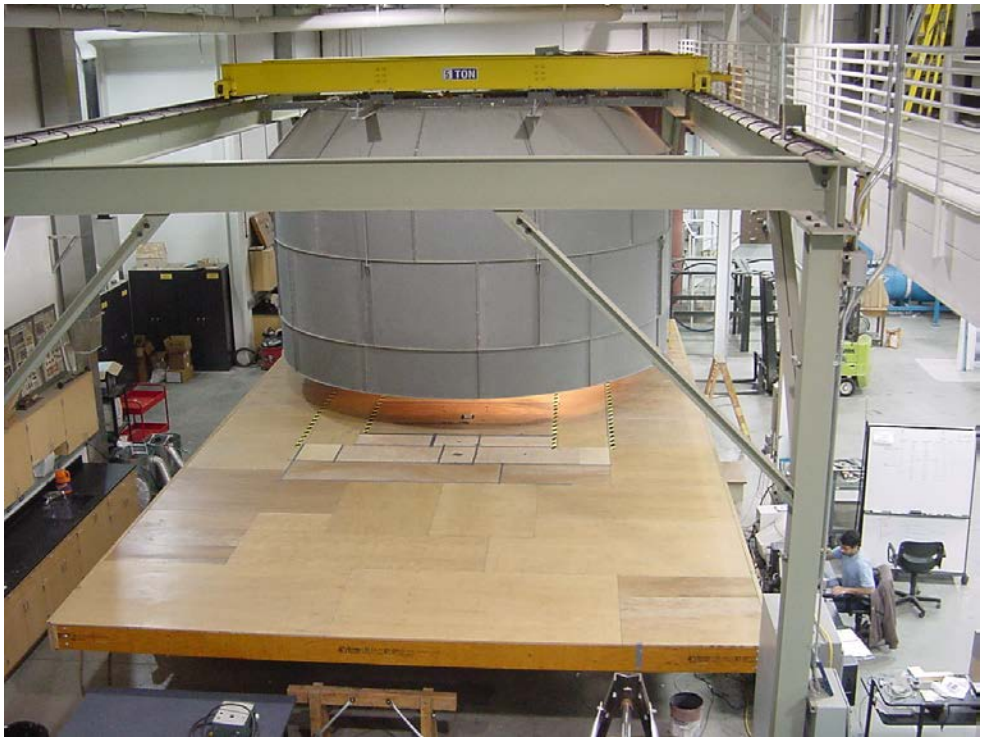

Figure 7.10, Tornado/Microburst Simulator at Iowa State University

Gable-Roof Building Model

The building model used in these tests was fabricated from acrylic and had plan dimensions (D) of 91mm by 91mm (3.6 in. by 3.6 in.). The eave height was 36mm with a maximum roof height (H) of 66mm (2.6 in.). The gable roof angle was 35°. The model is shown in Figure 7.11 and was fitted with 89 pressure taps. These taps were connected by plastic tubing to a Scanivalve electronic pressure scanner and a PC. All signals were corrected for the dynamic effects of the tubing. The building model itself is rigid and did not simulate any dynamic effects.

Figure 7.12 shows the numbering system for the pressure taps on the building as well as the coordinate system. All vortices travel from the negative to positive x-direction and approach the building at an angle, θ, as indicated. All vortices rotate counter-clockwise.

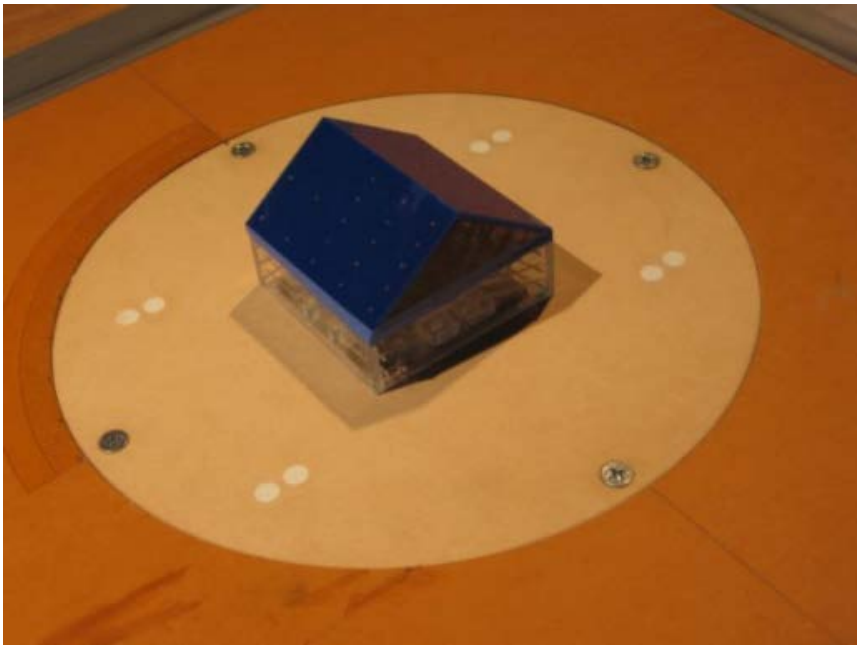

Figure 7.11, Gable-roof building model used in the tornado simulator tests.

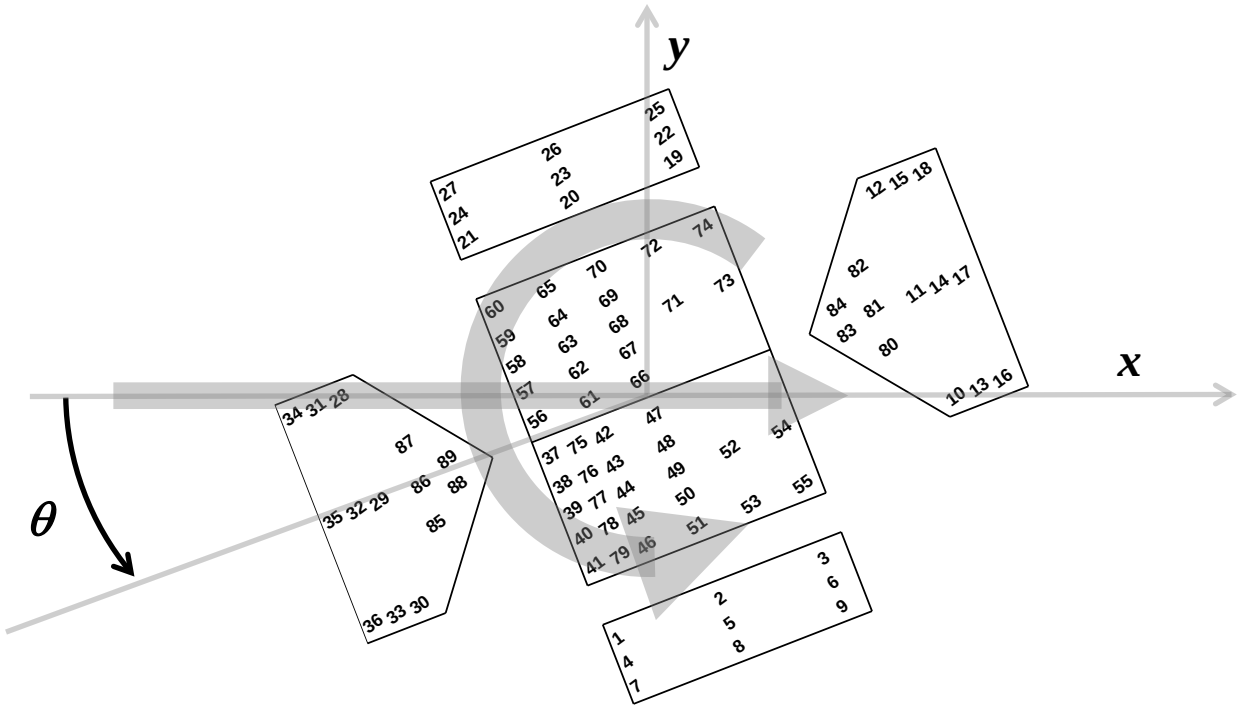

*Figure 7.12, Building model schematic showing pressure tap numbering, the x and y direction definitions, and the approach angle (**θ**) definition. The large arrows indicate the translation and rotation directions of the vortex; the vortex translated through the center of the building for all tests.*

Test Conditions

The building model has been tested in a range of vortex conditions. Vortex structure and size, vortex translation speed and vortex approach angle have all been varied. Table 7.3 summarizes the two vortex configurations that were included in this damage comparison—both the largest and the smallest swirl ratio vortices that the simulator can generate. The swirl ratio is a relative measure of rotation and axial flow rate through a vortex. Changing the swirl ratio changes both the radius and the structure of the vortex. More details on swirl ratio can be found in Haan et al. (2008). The vortex translation speed for this test was 0.5 ft/sec (0.15 m/s) and the approach angle (at which the vortex approached the building) of 0°. In the future, more conditions might be considered to statistically bracket the range, but this limited data set was chosen to simplify this first validation attempt.

Velocity measurements on these vortices were performed using a TFI Cobra probe located at the same position as the model but with the model absent. A 3-sec. averaging time

was used to quantify the gust velocities in the vortex as it translated past the building model location. Table 7.3 shows the maximum 3-sec. horizontal velocities acquired in these tests. These velocities were used to scale the measured wind loads to full scale. More details on velocity measurements can be found in Fleming et al. (2013). These velocities were also used (along with the building height) to estimate the Reynolds numbers of the building model tests. In this project, the Re values ranged from 3.9×10^5 to 5.2×10^5—it has conventionally been assumed that sharp-edged bluff body flows are relatively independent of Re effects for Re greater than ~3×10^4.

Table 7.3, Parameters for the tornado-like vortex used in the project. R_c is the radius of the vortex at the location of maximum tangential wind speed, Re is the Reynolds number based on building height, and R_c/D is the ratio of the vortex radius to the building plan dimension.

Vortex Type	V_{Hmax} (m/s)	Swirl ratio	R_c (m)	Re	R_c/D
V15	8.87	0.08	0.18	3.9×10^5	2.0
V55	11.86	1.14	0.51	5.2×10^5	5.6

7.2.2 Character of Tornado-Induced Loading

This section describes the character of tornado-induced loading while the next section describes how loads measured in the lab can be extrapolated to full-scale values. One way to conceive of the mechanism of tornado-induced pressures on a building is to think of pressures being generated both from the typical effects of wind and from the effect of the negative static pressure that is generated in the core of a tornado vortex. The effect of the static pressure drop in the core can be seen from any of the pressure time series from these tests. They all have a similar large drop right as the vortex passes. Example pressure signals are shown in Figure 7.13 from a wall tap and from a roof tap. These examples with the large pressure drop are typical of every pressure tap.

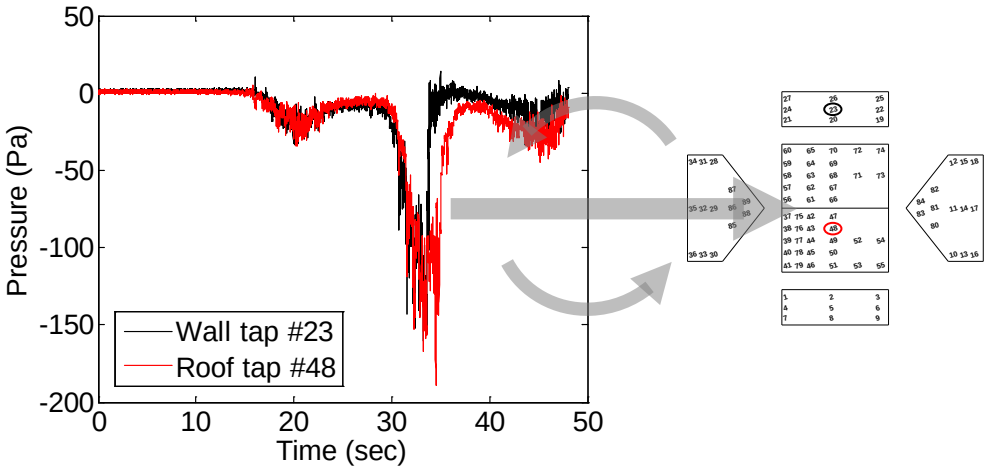

Figure 7.13, Example time series from a wall pressure tap and a roof pressure tap showing the large drop in pressure that occurs as the vortex passes the building. The large arrows indicate the direction of translation and rotation of the vortex.

The effect of the wind can be seen fairly clearly in the integrated forces. When pressure signals like those shown in Figure 7.13 are integrated over the building surface, forces can be estimated. Figure 7.14 shows coefficients for three components of force as the tornado vortex passes the building. As the leading edge of the vortex core interacts with the building, the building is pushed in the +y direction. As the trailing edge of the core passes, the building is pushed in the –y direction. The large uplift force (+z) shown in the figure is generated by the static pressure drop in the core.

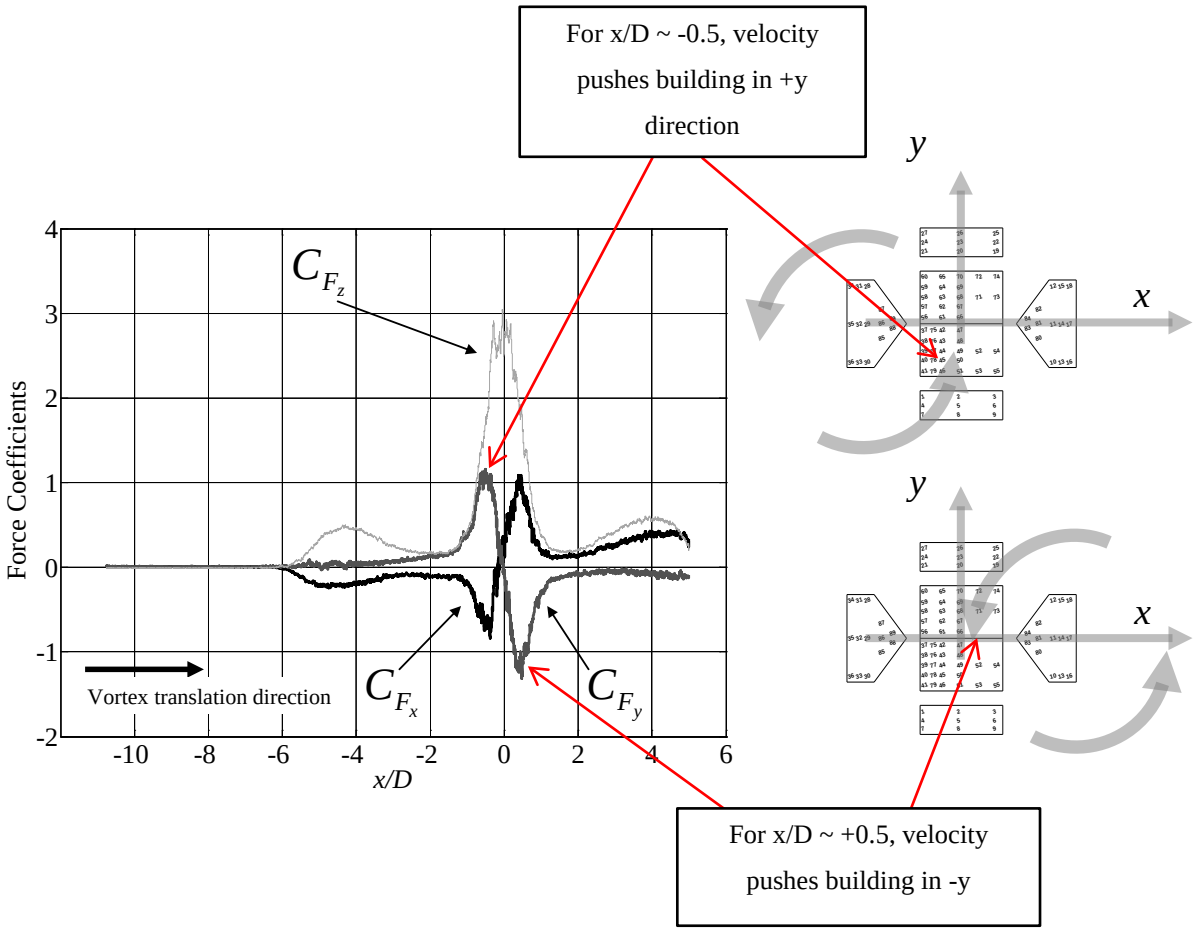

Figure 7.14, Overall tornado-induced forces estimated from integrating pressures about the building model. The effect of the wind velocity can be seen most clearly by looking at $\boldsymbol{C_{F_y}}$*. Just before the vortex center hits the building (negative value of x/D), the vortex velocity pushes the building in the positive y-direction. Just after the vortex passes, the vortex velocity pushes in the negative y-direction.*

7.2.3 Scaling Laboratory Data to Full Scale

Estimating full scale wind forces from laboratory measurements relies on the assumption that the force coefficients at full-scale and at model scale are equivalent as shown in Eq. (7.4) below. The subscripts "fs" and "m" stand for "full scale" and "model," respectively.

$$C_{F_{fs}} = C_{F_m} \tag{7.4}$$

These coefficients can be expressed in terms of forces, F, velocities, V, and areas, A, as:

$$\frac{F_{fs}}{V_{fs}^2 A_{fs}} = \frac{F_m}{V_m^2 A_m} \tag{7.5}$$

If equation (7.5) is rearranged as follows, the full-scale force estimate can then be expressed in terms of the length and velocity scales (λ_L and λ_V, respectively) as follows:

$$F_{fs} = F_m \frac{V_{fs}^2}{V_m^2}\frac{A_{fs}}{A_m} = F_m \frac{1}{\lambda_V^2}\frac{1}{\lambda_L^2} \tag{7.6}$$

The forced measured in the wind tunnel is a function of the radial distance, r, from the center of the vortex. F_m represents the vector sum of the three components of force on the building model as shown in Eqn. (7.7).

$$F_m(r) = \sqrt{F_x^2(r) + F_y^2(r) + F_z^2(r)} \tag{7.7}$$

The length and velocity scales were found from the parameters of the Moore tornado itself. The length scale was estimated by examining a plot of assessed damage level versus distance from the center of the vortex. It was assumed that the worst damage would occur within the radius of maximum wind speed—the edge of the "core" of the vortex. Therefore, the mean distance to the EF4 damage was used as the core radius for the Moore tornado. This distance was 490 ft (149m). Calculating a length scale, λ_L, between the size of the Moore vortex and the size of the laboratory V55 vortex produces a value of 1/295. At this scale, the building model represents something like a large industrial building or an apartment building.

The velocity scale was found by comparing the Moore vortex peak speed to the maximum horizontal velocity peak measured in the laboratory. The peak Moore wind speed was reported to be 210 mph (94 m/s)—as discussed in Chapter 1—and the laboratory peak was 11.86 m/s as shown in Table 7.3. This results in a velocity scale, λ_V, of 1/7.5.

An example plot of $F_{fs}(r)$ computed with Eqn (7.6) for one simulator trial is shown in Figure 7.15. A total of ten simulator trials were conducted for this case, and data from all ten trials were included in the statistics discussed in the next section.

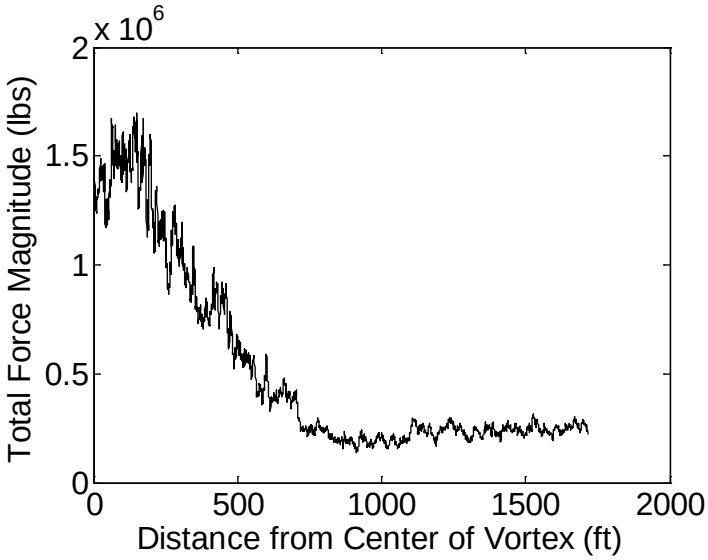

Figure 7.15, Example of full-scale tornado-induced wind loading ($\boldsymbol{F_m}(\boldsymbol{r})$) estimated from laboratory measurements. The incidence angle is 0° and the vortex type was V55. This example represents one of ten runs conducted at this condition.

7.2.4 Comparison between Field Damage Data and Laboratory Estimates

This section presents a comparison between the full-scale force estimates that were derived from laboratory measurements and the damage assessments performed in Moore. The section describes the data reduction procedure followed to make a reasonable comparison between the two, and it discusses the comparison itself and what implications it might have for how we interpret the laboratory simulations.

EF ratings from the 20 May 2013 Moore tornado were plotted as a function of distance from the center of the vortex. These ratings are shown in Figure 7.16. To compare force prediction data sets (such as the example shown in Figure 7.15) with the EF ratings assessed from the Moore damage surveys, some data reduction was conducted to make sense of the comparison. First, statistics were computed for each distance from the vortex center—specifically, from all 10 runs of the simulator, the mean, 25th percentile, and 75th percentile forces were calculated.

Second, it should be noted that a fragility curve type of relationship between forces and damage was not used in this case. Rather the force data were normalized such that the largest of these mean forces was given an EF rating of 4. This normalization makes an implicit assumption that the largest forces measured in the lab corresponded to the largest damage observed in the

field.

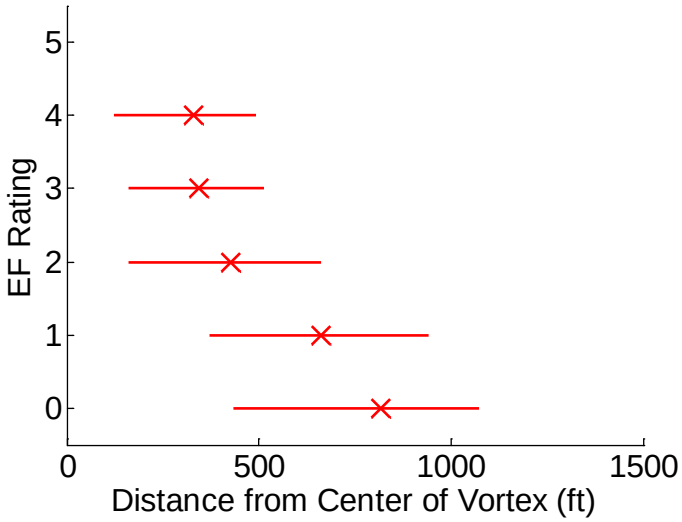

Figure 7.16, EF ratings from 20 May 2013, Moore tornado plotted against distance from vortex center. The symbols represent the mean distance for a given rating while the left and right ends of the lines represent 25th and 75th percentile distances.

The comparison is shown in Figure 7.17. The laboratory prediction does not decay quite as quickly as the field data, but the comparison is reasonable. The lab predictions shown are from a V55 vortex rather than the V15 vortex. The V55 vortex has a higher swirl ratio than V15, and therefore the V55 vortex has a two-celled structure while the V15 is single-celled. The fact that the comparison between Moore and V55 was better than the comparison between Moore and V15 might be an indication that the Moore tornado vortex was a two-celled or multi-celled vortex. Confirmation of this typically requires mobile radar data from the storm and some extra analysis. Unfortunately, these are not available for Moore.

This analysis highlights the promise of laboratory simulation—the shape of the curves is reasonably consistent, but it also highlights the need for a rational connection between predicted forces and resulting damage. The lab simulator can produce force predictions relatively easily, but estimating the resulting damage statistics requires a probabilistic framework involving fragility curves—something that builds on the innovative concepts found in van de Lindt et al. (2013).

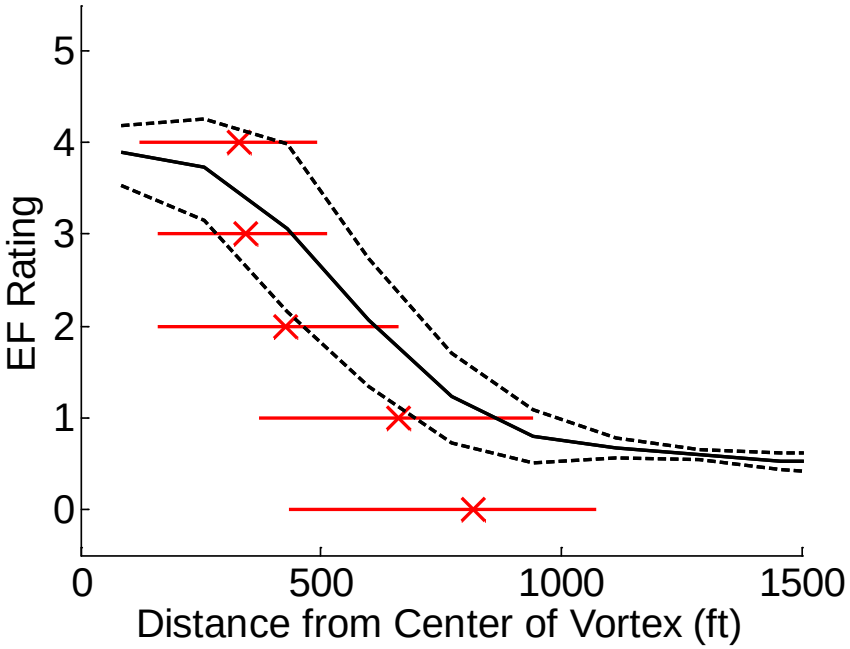

Figure 7.17, Comparison of Moore damage assessments (in red) with laboratory predictions (in black) from a V55 type vortex. The red symbols represent the mean distance for a given rating while the left and right ends of the red lines represent 25th and 75th percentile distances. The solid black line represents the mean EF prediction for each distance while the upper and lower dashed lines represent the 75th and 25th percentiles of these predictions.

7.2.5 Tornado Simulator Conclusions

Based on the observations made in Moore, OK, laboratory simulations, and similar observations made after the Tuscaloosa, AL and Joplin, MO tornados the following conclusions are advanced.

- The comparison between the damage data from the Moore tornado and the total force predictions from the laboratory tornado simulator shows promise for lab simulations. Although the lab simulator over predicted the damage for most radial positions, the shapes of the curves were reasonably consistent with each other.
- Improvements in the comparison between the lab force predictions and the damage survey results could be made with a more rational connection between predicted forces and resulting damage. This type of connection could be found using a probabilistic framework involving fragility curves.

Chapter 8 – Conclusions and Recommendations

The inspection team that visited Moore after the May 20th 2013 tornado contained experts in many different areas of science and engineering. For this reason, results of the investigation were comprehensive as well as technically detailed. As stated in the executive summary and introduction, target goals of the trip included describing a methodology for an easily reproducible rapid damage assessment, assessing performance of building components and storm shelters, analyzing how social media can positively impact communities in the wake of extreme events, and conducting specialized depth studies. The results of this report include:

- A geolocation data methodology has been developed and tested for use by extreme event damage assessment teams to collect, attribute, store, and distribute perishable damage data. Through a GIS internet portal, data and team findings are available for public viewing as well as analysis by members of the team or other experts interested in tornado damage data. The collection of LiDAR point cloud data in the aftermath of an extreme event provides a robust 3D data set that can be used to analyze structural damage even after a site has been cleaned up.
- Active social media data collection produced usable results. News reporters and storm chasers were obtaining and disseminating the most images in Moore. When approached, these professional shared tweets and images, as well as to disseminate the request to their followers, which grew the tweet count and useful images. This led to the conclusion that for future studies, citizen sensor requests should be directed to and disseminated through news reporters and storm chasers, as well as other "experts" involved with extreme events. Such groups include structural engineers, professional photographers, amateur/ham radio operators, and storm spotters.
- An analysis of storm shelter performance was conducted including above and below ground shelters. The results show that no inspected below ground shelters failed from perforation or penetration. Still, these shelters were sometimes found flooded by rain and severed water pipes, and in some cases the exits were blocked by debris. Above ground shelters also performed well, but one shelter was found to have been perforated by two metal poles. This was likely caused by poor consolidation of concrete between the foam forms due to the presence of plastic cross ties. In addition, examination of shared shelter

use showed that many residents of Moore took refuge in neighbors' shelters, and in some cases neighbors who were out of town left their shelter unlocked so that neighbors could access them.

- Residential structure damage patterns were examined and it was found that damage often initiated at garage doors and typically occurred at connections. Wall to foundation connections found in homes built since the 1999 tornado typically had more anchor bolts. Roof-to-wall connections were often toenailed and were observed to commonly fail. Failure of light-gage metal garage doors, particularly on garages that extended out from the house, typically led to pressurization of the garage, subsequent loss of roof over the garage, and collapse of the garage walls.
- The comparison between the damage data from the Moore, Oklahoma tornado of May 20th, 2013 and total force predictions from the laboratory tornado simulator shows promise for lab simulations. Although the lab simulator overpredicted the damage for most radial positions, the shapes of the curves were reasonably consistent with each other. Improvements in the comparison between the lab force predictions and the damage survey results could be made with a more rational connection between predicted forces and resulting damage. This type of connection could be found using a probabilistic framework involving fragility curves.
- Remotely sensed aerial imagery gives a comprehensive understanding of the location and extent of the storm, as well as flow and spreading of debris. These images also allow researchers to track long-distance transport of debris. Using aerial imagery from Moore, it was observed that debris flow is typically manifested in "streak lines" spreading out in thin lines away from the direction of travel of the storm. Long-distance debris transport showed that most heavy structural debris tends to be carried in the forward direction of the storm path.

Acknowledgements

The authors would like to acknowledge the National Science Foundation for their support through their RAPID grants program. The content of this report solely reflects the views of the authors and not the National Science Foundation.

The following students from several of the participating universities are also acknowledged for their contributions:

The University of Alabama: Shane Crawford, Alireza Geranmayeh, and David Burkhalter

University of Florida: Austin Thomas and Jeandona Doreste

University of Oklahoma: Seth Roswurm

References

ASTM C805/C805M, (2013). "Standard Test Method for Rebound Number of Hardened Concrete", ASTM International, West Conshohocken, PA, 2013.

CABO, 1995: One and Two Family Dwelling Code. International Code Council, Council of American Building Officials, Falls Church, VA, 350 pp.

City of Moore, Oklahoma (2013). Retrieved July 26, 2013 from http://www.cityofmoore.com/.

Cope, A. D., (2004). "Predicting The Vulnerability Of Typical Residential Buildings To Hurricane Damage", *Ph. D dissertation, link*: "http://fcmp.ce.ufl.edu/pubs/cope_a.pdf".

Ellingwood, B. R., Rosowsky, D. V., Yue Li, S., and Kim, J. H. (2004). "Fragility assessment of light-frame wood construction subjected to wind and earthquake hazards." ASCE J. Structural Engineering, 130(12), 1921-1930.

FEMA (2008). Taking Shelter From the Storm: Building a Safe Room for Your Home or Small Business. FEMA-320, Third Edition, August 2008.

FEMA, (2013): Oklahoma Tornadoes Situation Map, Retrieved July 5, 2013 from http://fema.maps.arcgis.com/home/webmap/viewer.html?webmap=5ebc42c2dee34fc0a31066331e8c02fb

FEMA, (1999): Midwest tornadoes of May 3, 1999. FEMA Publ. 342, Item 9-1035, 216 pp. Available online at [http://www.fema.gov/library/viewRecord.do?id=1423]

Fleming, M.R., Haan, Jr., F.L., Sarkar, P.P. "Turbulent Structure of Tornado Boundary Layers with Translation and Surface Roughness," *12th Americas Conference on Wind Engineering*, Seattle WA (2013).

Gardner, Anna, Mehta, Kishor C., Tanner, Larry J., Zhou, Zhongshan, Conder, Mark, Howard, Rob, Martinez, Mark S., and Weinbeck, Steve, (2000). The Tornadoes of Oklahoma City of May 3, 1999. Wind Science and Engineering Research Center, p. 1-38.

Gonzalez, Robert T, (2013): When tornadoes strike, which way do they travel? Retrieved August 23, 2013 from http://io9.com/when-tornados-strike-which-way-do-they-travel-513093207.

Google Maps. Google, (2013). Web. 11 July 2013. https://maps.google.com/.

Google Crisis Response. Google, (2013). Web. 11 July 2013. http://google.org/crisismap/2013-oklahoma-tornado?hl=en&llbox=35.35172%2C35.29037%2C-97.44147%2C-

97.56129&t=CUSTOM&layers=9%2C7%2C11%2C8%2Clayer2%2Clayer11%2C10%3A100.

Haan, Jr., F.L., Sarkar, P.P., Gallus, W.A., (2008): "Design, Construction and Performance of a Large Tornado Simulator for Wind Engineering Applications," *Engineering Structures*, v. 30, pp. 1146-1159.

Haan, F.L., Balaramudu, V.K., Sarkar, P.P, (2010): Tornado-Induced Wind Loads on a Low-Rise Building. ASCE *Journal of Structural Engineering*, 136, n. 1, pp.106-116.

KFOR.com, (2013). NewsChannel4 Oklahoma City. Interactive Map: 1999, 2003, 2013 Moore Tornadoes. Retrieved December 30, 2013, from http://kfor.com/2013/05/20/interactive-map-1999-2003-2013-moore-tornadoes/.

Kashani, A. G., Biswas, S., Crawford, P., Graettinger, A., Grau, D. (2013). Automated tornado wind speed estimation based on building damage data collected with terrestrial laser scanning. Journal of Computing in Civil Engineering, ASCE.

Lee, K., and Rosowsky, D. V. (2005). "Fragility assessment for roof sheathing failure in high wind regions." *Eng. Struct.*, 27(6), pp. 857-868.

Marshall, Timothy P., (2002). Tornado Damage Survey at Moore, Oklahoma. *Weather and Forecasting*, 17, pp. 582-598.

McDonald, J. R., & Mehta, K. C. (2006). A recommendation for an enhanced Fujita scale (EF-scale). Wind Science and Engineering Center, Texas Tech University.

Mishra, A.R., James, D.L., Letchford, C.W., (2008). Physical Simulation of a single-celled tornado-like vortex, Part B: Wind loading on a cubical model. Journal of Wind Engineering and Industrial Aerodynamics, 96, n. 8-9, pp. 1258-1273.

Natarajan, D., Hangan, H., Large eddy simulation of translation and surface roughness effects on tornado-like vortices (2012). *Journal of Wind Engineering and Industrial Aerodynamics*, 104-106 (2012) pp. 577-584.

National Weather Service, (2013). Tornado Outbreak of May 20, 2013. Retrieved July 2, 2013, from http://www.srh.noaa.gov/oun/?n=events-20130520.

NBC News, (2013). Satellite picture reveals the scar left behind by Moore tornado. Retrieved July 10, 2013 from http://www.nbcnews.com/science/satellite-picture-reveals-scar-left-behind-moore-tornado- 6C10219235.

New Day Tornado Shelters. (2013) Retrieved August 28, 2013 from http://www.newdaytornadoshelters.com/.

Norman Transcript, (2013). Time for clean slate for Moore Medical Center. Retrieved July 10, 2013 from http://normantranscript.com/headlines/x1472218848/Moving-past-Moore-Medical

Pan, Kai, Montpellier, Peter, and Zadeh, Masoud, (2002). Engineering Observations of the 3 May 1999 Oklahoma Tornado Damage. *Weather and Forecasting*, 17, pp. 599-610.

Prevatt, David O., William Coulbourne, Andrew J. Graettinger, Shiling Pei, Rakesh Gupta, and David Grau, (2012) "Joplin, Missouri, Tornado of May 22, 2011 – Structural Damage Survey and Case for Tornado-Resilient Codes," American Society of Civil Engineers, p. 64, October 15, 2012, ISBN: 9780784412503.

Reward Wall Systems, (2013). Retrieved July 1, 2013a, from http://rewardwalls.com/blog/2013/06/05/mooreoktornado/.

Prevatt, D. O., van de Lindt, J.W., Back, E., Graettinger, A. J., S. Pei, Coulbourne, W., Gupta, R., James, D. (2012). "Making the Case for Improved Structural Design: The Tornado Outbreaks of 2011," *Leadership and Management in Engineering*, 2012 (12), pp. 254-270

Sabareesh, G.R., Matsui, M., Tamura, Y., (2012). Dependence of surface pressure on a cubic building in tornado like flow on building location and ground roughness. *Journal of Wind Engineering and Industrial Aerodynamics*, 103 50-59.

Simmons, T. M., Sutter, D., Pielke, R. (2013) "Normalize tornado damage in the United States", *Environmental Hazards*, Vol 12 (2), pp. 132-147.

Storm Prediction Center, (2013). 0600 UTC Day 1 Convective Outlook. Retrieved July 11, 2013 from http://www.spc.noaa.gov/products/outlook/archive/2013/day1otlk_20130520_1200.html.

Tulsa World, (2013). Moore tornado tally: More than 12,000 homes damaged or destroyed. Retrieved July 10, 2013 from http://www.tulsaworld.com/article.aspx/Moore_Tornado_Aftermath_Storm_recovery_continues/20130523_777_0_MOORES121548.

United States Census Bureau, (2010): 2010 Census. Retrieved July 1, 2013, from http://factfinder2.census.gov/faces/tableservices/jsf/pages/productview.xhtml?pid=DEC_10_DP_DPDP1.

United States Census Bureau, (2012). Retrieved November 20, 2013, from http://factfinder2.census.gov/faces/tableservices/jsf/pages/productview.xhtml?pid=ACS_12_5YR_DP05.

van de Lindt, J., Pei, S., Dao, T.,Graettinger, A., Prevatt, D., Gupta, R., Coulbourne, W., (2013) Dual-Objective-Based Tornado Design Philosophy, ASCE *Journal of Structural Engineering*, 139, pp. 251-263.

Weather Underground, (2013): 10 Worst U.S. Tornado Outbreaks. Retrieved July 5, 2013 from http://www.wunderground.com/news/worst-tornado-outbreaks-20130228?pageno=5.

Zillow.com, (2013). Yahoo!-Zillow Real Estate Network. Web. 12 June 2013. http://www.zillow.com/homedetails/808-S-Silver-Leaf-Dr-Moore-OK-73160/21714332_zpid/.

Appendix

Table A1, Detailed results of building damage assessment and EF rating

House ID1	Damage Metrics									Expected Wind Speed (mph)	EF Rating
	Loss of roof or wall covering	Broken glasses	Failure of garage doors and walls	Uplift of roof decks	Failure of large section of roofs	Failure of some exterior walls	Failure of some interior walls	Failure of all walls	Slab swept clean		
1										65	EF0
2		*								79	EF0
3		*								79	EF0
4	*	*								96	EF1
5										65	EF0
6		*	*	*	*	*				120	EF2
7	*	*	*	*						100	EF1
8	*	*	*	*	*					125	EF2
9		*	*	*	*	*				135	EF2
10	*	*		*	*					125	EF2
11	*	*	*	*	*	*	*	*	*	170	EF4
12	*	*	*	*	*	*	*			150	EF3
13	*	*	*	*	*					140	EF2
14	*	*	*	*	*					130	EF2
15	*	*	*	*	*	*				135	EF2
16	*	*	*	*	*	*	*			150	EF3
17	*	*	*	*	*	*	*	*		152	EF3
18	*	*	*	*	*	*	*	*		152	EF3
19	*	*	*	*	*	*	*	*	*	170	EF4
20	*	*	*	*	*	*	*	*	*	170	EF4
21	*	*	*	*	*	*	*	*	*	170	EF4
22	n/a2	*								79	EF0
23	*	*		*	*	*				120	EF2
24	n/a2	*		*						97	EF1
25	n/a2	*	*	*						97	EF1
26	*	*	*	*	*	*				140	EF3
27	*	*	*	*	*	*	*			148	EF3
28	*	*	*	*	*	*	*	*		170	EF4
29	*	*	*	*	*	*	*			148	EF3
30	n/a2	*	*	*	*	*				130	EF2
31	n/a2	*	*	*		*				125	EF2
32	*	*	*							100	EF1
33	*	*	*							100	EF1
34	*	*	*	*	*					125	EF2
35	*	*	*	*	*					125	EF2
36	*	*		*						115	EF1
37	*	*	*	*	*	*				132	EF2
38	*	*	*	*	*	*				132	EF2
39	*	*	*	*	*	*	*	*		152	EF3
40	*	*	*	*	*	*	*			150	EF3
41	*	*	*	*	*	*	*			150	EF3
42	n/a2	*								100	EF1
43	n/a2	*	*							85	EF0

1 House IDs are based on those shown in Figures 2.9 and 2.10
2 Unable to identify the loss of covering material due to lack of color information